Planetary-Scale Shear Trajectories and Their Expression in Global Geological Geometry

Craig Stone

26 December 2025

Plain Language Summary

Many large geological features on Earth—such as curved mountain belts, sedimentary arcs, rift systems, and ocean basins—share recurring geometric patterns that extend across regional, continental, and sometimes near-hemispheric scales. These features are commonly interpreted in terms of local processes such as plate collisions, mantle flow, erosion, or faulting. In this study, we ask a broader question: whether some aspects of Earth's surface geometry and stress orientation reflect an underlying, planet-scale stress framework that interacts with—but is not reducible to—regional tectonic processes.

We compare observed stress directions from the World Stress Map with a mathematically derived global shear field associated with a prescribed true-polar-wander–like rotational geometry. Rather than evaluating only whether the model improves global mean alignment, we examine whether the geographic pattern of agreement and disagreement between model and observations is spatially organized.

Using permutation-based spatial statistics, we find that angular misfit values are not randomly distributed. Instead, they exhibit statistically significant spatial organization across multiple length scales, from regional domains (hundreds of kilometres) to near-hemispheric extents (thousands of kilometres). This long-wavelength structure persists even though the model does not outperform random Euler rotations in terms of global mean misfit, indicating that spatial organization and global alignment represent distinct and complementary diagnostic measures.

The same global shear framework is expressed qualitatively in a wide range of geological and geomorphic settings, including passive-margin sedimentary belts, arcuate mountain systems, oceanic bathymetric arcs, rift zone curvature, glacially sculpted terrains, and active plate-boundary geometries. The new results introduced in Section 6 further demonstrate that these patterns extend coherently across scale transitions, linking regional expressions of deformation to a broader, planet-scale stress topology.

These findings do not imply that a single mechanism controls all geological features, nor that plate tectonics is replaced by an alternative framework. Rather, they suggest that plate-scale and

regional processes operate within—and are subtly conditioned by—a persistent, long-wavelength stress architecture that organizes deformation over geological time.

Abstract

Large arcuate geological features occur across Earth's surface in sedimentary, tectonic, glacial, and oceanic environments. While most examples are traditionally interpreted in terms of local or regional processes, the possibility that such geometries reflect long-wavelength, globally organized structure has received limited systematic investigation.

Here we compare global geological and geophysical datasets with analytically derived surface shear trajectories associated with a prescribed class of true-polar-wander–like rotational geometries. Using a Vening Meinesz–style formulation, two conjugate families of shear trajectories (Net 1 and Net 2), together with invariant contours, are computed analytically on the sphere and projected independently of geological or geophysical observations.

Qualitative comparison reveals recurring geometric congruence between the modeled shear field and a wide range of Earth-surface features, including continental sediment arcs, major mountain belts, oceanic bathymetric curvature, rift-system segmentation, glacially sculpted terrains, and active plate-boundary architecture. Quantitative comparison with the World Stress Map (WSM) database shows that, although the model does not outperform random Euler rotations in terms of global mean angular misfit, the spatial distribution of misfit exhibits statistically robust, non-random geographic organization.

Permutation-based spatial autocorrelation analysis yields consistently positive and highly significant Moran's I values from regional ($\sim$250 km) through continental to near-hemispheric ($\sim$3000–4000 km) length scales, with smoothly decreasing magnitude as spatial scale increases. The new results introduced in Section 6 demonstrate that this organization persists coherently across scale transitions and cannot be explained by chance or by local tectonic processes alone.

Taken together, these results suggest that Earth's surface deformation and stress orientation operate within a persistent, planet-scale stress topology that interacts with, and subtly conditions, plate tectonics and regional geological evolution, functioning as an organizing framework alongside rather than in place of conventional tectonic mechanisms.

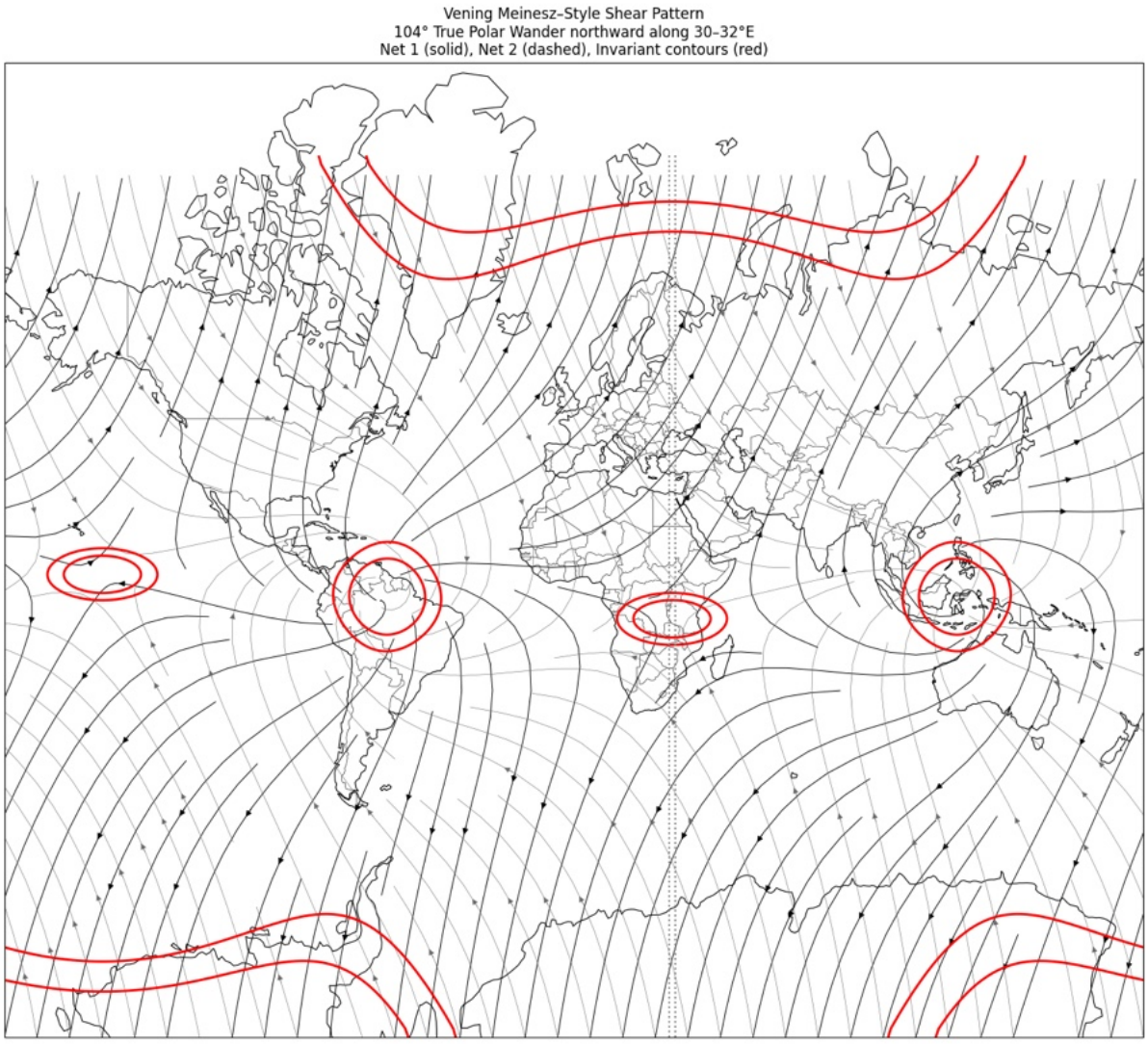

Figure 1: Vening Meinesz–style global shear pattern for a prescribed 104° northward true polar wander along the 31°E meridian. Solid curves indicate Net 1 shear trajectories, dashed curves Net 2 trajectories, and red curves invariant contours.

1 Introduction

Earth's lithosphere exhibits pervasive curvature at regional, continental, and planetary scales. Arcuate sediment belts, sweeping mountain chains, curved continental margins, bathymetric arcs, rift systems, and coherent basin chains occur across diverse tectonic environments and geological ages. Conventional explanations typically invoke local or regional boundary conditions—such as plate convergence, inherited basement fabrics, mantle flow, glaciation, or sediment routing—to account for individual cases [Turcotte and Schubert, 2014, Condie, 1997]. However, many of the largest arcuate systems cross geological provinces, persist across contrasting lithospheric ages, and dis-

play smooth, continuous curvature that is difficult to reconcile with segmented tectonic histories or short-wavelength forcing alone.

These observations raise a broader question: whether some aspects of Earth's surface geometry and stress orientation may be influenced by long-wavelength, planet-scale stress organization that interacts with—but does not replace—plate-tectonic and regional processes. Prior studies have occasionally suggested large-scale coherence in tectonic fabrics, stress alignment, or geomorphic curvature, but systematic evaluation of such organization using globally consistent analytical geometry and spatial statistics has been limited.

In this study, we evaluate whether a mathematically prescribed global shear field associated with a simple class of true-polar-wander–like rotational geometries exhibits meaningful correspondence with observed geological structure and contemporary stress orientation. The approach does not seek to reconstruct a specific geophysical event or mechanism. Rather, it tests whether the geometry of such a shear field can act as an organizing framework that is detectable in both the spatial pattern of stress misfit and the recurring curvature of major geological features.

A key methodological distinction in this work is the separation of two complementary questions. First, we assess whether the modeled shear field improves global mean alignment relative to random Euler rotations. Second—and more critically—we evaluate whether the spatial distribution of angular misfit values is geographically organized rather than randomly dispersed. A model may fail to minimise misfit in a global scalar sense while still capturing physically meaningful long-wavelength structure. Distinguishing between global alignment and spatial organization is therefore essential for correct interpretation.

The analyses presented here combine qualitative comparison of shear-trajectory geometry with continental- and ocean-scale geological features, and quantitative spatial-statistical evaluation of stress-orientation misfit using the World Stress Map database. The results, including the extended findings introduced in Section 6, indicate that non-random, multi-scale spatial organization persists from regional to near-hemispheric wavelengths, and that this organization is expressed coherently across diverse tectonic contexts. These observations motivate interpretation of Earth's deformation and surface geometry as operating within a persistent, planet-scale shear topology that interacts with and subtly conditions plate-tectonic processes over geological time.

2 Methods

2.1 Statistical Testing Framework

Two complementary statistical approaches are employed, reflecting the distinction between global scalar performance and spatially structured behaviour in the misfit field.

First, Euler-rotation null tests evaluate whether the modeled shear field provides improved *global mean* alignment relative to randomly oriented shear fields generated through uniformly sampled Euler rotations. These tests quantify aggregate angular misfit across all sites and therefore assess

only whether a given geometry minimises misfit in a scalar, globally averaged sense.

Second, spatial organization is evaluated using Moran's I with permutation-based null models. In this framework, angular misfit values are randomly reassigned among observation locations while preserving both sampling geometry and the underlying misfit distribution. This procedure tests whether neighbouring locations exhibit more similar misfit values than expected under spatial randomness, and is therefore insensitive to global mean alignment. It directly evaluates the presence, magnitude, and scale dependence of geographic structure in the misfit field.

These two tests address distinct but complementary questions and are interpreted accordingly throughout the manuscript and in the extended analyses presented in Section 6.

2.2 Prescribed True Polar Wander Geometry

The modeled stress framework is derived from a single prescribed true-polar-wander (TPW)–like rotational geometry, implemented as a rigid-body northward rotation of 104° about an axis fixed along the 31°E meridian. The transformation is treated purely geometrically, without assumptions regarding its timing, duration, or physical driver. The objective is not to reconstruct a specific TPW event, but to evaluate whether such a geometry generates a shear topology consistent with observed large-scale stress orientations and geological curvature.

2.3 Construction of the Global Shear Field

The surface stress field is represented by two orthogonal families of analytically derived shear trajectories:

- **Net 1**: trajectories aligned with maximum differential shear induced by the prescribed reorientation;
- **Net 2**: trajectories orthogonal to Net 1, representing the conjugate shear accommodation system.

Invariant contours are computed as loci of minimal differential shear and represent regions expected to favour long-term structural persistence and curvature stability. All trajectories and contours are generated analytically on the sphere and projected globally without tuning or fitting to geological or geophysical datasets.

2.4 Datasets and Visualisation

Independent datasets include global plate boundaries, bathymetry and gravity compilations, geological province maps, surface-sediment composition, digital-elevation models, satellite imagery, and the 2025 World Stress Map (WSM) database. Multiple cartographic projections, including polar stereographic views, are employed to minimise projection bias and to test the robustness

of geometric relationships across latitudes. Section 6 extends the same framework to evaluate cross-scale consistency in misfit organization and shear-trajectory correspondence.

Terminology and Scale Definitions

For clarity and consistency, we adopt the following scale terminology throughout the Results and Discussion. *Regional scales* refer to spatial wavelengths of order ∼250–500 km, encompassing local tectonic domains and plate-boundary systems. *Continental to transcontinental scales* refer to wavelengths of approximately 500–1500 km, spanning major lithospheric provinces and multi-plate regions. *Planetary-scale organization* denotes wavelengths 1500 km, extending across multiple plates and approaching hemispheric dimensions; the term *near-hemispheric* denotes the upper portion of this range (3000–4000 km), where neighbourhood extents span a substantial fraction of a hemisphere without implying global uniformity.

Throughout, *spatial organization* refers to statistically resolvable geographic structure in the misfit field as quantified by Moran's I, whereas *global alignment* denotes scalar, globally averaged angular misfit. The coexistence of weak or non-significant global alignment with strongly significant spatial organization is therefore interpreted as evidence for long-wavelength stress structure operating alongside, rather than replacing, regional tectonic processes—an interpretation further reinforced by the scale-consistent behaviour documented in Section 6.

3 Results: Regional Case Studies

The following case studies illustrate how the modeled shear framework is expressed across contrasting tectonic, geomorphic, and depositional environments. In each example, geometric correspondence is evaluated in terms of (i) alignment with Net 1 and Net 2 shear trajectories or invariant contours, (ii) independence from purely local boundary conditions, and (iii) coherence across scale transitions. These regional observations complement the quantitative spatial-statistical results and provide contextual evidence for a persistent, long-wavelength shear topology that interacts with, rather than replaces, plate-tectonic and surface processes.

3.1 Southeastern United States Sediment Arc

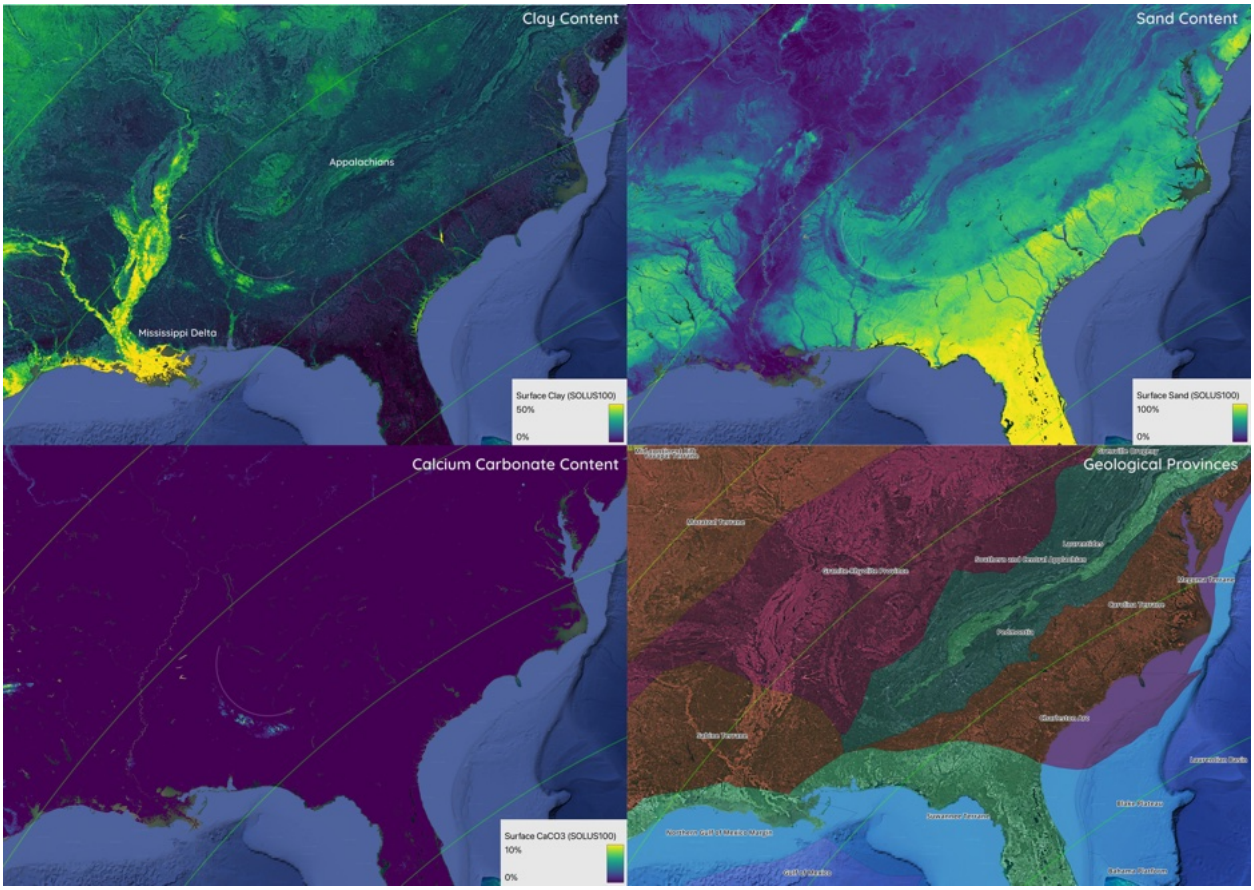

Figure 2: Four-panel comparison of clay, $CaCO_3$, sand, and geological provinces in the southeastern United States. A continent-scale arcuate belt aligns with invariant shear contours and crosses multiple geological provinces.

The arcuate sedimentary belt spanning the southeastern United States (Figure 2) represents one of the clearest expressions of the modeled global shear framework acting within a passive-margin setting. Conventional interpretations emphasise Appalachian orogenic inheritance, differential erosion, fluvial routing, and marine sediment redistribution. While these processes are important contributors, they do not readily explain the remarkable geometric continuity, large radius of curvature, and cross-provincial coherence of the arc across multiple sediment classes and lithospheric domains.

When examined in the context of the modeled shear field, the sediment arc aligns closely with invariant shear contours rather than with present-day drainage basins, coastline geometry, or individual tectonostratigraphic boundaries. The arc persists across terranes of differing lithology and age, including Paleozoic orogenic belts, Mesozoic rifted margins, and Cenozoic sedimentary platforms, indicating control by a stress geometry that transcends local structural segmentation.

Notably, the correspondence is expressed simultaneously in clay-rich sediments, carbonate dis-

tributions, and sandy deposits, each characterised by distinct transport pathways and depositional mechanisms. The convergence of these independent sedimentary signals along the same arcuate trajectory argues against coincidental alignment and instead points to a shared, long-wavelength controlling framework. Within the shear-net interpretation, the arc occupies a zone of minimal differential shear, a setting expected to favour long-term sediment accumulation and curvature stability while suppressing disruptive deformation.

Through repeated episodes of erosion, sea-level fluctuation, and sediment reworking, this inherited stress architecture appears to have been progressively amplified rather than erased. The southeastern sediment arc therefore functions as a geomorphic and sedimentological recorder of the broader shear topology, consistent with the cross-scale organisational behaviour demonstrated statistically in Section 6.

This interpretation does not displace established Appalachian or passive-margin models; instead, it situates them within a hierarchical framework in which local processes operate within, and are subtly conditioned by, a persistent planet-scale stress organization. In this sense, the southeastern United States sediment arc is not an isolated regional anomaly, but a continental-scale manifestation of the same shear geometry expressed in other tectonic and depositional systems worldwide.

3.2 The Himalayan Arc

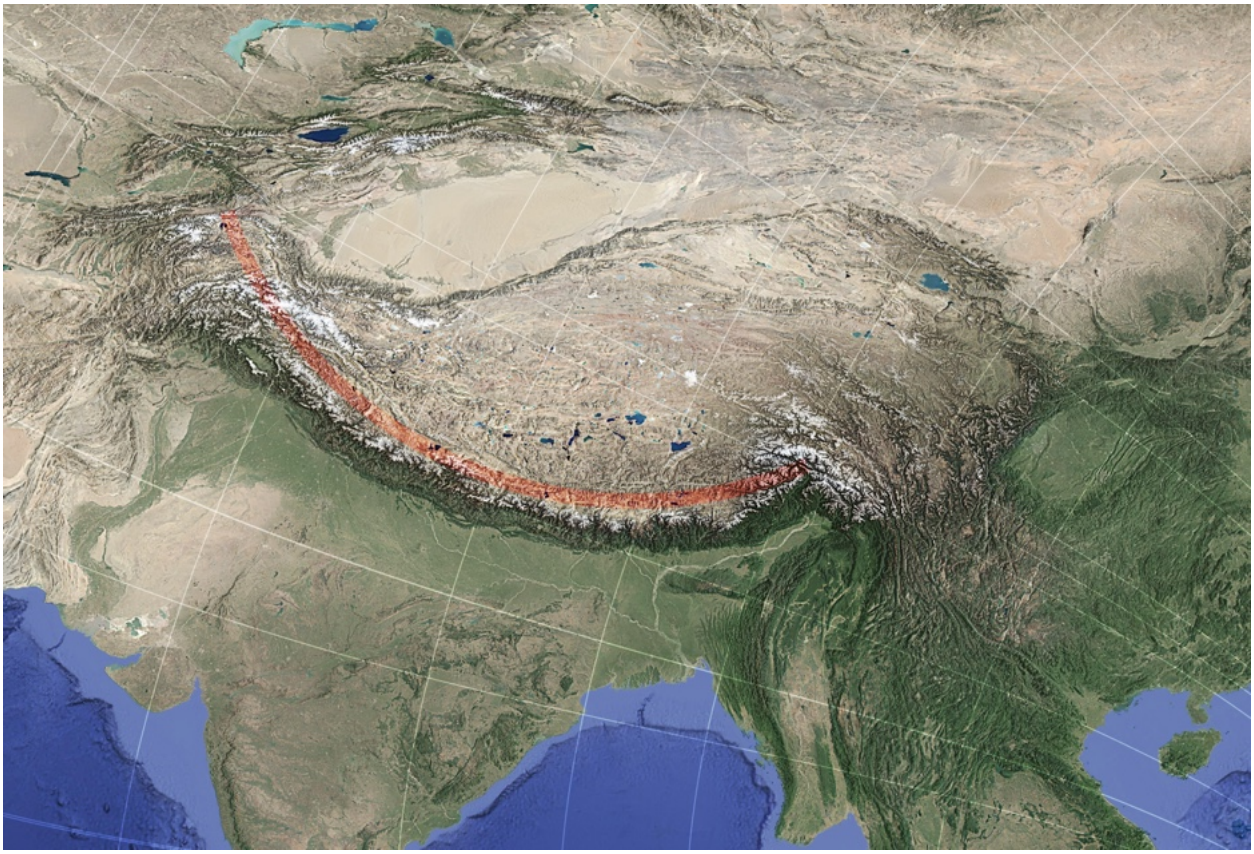

Figure 3: The Himalayan mountain belt forms a geometrically smooth arc that lies parallel to one shear family and orthogonal to the conjugate family.

The Himalayan orogen constitutes one of the most striking large-scale arcuate features on Earth, traditionally interpreted as the consequence of continent–continent collision between the Indian and Eurasian plates. This tectonic framework explains crustal shortening, uplift, and seismicity, but it does not, by itself, account for the exceptional geometric regularity and long-radius curvature of the Himalayan arc over more than 2,500 km, nor for its consistent orientation with respect to broader stress trajectories.

Within the modeled global shear framework, the Himalayan arc exhibits near-ideal orthogonality to one family of shear trajectories (Net 1) while remaining broadly parallel to the conjugate family (Net 2). This dual geometric relationship is mechanically non-trivial: it places the orogen within a transition zone where principal shear directions rotate from dominantly compressional to tangential regimes. In such a configuration, convergence is predisposed to organise into a smooth, laterally continuous curvature rather than fragmenting into irregular salients or segmented thrust belts.

The persistence of this geometry across regions of contrasting crustal thickness, lithological inheritance, and convergence history suggests that the Himalayan arc represents not merely a local

collision artifact, but a lithospheric-scale response embedded within a pre-existing, long-wavelength stress topology. In this interpretation, the India–Asia collision supplies the energetic forcing, while the global shear field constrains the geometric pathways along which shortening is accommodated.

This perspective assists in reconciling several long-standing observational asymmetries, including the coherence of foreland-basin development, the continuity of major thrust systems, and the relative uniformity of arc curvature despite significant variations in convergence rate and slab geometry along strike. These behaviours are more readily understood when deformation is viewed as operating within a guiding shear architecture rather than being governed solely by local structural inheritance.

Analogous geometric relationships occur in other arcuate systems examined in this study—including the Andes, the Banda Arc, and selected intracontinental curvature belts—each occupying regions where the modeled shear field predicts stable, low-variance stress configurations across multiple spatial scales. The Himalayan arc therefore represents an end-member case in which strong tectonic forcing interacts with a persistent, planet-scale shear organization that is also expressed in more weakly deformed or passive-margin environments.

In summary, the Himalayan arc is best interpreted as the visible outcome of continental collision occurring within a pre-organised, long-wavelength shear field. This interpretation preserves the explanatory strengths of plate-tectonic theory while situating orogenic curvature within a broader hierarchical framework consistent with the cross-scale organisational behaviour demonstrated in Section 6.

3.3 Central America and the Caribbean

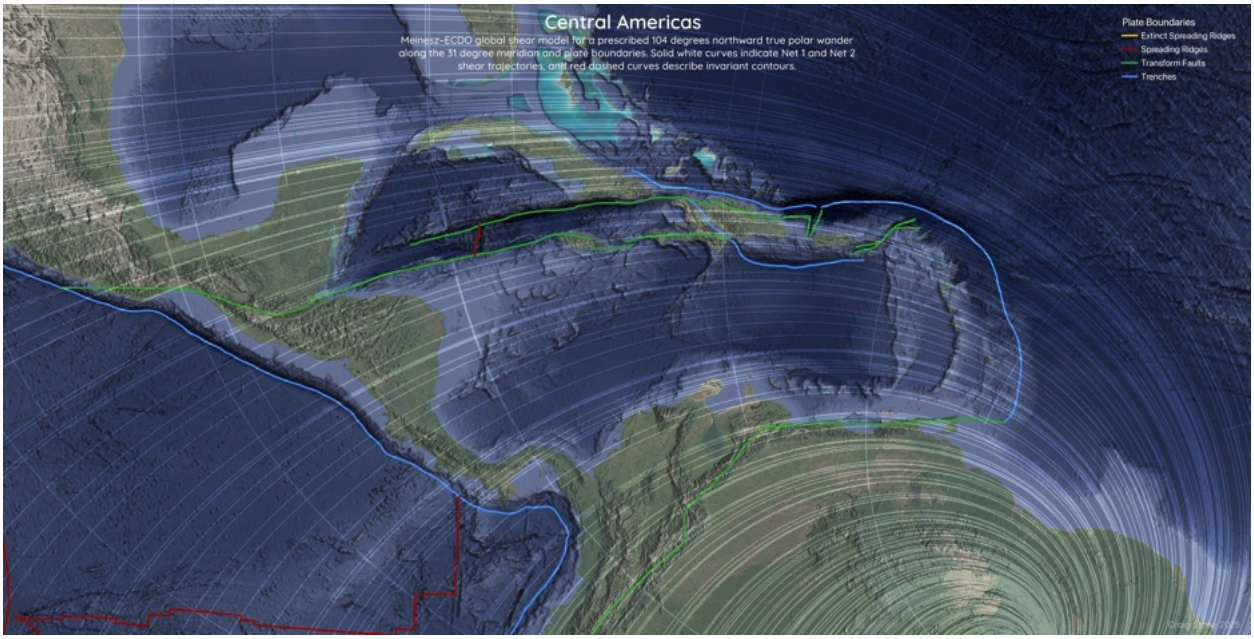

Figure 4: Central America and the Caribbean showing strong geometric congruence between plate boundaries and the modeled global shear field.

3.4 Central America and the Caribbean: Shear-Guided Arc Segmentation and Plate-Boundary Organization

Central America and the Caribbean constitute one of the most tectonically intricate regions on Earth, involving interactions among multiple major and minor plates, variable subduction polarity, transform faulting, microplate rotation, and inherited continental fragments. Conventional plate-kinematic models successfully describe relative motions within this system, but they do not fully account for the pronounced geometric coherence, curvature continuity, and segmentation observed across arcs, basins, and fault systems at regional to supra-regional scales.

Within the modeled global shear framework, Central America and the Caribbean occupy a domain of pronounced shear curvature and net convergence associated with the western Euler-point sector of the field. The dominant arcs of the Lesser Antilles, the Central American volcanic front, and the curved margins of the Caribbean Plate closely parallel modeled shear trajectories rather than simply following instantaneous plate-motion vectors. This alignment persists across transitions from oceanic to continental lithosphere and across boundaries separating subduction-dominated, transform-dominated, and extensional regimes, indicating control by a stress organization that transcends local kinematic boundaries.

A particularly diagnostic expression of this control is the smooth, large-radius curvature of the Caribbean Plate margins. Instead of forming a polygonal outline, the plate boundary traces arcs that correspond closely to invariant shear contours—loci of minimal differential shear that favour

structural persistence through time. This geometry provides a natural explanation for the long-term coherence of the Caribbean Plate despite internal deformation, microplate interaction, and prolonged tectonic isolation.

Rift boundaries and major transform corridors exhibit mixed but non-random relationships to the shear nets. Several large transforms align tangentially with one of the two shear families, while others rotate progressively to accommodate transitions between shear-dominated and kinematically dominated sectors. This behaviour is consistent with stress-guided partitioning of deformation, in which plate motions operate within, rather than independently of, an inherited long-wavelength shear topology.

Seismicity and volcanism reinforce this interpretation. Earthquake epicentres ($M \geq 4.5$ over the past 25 years) cluster preferentially along shear-aligned corridors, particularly where trajectories curve or converge, and active volcanic centres similarly concentrate within zones where the modeled field predicts enhanced strain localization. The spatial coincidence of active deformation with predicted shear geometry is notable given the rapid tectonic evolution and high strain rates characteristic of the region.

Taken together, the Central America–Caribbean system demonstrates that the global shear organization remains legible even in highly dynamic, plate-boundary environments. Rather than obscuring the underlying geometry, tectonic complexity amplifies its expression, revealing a persistent, multi-scale constraint on the orientation, curvature, and segmentation of plate-boundary structures—behaviour consistent with the cross-scale spatial organization quantified in Section 6.

3.5 South Indian Ocean Tectonic Arc

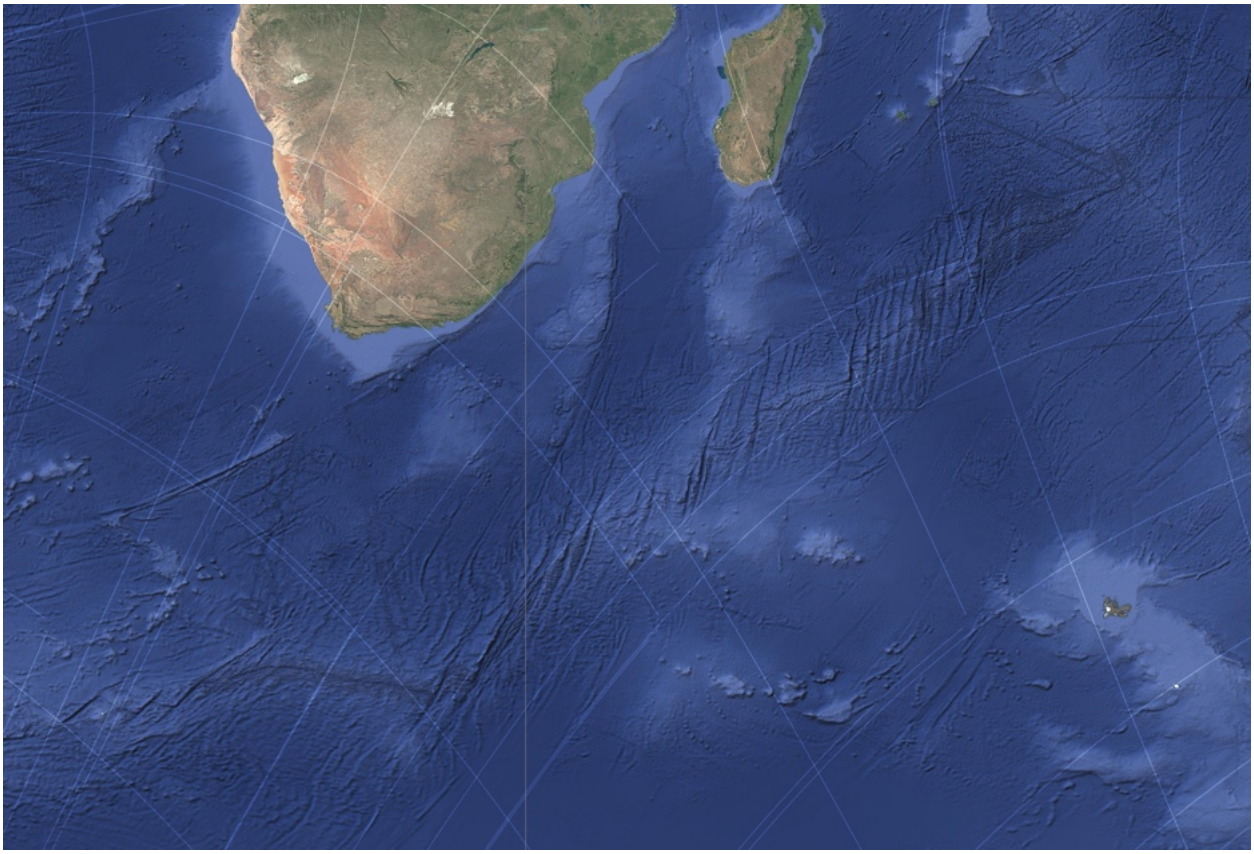

Figure 5: A vast tectonic arc in the southern Indian Ocean displaying strong congruence with modeled shear trajectories.

The southern Indian Ocean hosts one of the least discussed yet most geometrically coherent arcuate tectonic features identified in this study. Extending across abyssal plains and intersecting multiple spreading systems, the arc is commonly attributed to combinations of ridge propagation, transform segmentation, and inherited mantle structure. While these processes contribute to its development, they do not, on their own, account for the smooth, large-radius curvature and persistence of the feature across regions with markedly different spreading histories.

Within the modeled global shear framework, the South Indian Ocean arc aligns closely with invariant shear contours, occupying a domain of minimal differential shear under the prescribed rotational geometry. This alignment is particularly significant because oceanic lithosphere is continuously generated. The preservation of coherent curvature in such a setting implies that the organizing stress geometry is both long-wavelength and repeatedly imposed through successive episodes of lithospheric accretion.

Bathymetric and gravity data indicate that ridge segments, fracture zones, and subtle topographic highs preferentially conform to the modeled curvature rather than to local spreading directions alone. In several regions, ridge axes rotate smoothly to remain approximately orthogonal

to nearby shear trajectories, while transform offsets tend to align parallel to one of the two shear families. This behaviour mirrors that observed along the Mid-Atlantic Ridge and supports the interpretation that ridge segmentation and propagation are biased by an externally imposed shear topology rather than emerging solely from local kinematic constraints.

The diagnostic value of this feature lies in its predominantly oceanic context, largely free from continental inheritance. Its morphology must therefore arise from interactions among mantle flow, lithospheric accretion, and a persistent, planet-scale stress organization. In this setting, the global shear field provides a parsimonious explanation for the spatial coherence of ridge initiation, abandonment, and segmentation through time.

Even as spreading centres migrate and plate configurations evolve, the invariant shear geometry remains fixed relative to the global frame, enabling successive generations of oceanic crust to inherit similar curvature. The resulting composite bathymetric signature integrates the cumulative effect of long-wavelength shear organisation over tens of millions of years—behaviour that is consistent with the scale-persistent spatial structure demonstrated statistically in Section 6.

In summary, the South Indian Ocean tectonic arc represents a compelling oceanic manifestation of the global shear framework. Its correspondence with invariant contours strengthens the inference that the modeled shear field reflects a real and long-lived component of Earth's stress architecture, influencing both continental and oceanic tectonics across multiple spatial and temporal scales.

3.6 Sulawesi and Western Pacific Bathymetry

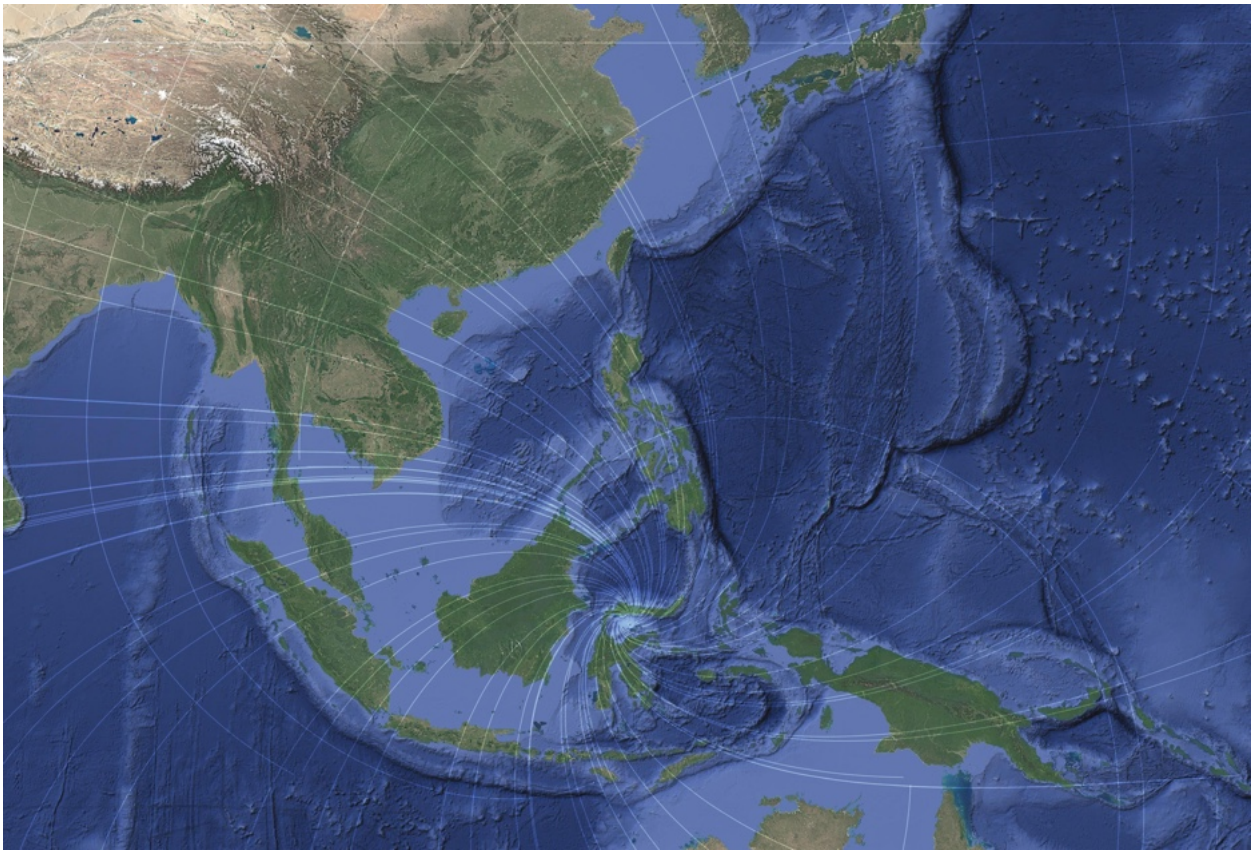

Figure 6: Primary and secondary bathymetric arcs near Sulawesi aligned with predicted shear trajectories.

The Sulawesi–Banda region represents one of the most structurally complex tectonic environments on Earth, characterised by tightly curved island arcs, deep bathymetric basins, rapid slab rollback, back-arc spreading, and intense seismic and volcanic activity. Conventional models explain this complexity through interacting processes including microplate rotation, slab tearing, variable subduction polarity, and evolving plate-boundary geometries. While these mechanisms account for the kinematics, they do not, on their own, explain the exceptional geometric coherence, nested curvature, and near-spiral morphology of the Banda Arc and surrounding basins.

Within the modeled global shear framework, the Banda Sea and adjacent arcs occupy a domain of pronounced shear convergence and rotational confinement. Both Net 1 and Net 2 trajectories curve strongly into the region, producing a tightly wound shear vortex whose geometry closely mirrors the observed bathymetry, trench curvature, and volcanic-arc alignment. The Banda Arc itself traces an almost continuous segment of an invariant contour, while subsidiary ridges and basins alternate between parallel and orthogonal relationships to the local shear directions.

This configuration implies that the Sulawesi–Banda system resides within a high-curvature

segment of the planetary-scale shear topology, where long-wavelength stress trajectories impose strong directional bias on deformation. In such a regime, modest lithospheric heterogeneity or inherited weakness can be rapidly amplified into rotational tectonics. Microplate rotations therefore emerge not as the primary cause of curvature, but as mechanical responses to an imposed shear geometry that favours angular-momentum conservation within a confined domain.

Bathymetric features northeast of Sulawesi exhibit smaller-scale arcuate basins and ridges that replicate the same geometric relationships at reduced wavelength, suggesting a self-similar or fractal expression of the underlying shear organisation. These features are difficult to reconcile with isolated slab-dynamic processes, yet follow naturally if the lithosphere is responding to a continuous, long-wavelength stress network.

Seismicity and volcanism display complementary spatial coherence. Earthquake hypocentres cluster preferentially along shear-aligned corridors and curvature-transition zones, while volcanic centres concentrate where the modeled field predicts changes in shear regime from compressional to extensional dominance. This pattern is consistent with stress-guided melt focusing and fault reactivation governed by shear geometry rather than by plate-boundary position alone.

In this framework, the Sulawesi–Banda system constitutes an end-member expression of rotational tectonics embedded within a persistent planet-scale shear organisation. Its apparent complexity reflects the clarity with which the underlying geometry is expressed, and its behaviour is consistent with the cross-scale spatial organisation and curvature stability demonstrated quantitatively in Section 6.

3.7 Mid-Atlantic Ridge

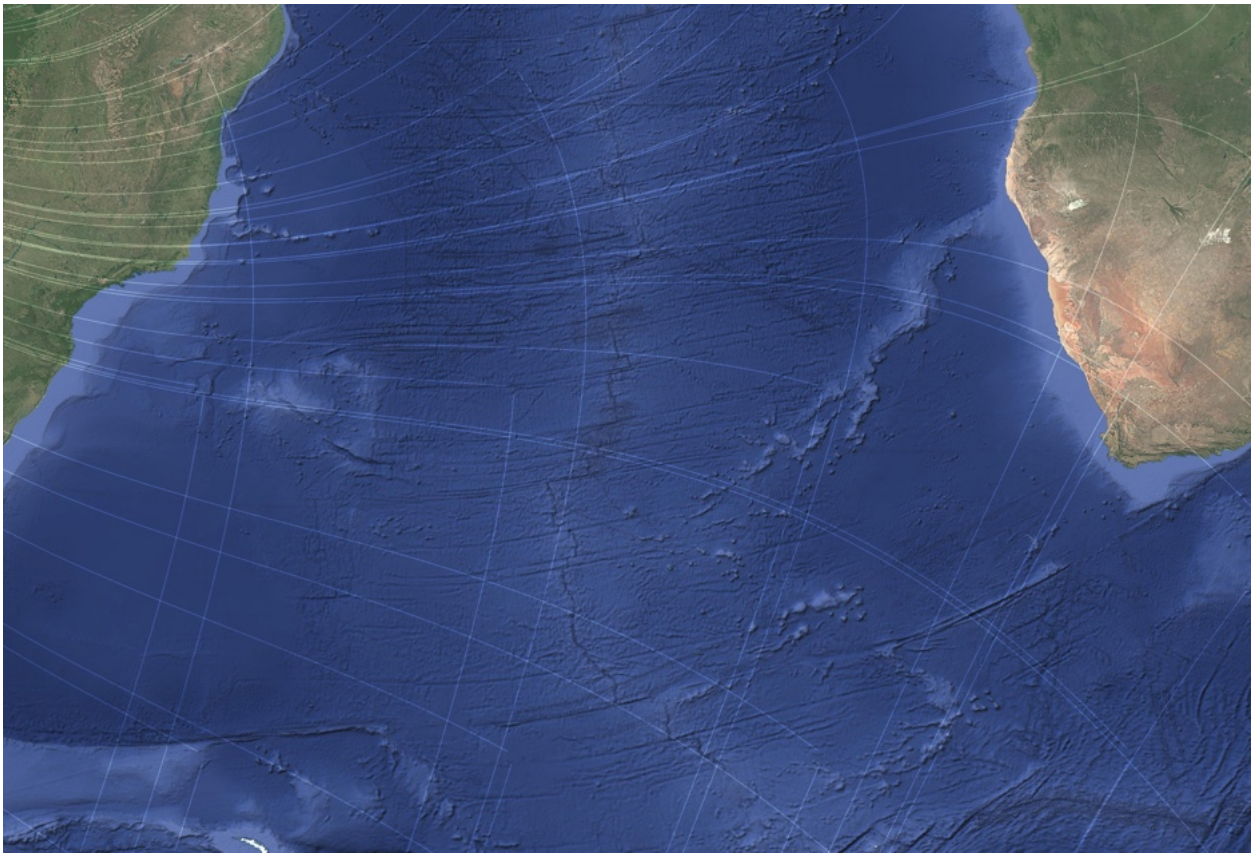

Figure 7: The Mid-Atlantic Ridge exhibits alternating alignment with Net 1 and Net 2 shear families along strike.

The Mid-Atlantic Ridge (MAR) provides a particularly powerful test of the modeled global shear framework because it is an actively forming plate boundary in which new lithosphere is continuously created. Any persistent geometric correspondence in such a setting must therefore reflect an organising boundary condition that is repeatedly expressed through ongoing accretion, rather than a purely fossil inheritance.

In conventional interpretations, MAR morphology is attributed to the interaction of plate divergence, mantle upwelling, transform segmentation, and spreading-rate variability. While these factors are essential to ridge dynamics, they do not, by themselves, explain the systematic alternation in ridge-segment orientation and curvature observed along thousands of kilometres of ridge axis.

When compared with the modeled shear field, the MAR displays a striking pattern of alternating alignment with Net 1 and Net 2 trajectories. Ridge segments rotate gradually to remain approximately orthogonal to the locally dominant shear direction, while intervening transform faults tend to align parallel to the complementary shear family. This behaviour repeats quasi-periodically from

the North Atlantic through the equatorial region into the South Atlantic, indicating a persistent geometric bias rather than stochastic segmentation.

Such alternation arises naturally if spreading is geometrically conditioned by a long-wavelength shear topology that operates alongside plate divergence. In this interpretation, spreading is accommodated most efficiently where ridge axes develop orthogonal to maximum shear gradients, while lateral offsets concentrate along shear-parallel orientations that minimise resistance to differential motion. The result is a ridge system whose large-scale sinuosity reflects interaction between local accretionary processes and a broader, planet-scale stress organisation.

The coexistence of ridge propagation, segment abandonment, and transform migration within this geometry reinforces the view that the shear framework does not replace plate-tectonic processes, but constrains the form through which they are expressed. The persistence of these relationships through time implies that successive generations of newly formed lithosphere inherit the same long-wavelength curvature, consistent with the scale-stable spatial organisation documented statistically in Section 6.

Importantly, the behaviour of the MAR parallels that observed in continental rift systems such as the East African Rift and oceanic arcs in the southern Indian Ocean, where alternating alignment with the two shear families is similarly expressed. This cross-regime consistency strengthens the inference that the modeled shear field captures a fundamental component of Earth's stress architecture rather than a phenomenon confined to any single tectonic environment.

In summary, the Mid-Atlantic Ridge demonstrates that the global shear organisation is not merely a relic preserved in ancient lithosphere, but an active geometric constraint influencing present-day plate-boundary evolution. Its alternating alignment with the two shear nets provides compelling evidence for long-wavelength planetary stress structure operating in concert with plate-tectonic divergence.

3.8 North American Arcuate Lake Chain

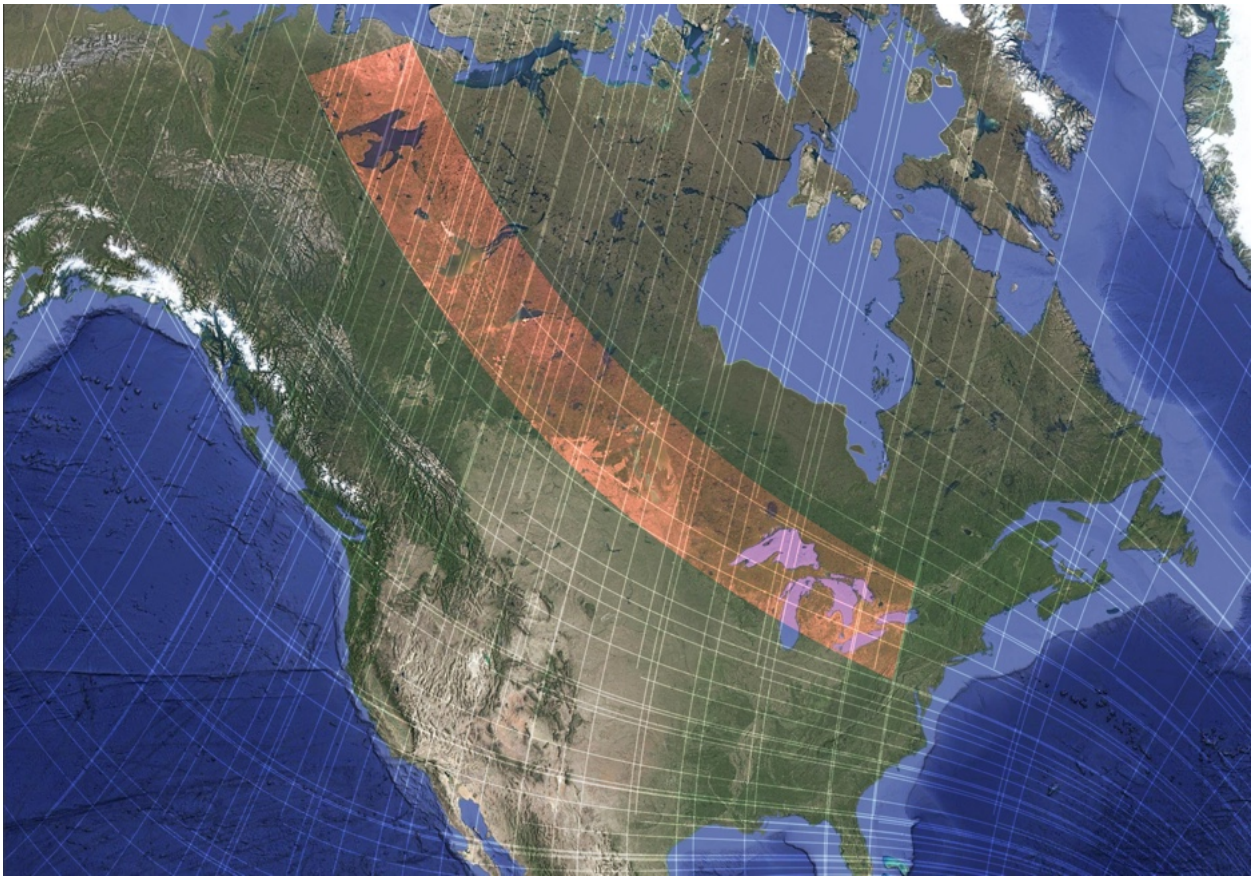

Figure 8: A continental-scale arc of large lakes across North America aligned with invariant shear contours.

Across central and eastern North America, a prominent northwest–southeast–trending arc of large lakes extends from the Canadian Shield through the Great Lakes region into the northeastern United States. This sequence includes Great Bear Lake, Great Slave Lake, Lake Winnipeg, Lake Superior, Lake Michigan, Lake Huron, Lake Erie, and Lake Ontario, together with numerous subsidiary basins distributed across the Shield. Conventional interpretations emphasise glacial excavation of pre-existing depressions and selective erosion along lithological boundaries. Although glaciation played a decisive role in deepening and shaping individual basins, it does not by itself account for the large-scale arcuate coherence, continuity across cratonic blocks, or the repeated correspondence between basin margins and deep structural fabrics.

Within the modeled global shear framework, the lake chain aligns closely with one of the dominant invariant-contour trajectories, with local modulation where the conjugate shear family intersects the belt. The resulting geometry is gently curvilinear rather than linear or rift-parallel, and persists across multiple tectonic provinces, including Archean cratons, Proterozoic orogens, and Phanerozoic sedimentary platforms. This cross-provincial continuity is consistent with control

by a long-wavelength stress organisation rather than by isolated, province-specific processes.

Lake Superior provides a diagnostic example. Its elongated, asymmetric basin follows a shear-aligned trajectory that intersects the Midcontinent Rift at a high angle. While the rift supplied pre-existing weakness and magmatic thickening, the ultimate basin geometry appears to reflect superposed shear organisation rather than pure extensional inheritance. Similar relationships are observed in Lakes Michigan and Huron, whose orientations deviate from local stratigraphic grain yet conform closely to the modeled shear net.

Further north, the large arcuate basins of Great Bear and Great Slave lakes occupy a region of distributed shear convergence near the Fort Simpson Arc. In such settings, the modeled field predicts broad, low-relief subsidence zones that are preferentially reactivated under repeated loading and unloading. The continuity of lake orientation across the transition from stable craton to reworked Proterozoic belts supports a tectonic origin rooted in long-wavelength stress topology rather than isolated rifting events.

Glaciation acted as an efficient amplifying and revealing agent. Ice streams preferentially exploited shear-aligned structural weaknesses, deepening and widening preconditioned depressions while preserving their inherited curvature. Many basin margins coincide with bedrock lineaments, gravity anomalies, and seismic discontinuities that predate the last glacial maximum by hundreds of millions of years, reinforcing the interpretation of tectonic preconditioning.

Taken together, the North American arcuate lake chain can be understood as a surface expression of a persistent, continent-scale shear organisation that has been episodically reactivated and geomorphically enhanced through glacial processes. Its coherence across geological provinces and scales is consistent with the long-wavelength spatial organisation quantified in Section 6, and supports the inference that the modeled shear framework exerts durable control on landscape evolution even in otherwise tectonically quiescent continental interiors.

3.9 United Kingdom Bimodal Morphology

Figure 9: Bimodal geomorphic orientation in the United Kingdom, particularly Scotland, aligned with both shear families.

The British–Irish Isles exhibit a strikingly bimodal geomorphological and structural fabric that has long been recognised but remains only partially explained within conventional tectonic narratives. Standard interpretations emphasise Caledonian and Variscan orogenesis, later reactivation during Atlantic rifting, and extensive modification by Pleistocene glaciation. While each of these processes contributed materially to the present-day landscape, they do not fully account for the persistent, large-scale directional coherence observed across disparate lithologies, ages, and tectonic provinces.

Within the modeled global shear framework, the United Kingdom occupies a region where Net 1 and Net 2 trajectories intersect at moderate angles, producing a dual shear fabric that is clearly expressed in topography, drainage orientation, and bedrock structure. This bimodality is especially evident in Scotland, where major lineaments, fjord systems, loch orientations, and mountain ranges alternate between alignments parallel to each shear family. The Highlands, Grampians, and Northern Isles together preserve a directional memory that transcends individual orogenic episodes and subsequent phases of tectonic reactivation.

Scotland provides the clearest expression of this geometry owing to limited sedimentary cover

and extensive glacial stripping, which preferentially excavated along shear-aligned weakness zones. The resulting landscape functions as a natural strain recorder, revealing the orientation of mechanically favoured planes. Notably, many glacial valleys and sea lochs exploit structures oblique to known Caledonian thrust trends yet closely parallel to the modeled shear trajectories, indicating reactivation under later stress regimes rather than simple inheritance from early Palaeozoic deformation.

England and Wales, although more subdued topographically, preserve the same dual orientation in river networks, escarpments, and basin margins. The Pennine spine, the Welsh uplands, and the structural grain of southern England collectively reflect alternating shear control, even where post-Mesozoic tectonic activity has been limited. Comparable behaviour is observed in Ireland, where major basins, coastal embayments, and regional lineament systems align with the same two dominant shear directions.

This bimodal expression implies that the lithosphere beneath the British–Irish Isles has repeatedly experienced stress fields consistent with the global shear organisation, leading to cumulative reinforcement of specific orientations through multiple tectonic and climatic cycles. Rather than being overprinted or erased, earlier structures were selectively reactivated when favourably oriented relative to the imposed shear geometry, producing the observed persistence of landscape-scale anisotropy.

In this interpretation, glaciation acted primarily as an amplifying and revealing agent. Ice flow preferentially followed mechanically weakened, shear-aligned pathways, enhancing relief along these orientations without dictating them. The strong correspondence between shear trajectories and geomorphology therefore reflects tectonic preconditioning expressed through repeated erosional reworking—behaviour consistent with the scale-persistent spatial organisation demonstrated quantitatively in Section 6.

In summary, the United Kingdom and Ireland represent a mid-latitude example of distributed bimodal shear expression, where neither shear family dominates completely. The resulting dual-oriented morphology provides compelling evidence that long-wavelength, globally coherent stress organisation can exert durable control over landscape evolution even in regions that are tectonically quiescent in the recent geological past.

3.10 East African Rift System

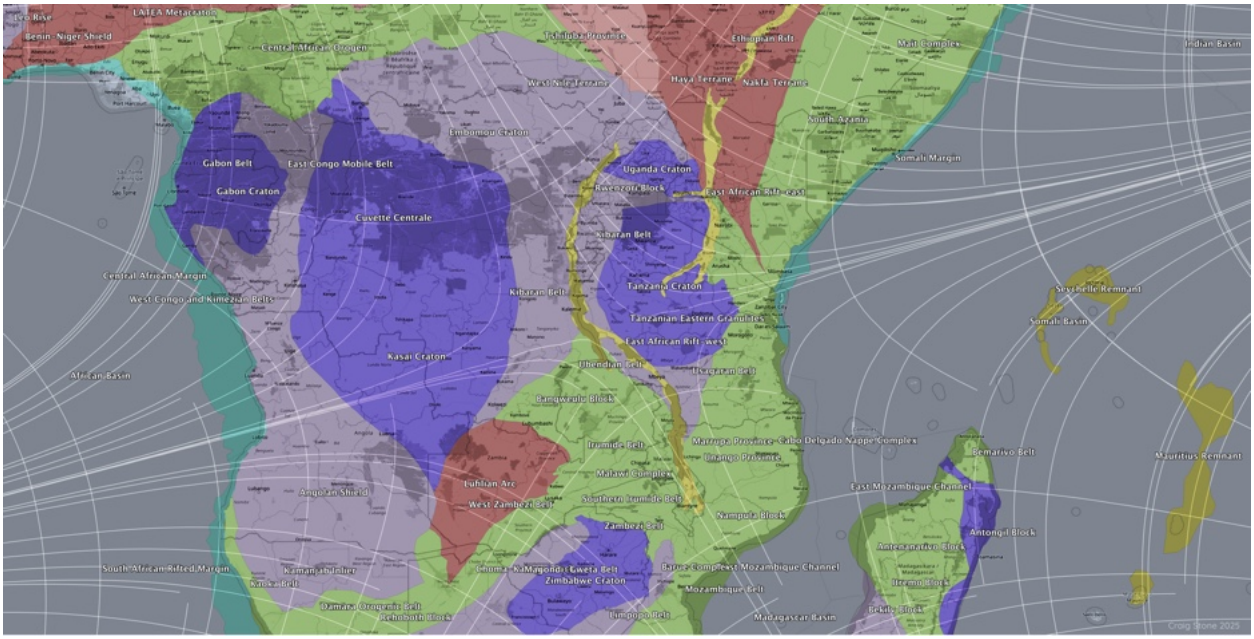

Figure 10: Double-arc geometry of the western East African Rift coincident with convergence of Net 1 and Net 2 near 14°S, 31°E.

The East African Rift System (EARS) has traditionally been interpreted as a classic example of continental rifting driven by mantle upwelling, lithospheric thinning, and plate-boundary reorganisation. This framework explains the overall extensional regime, magmatism, and basin development, but it does not fully account for the pronounced arcuate geometry of the system, nor for the existence of two partially overlapping rift branches that curve coherently across multiple tectonic provinces.

Within the modeled global shear framework, the EARS occupies a region of marked convergence between Net 1 and Net 2 trajectories centred near approximately 14°S, 31°E. This location coincides closely with the transition between the eastern and western rift branches, where deformation shifts from distributed extension to more strongly focused rifting and volcanism. The resulting geometry naturally favours the development of paired arcuate structures rather than a single linear rift corridor.

The western branch traces a smooth arc that aligns closely with one of the dominant shear families, whereas the eastern branch exhibits alternating alignment between the two nets. This dual behaviour mirrors the broader bimodal stress configuration predicted by the model and provides a geometric explanation for the long-recognised asymmetry between the branches. Rather than representing independent or successive rifting events, the paired arcs can be interpreted as complementary expressions of the same imposed long-wavelength stress organisation acting on lithosphere with variable rheology and thermal state.

Zones of elevated seismicity and active volcanism cluster preferentially within regions of shear convergence and curvature transition, where the modeled field predicts enhanced strain localisation and rotational stress gradients. These conditions are favourable for magma ascent, dyke emplacement, and fault reactivation, and the spatial association persists across both Precambrian cratons and younger mobile belts. This behaviour underscores the independence of the pattern from local lithologic control and supports interpretation in terms of a guiding stress topology.

The longevity of the EARS further reinforces this view. Episodes of extension and magmatism have recurred intermittently since at least the Paleogene, yet the large-scale curvature and branch geometry have remained remarkably stable. Such persistence is consistent with episodic reactivation of an inherited, shear-guided lithospheric architecture rather than with transient plume-driven extension acting in isolation.

In this interpretation, mantle upwelling and thermomechanical weakening act as facilitators that enable deformation to exploit mechanically favourable pathways established by the global shear organisation. The East African Rift thus emerges as a continental-scale analogue to other double-arc and curvature-stabilised systems documented in this study, and its behaviour is consistent with the scale-persistent spatial organisation quantified in Section 6.

3.11 Greenland, Hudson Bay, and the Nastapoka Arc

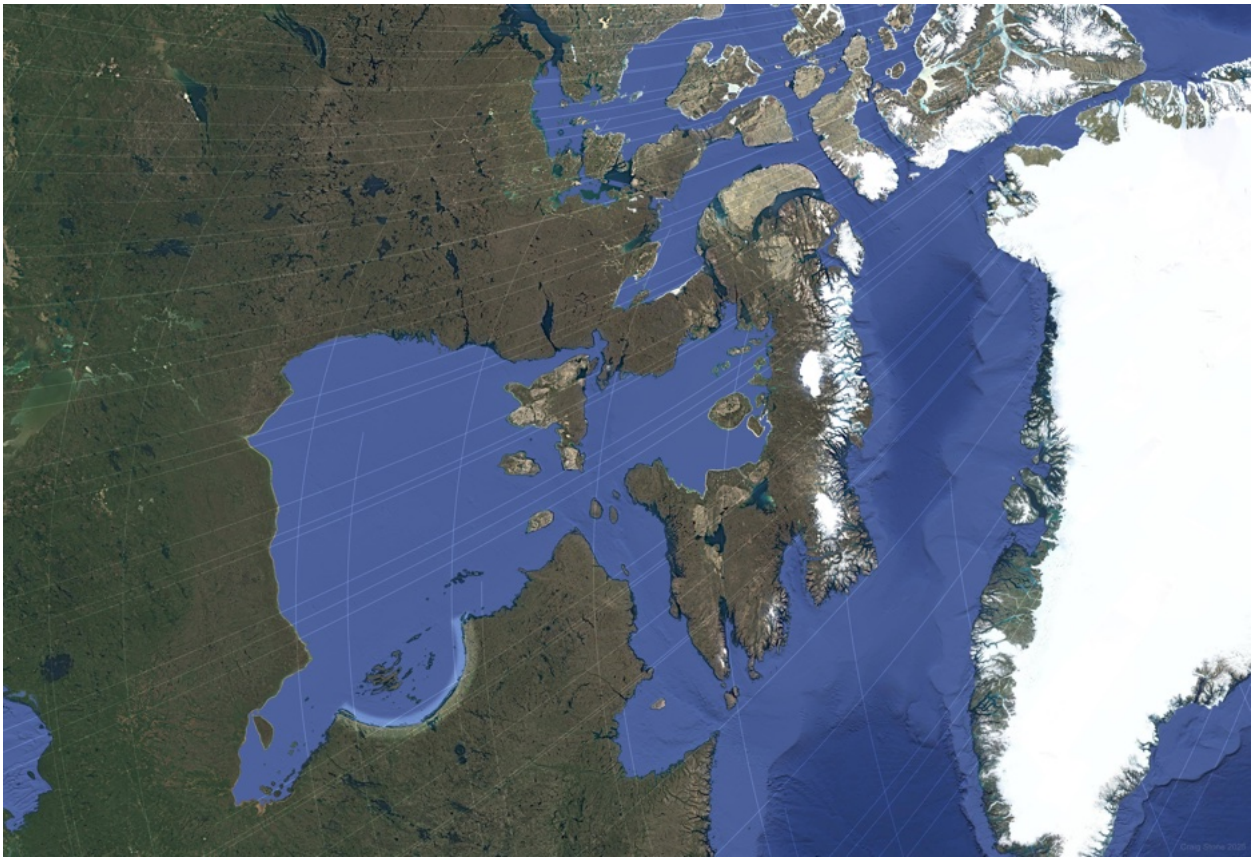

Figure 11: Greenland and Hudson Bay in polar stereographic projection showing bimodal agreement with shear nets and the arcuate Nastapoka structure.

High-latitude regions provide a stringent test of global stress-geometry models because projection artefacts are minimised in polar views and because cratonic lithosphere dominates over young plate-boundary deformation. When examined in polar stereographic and orthographic projections, Greenland, Hudson Bay, and the Nastapoka Arc exhibit some of the clearest and least ambiguous expressions of the modeled global shear framework identified in this study.

Greenland displays a pronounced bimodal structural and geomorphic fabric that aligns closely with both Net 1 and Net 2 trajectories. Fjord systems, coastal embayments, and interior lineaments alternate systematically between the two shear orientations, and this pattern persists even beneath extensive ice cover, as revealed by subglacial topography and bedrock structure. The coherence of this bimodality across Archean cratons and Proterozoic mobile belts suggests long-term preservation of shear-aligned weakness zones embedded within a persistent, long-wavelength stress organisation.

Hudson Bay occupies an especially significant position within the modeled field. Its broad, shallow, and weakly polygonal basin coincides with a region of shear convergence and minimal differential stress, consistent with an invariant or low-strain node in the global shear topology. Such

locations are predisposed to long-term subsidence, thermal relaxation, or crustal thinning without strong directional deformation, providing a natural geometric explanation for the stability of the basin through repeated cycles of glaciation, isostatic rebound, and regional tectonic quiescence.

The Nastapoka Arc, forming the southeastern margin of Hudson Bay, represents one of the most geometrically precise large-scale arcuate structures preserved in continental crust. Its curvature, continuity, and persistence across multiple geological provinces closely mirror nearby invariant shear contours. While impact-related origins have been proposed historically, the absence of unequivocal shock features, combined with the arc's conformity to the broader continental stress geometry, supports interpretation as a shear-guided curvature feature that has been selectively exposed and sharpened by glacial erosion rather than generated by it.

Importantly, the Greenland–Hudson Bay–Nastapoka system mirrors other arcuate and curvature-stabilised features documented in this study—including the Himalayan Arc, the Banda Arc, and the southeastern North American sediment belt—each located within regions where the modeled shear field predicts stable, low-variance stress configurations across multiple spatial scales. The recurrence of this behaviour across hemispheres and tectonic contexts strengthens the inference that these features are expressions of a persistent, planet-scale stress organisation rather than independent coincidences.

In this interpretation, glaciation acts primarily as a revealing and amplifying agent, preferentially eroding along mechanically weakened, shear-aligned zones and enhancing the visibility of inherited curvature. The exceptional clarity of these Arctic examples reflects the combined effects of cratonic rigidity, limited sedimentary cover, and repeated erosional stripping, which together preserve a high-fidelity record of the underlying shear topology—behaviour consistent with the scale-persistent spatial organisation quantified in Section 6.

3.12 Northwestern Canada and the Fort Simpson Arc

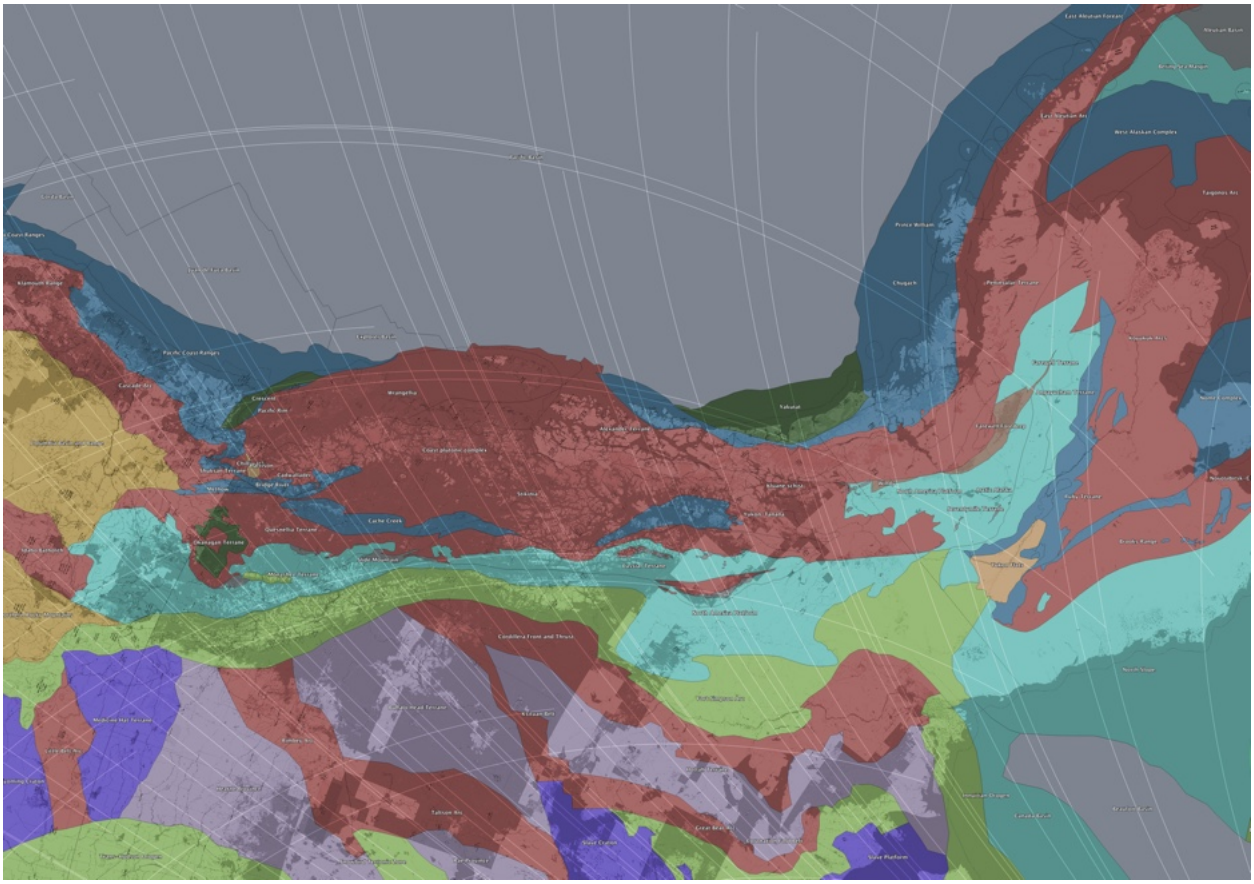

Figure 12: Northwestern Canada showing multiple agreements with shear nets, including the Fort Simpson Arc and transition from the Coast Plutonic Complex to the East Aleutian Arc.

The Fort Simpson Arc anomaly (FSA) of northwestern Canada has traditionally been interpreted as an Early Proterozoic magmatic arc, based on its curvilinear aeromagnetic signature, associated positive gravity anomalies, and U–Pb zircon ages clustering near ∼1.85 Ga from granitoid basement exposures. This interpretation, while well supported by geochronological and petrological evidence, encounters several persistent geometric and tectonic ambiguities that warrant re-examination in light of the global shear-net framework developed here.

Previous syntheses note that the Fort Simpson anomaly is not a simple linear feature, but instead broadens and curves westward into large elliptical magnetic highs near Great Bear Lake, among the most extensive aeromagnetic features in North America. Even within conventional interpretations, these western highs are acknowledged as potentially distinct basement elements that appear unified only through filtered geophysical datasets. Moreover, the Fort Simpson domain exhibits a long history of reactivation, influencing later extensional basins, dyke swarms, hydrothermal systems, and lithospheric segmentation over a time span exceeding one billion years.

When examined in polar and Arctic projections, the Fort Simpson Arc displays a close geometric

correspondence with one of the principal branches of the modeled global shear net. In particular, the curvature, bifurcation, and apparent bimodality of the Fort Simpson structure coincide with zones of net convergence and rotation in the shear trajectories. This correspondence is independent of stratigraphic boundaries, terrane affinities, or magmatic age constraints, suggesting a kinematic control that predates and outlasts any single tectono-magmatic episode.

Within this framework, Early Proterozoic arc magmatism is reinterpreted not as the origin of the Fort Simpson structure, but as one expression of a pre-existing lithospheric shear corridor. Such corridors are expected to localize mantle upwelling, magma ascent, and crustal underplating during periods of favorable stress orientation, while remaining mechanically weak and prone to reactivation under subsequent stress regimes. The coincidence of the Fort Simpson anomaly with positive gravity signatures is consistent with shear-focused lower-crustal densification or mafic underplating, rather than requiring a uniquely arc-related mechanism.

This reinterpretation resolves several longstanding difficulties associated with an arc-only model. The pronounced curvature and elliptical geometry of the Fort Simpson anomaly, its apparent continuity despite internal geological heterogeneity, and its repeated reactivation through Proterozoic and Phanerozoic time are all natural consequences of long-lived lithospheric shear structures, but are atypical of transient subduction-related arcs. Importantly, this perspective does not negate the arc-related geochemical and geochronological evidence documented in earlier studies; rather, it reframes arc magmatism as a secondary response to an inherited stress architecture.

In this view, the Fort Simpson Arc anomaly represents a lithospheric-scale shear feature that has acted as a persistent organizer of deformation and magmatism since at least the Paleoproterozoic. Its alignment with the global shear net supports the broader hypothesis that certain first-order continental geological features are governed by planet-scale kinematic patterns associated with large-amplitude true polar wander, rather than by isolated plate-boundary processes alone.

3.13 Arctic Polar Projection: Coherence of Shear Trajectories with Circum-Arctic Geological Provinces

Figures 13 and 14 present the modeled shear trajectories projected in an Arctic polar stereographic view and compared against independently mapped geological provinces and surface morphology. In this geometry, the large-scale structure of the shear field becomes especially transparent: trajectories organize into smooth, continuous arcs that radiate and spiral coherently around the polar region, intersecting the circum-Arctic margins at consistent and repeatable angles.

In Figure 13, the shear trajectories are overlaid on a global tectonic and terrane compilation. A striking correspondence is observed between the modeled flow lines and the boundaries, elongation axes, and curvature of major Arctic geological provinces, including cratonic margins, accreted terranes, sedimentary basins, and orogenic belts. Notably, several major province boundaries appear to track the shear trajectories over distances of thousands of kilometers, despite spanning lithologies and tectonic histories that are traditionally treated as unrelated. This coherence extends across

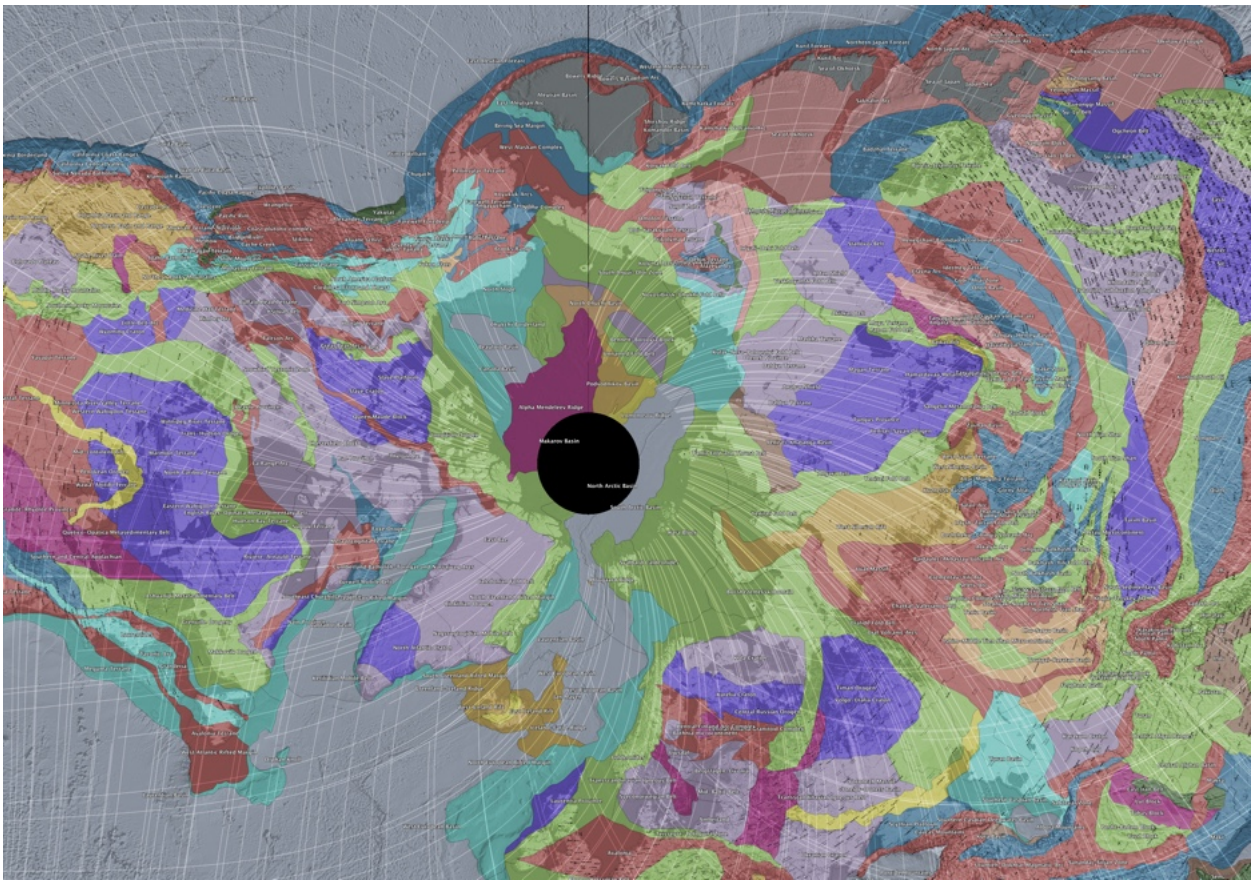

Figure 13: Arctic polar projection showing analytically derived shear trajectories overlaid on a global tectonic and geological province compilation. The shear lines exhibit strong geometric correspondence with the curvature, orientation, and boundaries of major circum-Arctic geological provinces across North America, Greenland, and Eurasia.

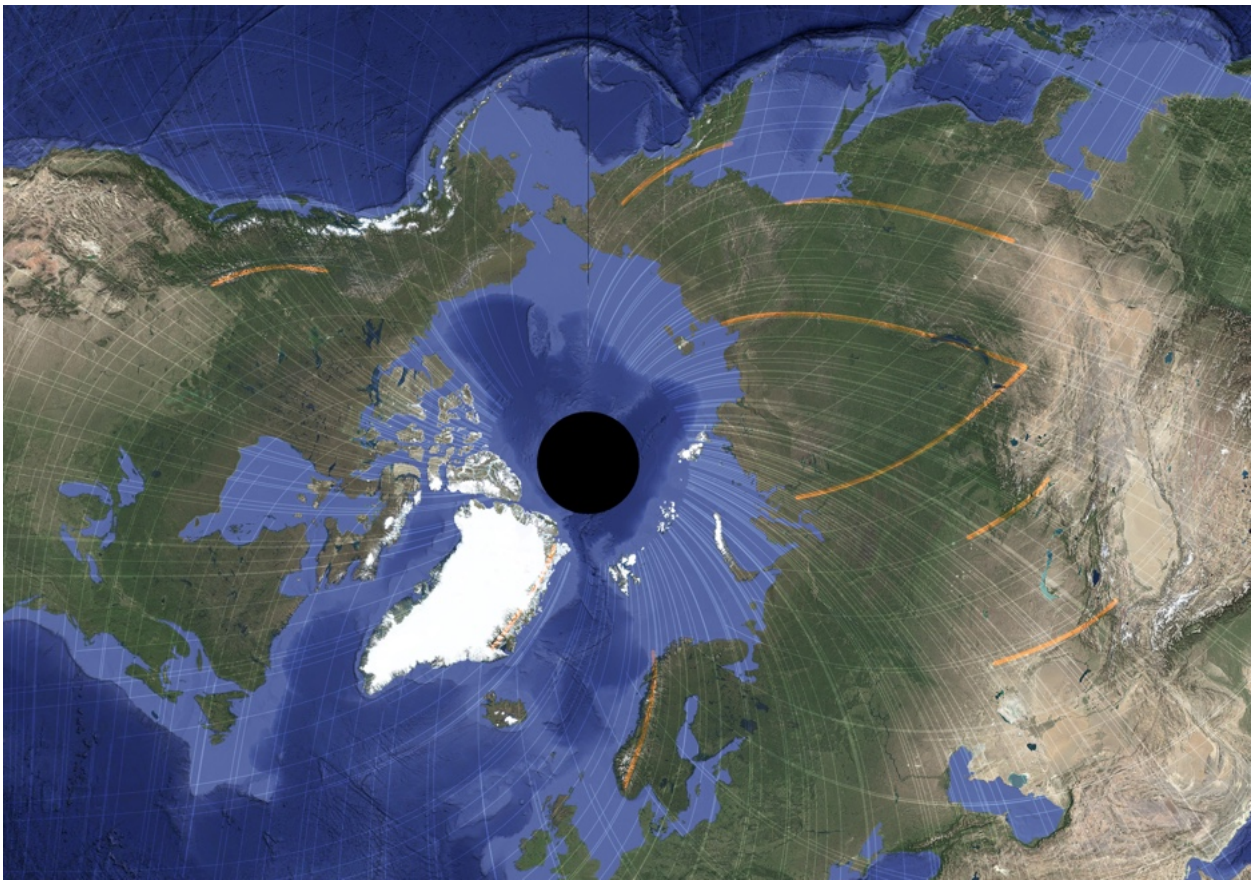

Figure 14: Arctic polar projection of shear trajectories over satellite imagery and bathymetry. Large-scale coastal arcs, continental shelf edges, submarine ridges, and basin margins frequently align with the modeled shear field, highlighting coherence across both continental and oceanic domains.

North America, Greenland, Eurasia, and the Barents–Kara sector, suggesting that the alignment is not a localized artifact but a basin-scale phenomenon.

Figure 14 shows the same shear trajectories superimposed on satellite imagery and bathymetry. Here, the correspondence extends beyond mapped tectonic units to geomorphic expression: continental shelf edges, submarine ridges, basin margins, and large-scale sedimentary curvature frequently parallel the modeled shear lines. Particularly along the Eurasian Arctic margin and the North Atlantic–Arctic transition, arcuate bathymetric and coastal features follow the predicted shear geometry with minimal deviation. The persistence of this alignment across both exposed continental crust and submerged oceanic domains indicates that the signal is not confined to a single depositional or tectonic regime.

Taken together, these polar views provide one of the clearest demonstrations in the study of long-wavelength geometric congruence between the analytically derived shear field and Earth's surface structure. The Arctic is unique in that it aggregates multiple plates, terranes, and basin systems around a common geometric focus, reducing visual ambiguity and emphasizing global-scale organization. The coherence observed here is difficult to reconcile with purely local or plate-specific processes alone, and instead supports the interpretation that a planet-scale stress topology—compatible with whole-Earth reorientation or true polar wander–like kinematics—has acted as a persistent organizing influence on Arctic tectonic and sedimentary architecture.

3.14 Mid- to High-Latitude Glacial Morphology and Shear-Guided Landscape Expression

Across numerous mid- and high-latitude regions, glacially sculpted terrains exhibit recurring directional coherence that aligns with the modeled global shear framework. These expressions occur in settings ranging from formerly glaciated continental interiors to high-relief fjord systems and cratonic margins, where Pleistocene and earlier glacial activity has repeatedly interacted with inherited structural anisotropy.

In many such regions, valley networks, fjord orientations, drumlin fields, and basin alignments display systematic alternation between the two modeled shear families, or preferential occupation of invariant-contour domains. This behaviour is observed in Scandinavia, the Canadian Shield, Greenland, coastal Patagonia, and segments of the Scottish Highlands, where glacial erosion has preferentially exploited shear-aligned weakness zones and curvature-stable domains.

These relationships are not readily explained by ice-flow dynamics alone. While ice-sheet geometry and basal processes strongly influence erosion patterns, they do not by themselves account for the persistence of large-radius curvature, repeated directional bimodality, or coherence across lithologically and tectonically contrasting terranes. Instead, the observed morphology is more consistent with selective enhancement of pre-existing, shear-guided structural fabrics through repeated cycles of glacial occupation and unloading.

Invariant-contour regions in particular tend to coincide with broad, low-strain basins and gen-

tly curving depressions that act as long-term sediment traps or loci of glacial lake development. Conversely, shear-trajectory corridors correspond to linear to curvilinear zones of enhanced incision, fjord development, and valley deepening, where stress-aligned structures provide mechanically favourable pathways for focused erosion.

This behaviour parallels that documented in the North American arcuate lake chain and in parts of Greenland and Scandinavia, where landscape anisotropy and curvature stability persist across multiple glacial cycles. The coherence of these relationships across continents and hemispheres supports interpretation of glacial morphology as an amplifying and revealing agent acting upon a longer-lived, planet-scale shear organisation rather than as an independent generator of curvature.

Taken together, these glacially expressed examples reinforce a broader pattern evident throughout the case studies: regions of persistent curvature, directional bimodality, and organised anisotropy tend to occur where the modeled field predicts stable stress geometry across scales. This behaviour is consistent with the statistically significant spatial organisation of misfit demonstrated in Section 6, further linking geomorphic expression to the same long-wavelength stress topology inferred from the stress-orientation analyses.

3.15 Ocean-Basin Curvature, Transform Systems, and Shear-Conditioned Segmentation

Beyond the specific examples discussed above, large portions of the global ocean floor exhibit recurring patterns of curvature, segmentation, and transform-fault alignment that are consistent with the modeled global shear framework. These expressions occur across multiple spreading systems and age provinces, including the South Atlantic, southwest Indian Ocean, equatorial Atlantic, and sectors of the Pacific basin.

In many of these regions, ridge-axis orientation, transform offsets, and fracture-zone geometries display systematic alternation between relationships parallel and orthogonal to the two modeled shear families. Ridge segments commonly rotate gradually along strike to maintain approximate orthogonality to the locally dominant shear trajectory, while major transforms preferentially align tangentially to the complementary net. This behaviour parallels that documented along the Mid-Atlantic Ridge but is repeated independently across widely separated plate-boundary environments.

Curvature in abyssal-plain fabrics and gravity-lineation networks further reinforces this interpretation. Instead of forming purely rectilinear fracture-zone patterns, many basins exhibit smooth, long-radius deflections whose geometry corresponds closely to invariant-contour domains in the modeled field. These curvature-stable regions coincide with areas of reduced differential shear, where long-term structural persistence and gradual reorientation of spreading fabrics are mechanically favoured.

Importantly, these oceanic expressions occur in settings largely free from continental inheritance, implying that their organisation emerges from interactions among mantle upwelling, plate divergence, and a persistent, long-wavelength stress topology rather than from pre-existing crustal fabric

alone. The repeated expression of shear-conditioned segmentation across independent spreading systems suggests a global organising influence rather than a series of unrelated regional coincidences.

The behaviour of these basins mirrors that seen in continental rift systems and arcuate mountain belts: segmentation, curvature stability, and directional alternation are expressed most clearly where the modeled field predicts strong shear gradients or convergence between the two nets. This cross-regime coherence supports interpretation of ocean-basin geometry as a dynamically evolving but shear-constrained expression of plate-boundary processes—consistent with the scale-persistent spatial organisation quantified in Section 6.

In summary, the global distribution of ridge curvature, transform alignment, and fracture-zone segmentation provides additional evidence that long-wavelength shear organisation exerts a durable geometric influence on the development of ocean-basin structure, operating in concert with, rather than in opposition to, the kinematic framework of plate tectonics.

3.16 Continental Margin Curvature, Passive-Margin Arcs, and Long-Wavelength Structural Guidance

Curved passive margins and continental-shelf arcs occur along several major continental outlines, including segments of the West African margin, northern South America, the western Australian shelf, and portions of the Antarctic and Arctic continental rims. These features are commonly attributed to variations in rift propagation, diachronous breakup, sediment loading, or flexural response to differential margin subsidence. While these processes play important roles in shaping margin architecture, they do not fully account for the persistence of smooth, large-radius curvature that transcends basin boundaries, stratigraphic transitions, and breakup histories.

When examined within the modeled global shear framework, many of these passive-margin arcs coincide with invariant-contour domains or trace trajectories that are parallel to one of the two shear families over distances of hundreds to thousands of kilometres. The congruence is particularly evident where margin curvature remains coherent across multiple rift episodes or across transitions from volcanic to non-volcanic margin segments, implying control by an organising stress geometry rather than by locally restricted breakup kinematics alone.

Several major continental shelves display gently sweeping curvature in shelf-edge trajectories and sediment-wedge outlines that follow shear-aligned pathways despite contrasts in sediment supply, basin subsidence history, or margin thermal state. In these cases, depositional architecture appears to have evolved within a preconditioned stress topology that favoured curvature stability and long-term geometric persistence, with stratigraphic processes amplifying rather than generating the underlying planform geometry.

Where transform-bounded margin segments intersect shear-trajectory corridors, margin curvature commonly tightens and structural segmentation becomes more pronounced. Conversely, margins coincident with invariant-contour regions exhibit broad, laterally continuous curvature with reduced structural partitioning. This systematic variability is consistent with deformation

and margin evolution being conditioned by spatial gradients in the long-wavelength shear field.

These relationships parallel behaviours documented in passive-margin sediment belts, arcuate rifts, and ocean-basin curvature systems elsewhere in this study. In each case, large-radius curvature and directional stability are most clearly expressed where the modeled field predicts low-variance or convergent shear geometry across scales. The recurrence of this pattern suggests that passive-margin curvature is not solely the by-product of breakup mechanics, but reflects interaction between plate separation, sedimentation, and a persistent, planet-scale stress organisation.

In this interpretation, passive margins act as long-term recorders of curvature-stable domains within the global shear topology. Their planform geometry evolves through the cumulative superposition of rifting, thermal subsidence, and sediment loading on an inherited geometric framework—behaviour consistent with the scale-persistent spatial organisation demonstrated quantitatively in Section 6.

3.17 Synthesis of Regional Expressions and Cross-Scale Geometric Consistency

The regional case studies presented above demonstrate that geometric correspondence between the modeled global shear field and Earth-surface structure is not confined to any single tectonic setting, lithospheric age, or geomorphic environment. Instead, similar relationships recur across passive margins, active plate boundaries, intracontinental domains, glacial landscapes, and ocean-basin systems. In each context, curvature stability, directional bimodality, and preferential alignment with one or both shear families are expressed most clearly where the modeled field predicts low-variance or convergent shear geometry across multiple spatial scales.

A common pattern emerges across these examples. Regions coincident with invariant-contour domains tend to host broad, curvature-stable basins, sedimentary arcs, and long-radius morphological sweeps, whereas shear-trajectory corridors preferentially localise incision, rifting, fault reactivation, ridge segmentation, and arcuate orogenic development. These behaviours are observed irrespective of whether deformation is currently active or episodic, suggesting that the underlying geometry functions as a persistent organising framework rather than a transient tectonic imprint.

Crucially, the qualitative correspondence documented in these regional systems mirrors the statistically resolvable spatial organisation of stress-orientation misfit demonstrated in Section 6. The same domains that exhibit coherent geological curvature frequently coincide with regions where misfit values cluster geographically across regional to near-hemispheric scales, even where the global mean alignment test remains non-diagnostic. This parallelism reinforces the interpretation that spatial organisation and geometric expression represent complementary manifestations of the same long-wavelength stress topology.

The recurrence of shear-guided curvature across independent tectonic provinces argues against coincidental alignment or purely anthropogenic mapping bias. Instead, the cross-scale and cross-regime coherence suggests that regional processes—such as plate convergence, rifting, glaciation, sedimentation, and mantle upwelling—operate within, and are subtly conditioned by, a broader,

planet-scale stress organisation. In this framework, local mechanisms provide the energetic forcing, while the long-wavelength shear geometry constrains the pathways through which deformation and landscape evolution are expressed.

Taken together, the regional observations and statistical results support the interpretation that the modeled global shear framework captures a persistent component of Earth's stress architecture. This component does not replace plate tectonics, but acts alongside it as an organising constraint that influences curvature development, structural reactivation, and spatial patterning of deformation from regional to near-hemispheric scales.

—

4 Global Plate Boundary Comparison

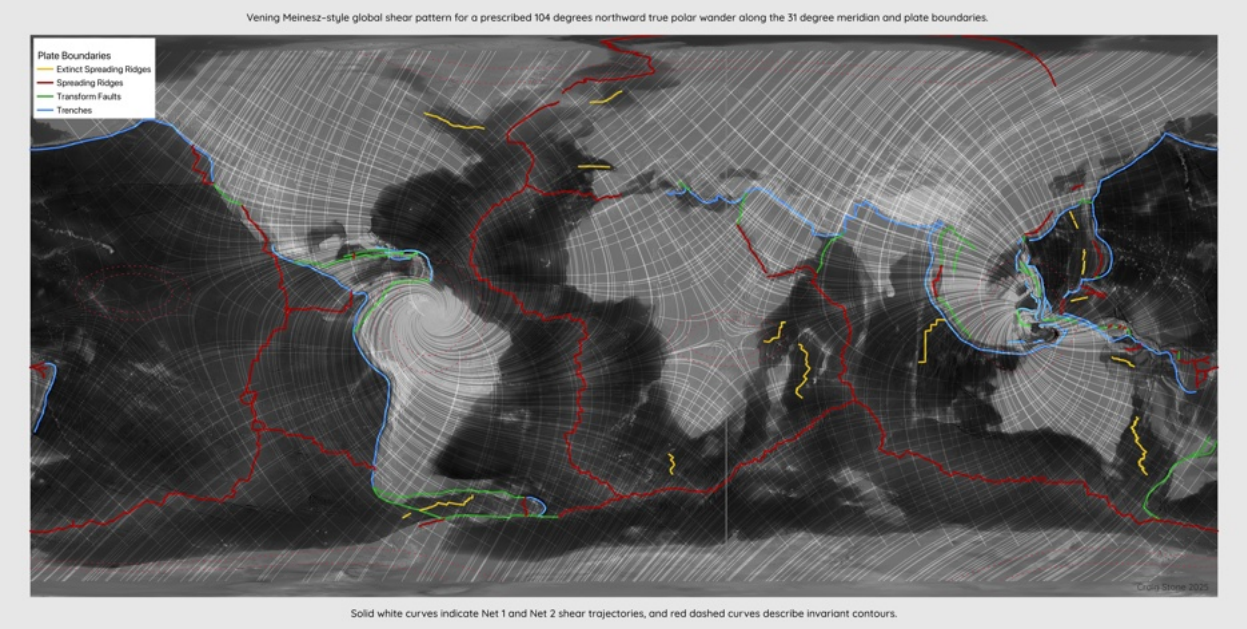

Figure 15: Comparison of the global shear model with modern plate boundaries. Strong geometric correspondence is observed across subduction arcs, transforms, and extinct ridges.

—

4.1 Comparative Behaviour of the Two Euler-Point Domains

The two Euler-point regions defined by the prescribed 104° northward true polar wander (TPW) along the 31°E meridian provide a natural experiment for evaluating how the modeled global shear field couples into contrasting tectonic environments (Figures 16 and 17). Although both regions exhibit clear correspondence with the Venning–Meinesz–style shear trajectories, the mode of conformance differs in ways that are geologically informative.

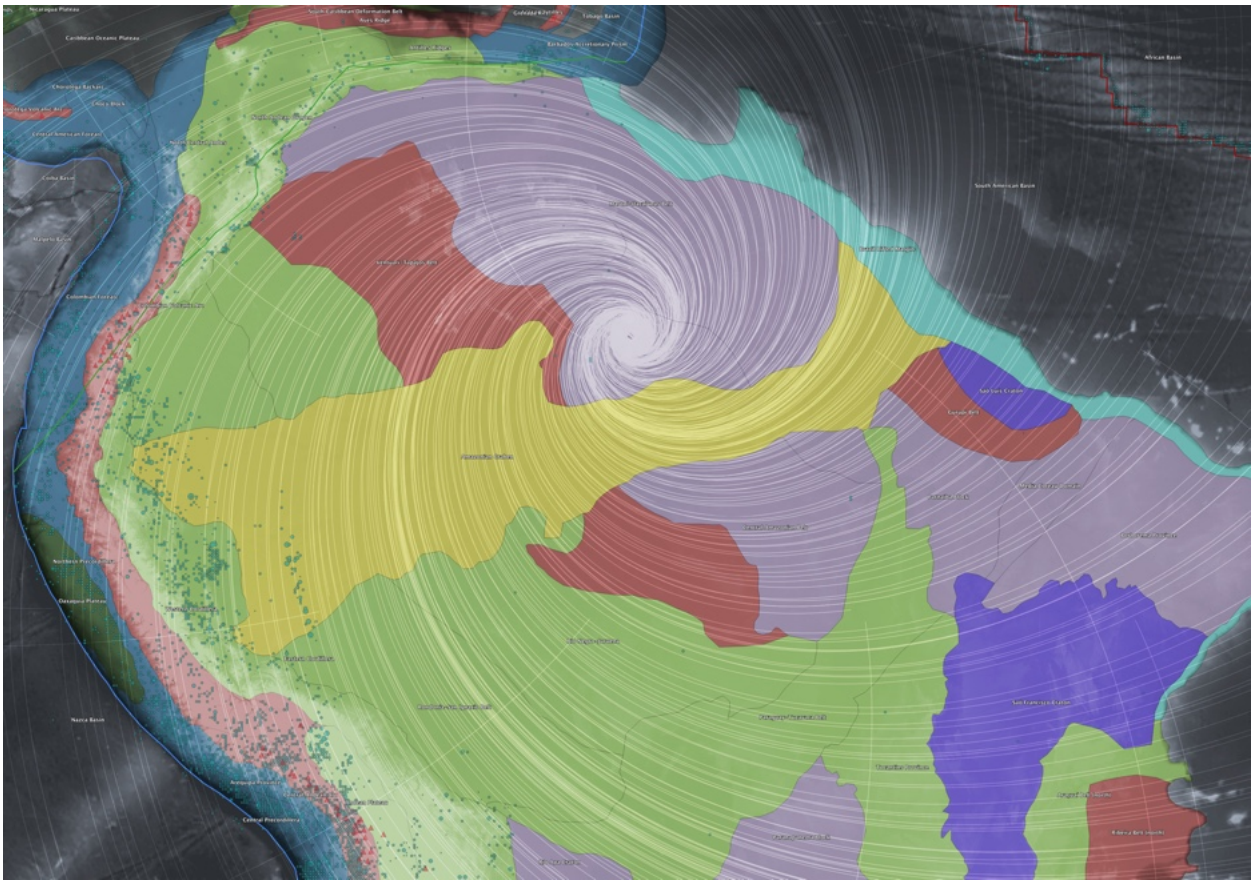

Figure 16: Western Euler-point domain showing the Venning–Meinesz–style shear trajectories overlaid on geological provinces, plate boundaries, earthquake epicenters (M≥4.5), and volcanic centers.

Western Euler Domain. The western Euler point, centered over northern South America and the Caribbean (Figure 16), exhibits the strongest and most internally consistent agreement between the shear model and observed geology. In this domain, shear trajectories form tightly wrapped spiral patterns that closely parallel Precambrian cratonic margins, mobile belts, and long-lived deformation zones. Major rift and transform boundaries, earthquake epicenter distributions (M≥4.5 over the past 25 years), and active to historically active volcanic centers preferentially align tangentially to the modeled shear flow.

Notably, both ancient tectonic fabrics and present-day deformation are organized predominantly along shear-parallel trajectories rather than orthogonal to them. This indicates that the shear field has acted as a persistent organizing stress over multiple tectonic cycles, repeatedly reactivating inherited lithospheric weaknesses in geometrically consistent orientations. The high degree of spatial coherence suggests that thick, mechanically heterogeneous continental lithosphere is capable of preserving and expressing low-order global stress modes over geological timescales.

Eastern Euler Domain. The eastern Euler point, located within the Indonesia–Sunda–Banda tectonic collage (Figure 17), presents a contrasting but equally informative expression of the same

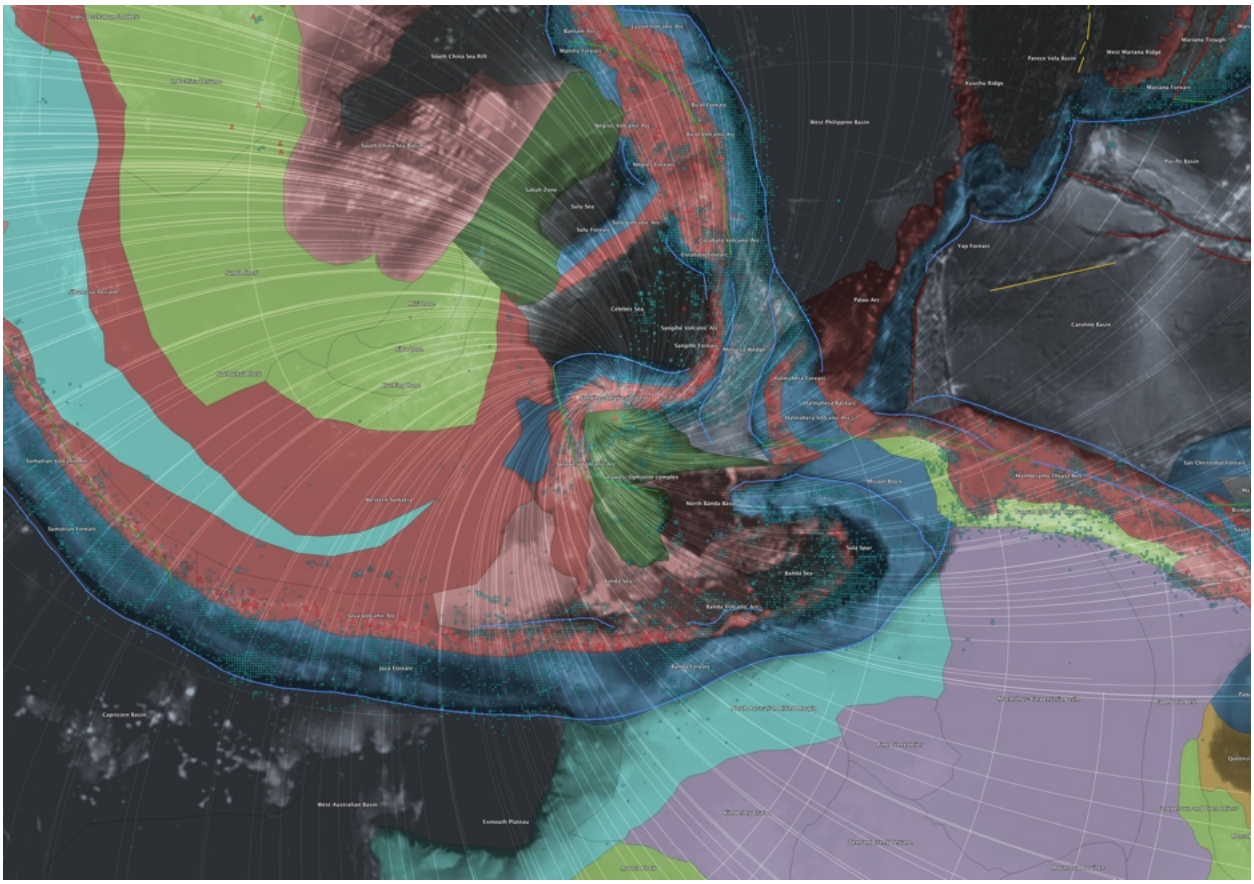

Figure 17: Eastern Euler-point domain (Indonesia–Sunda–Banda region) illustrating the relationship between modeled shear trajectories, arcuate subduction systems, seismicity, and active volcanism.

underlying shear structure. This region is characterized by rapid plate convergence, slab rollback, arc–continent collision, and distributed back-arc deformation. Despite this complexity, several robust correspondences with the shear model remain evident.

Major arcuate subduction systems, including the Banda and Sunda arcs, follow curvature consistent with modeled shear trajectories rather than simple relative plate-motion vectors. Earthquake hypocenters cluster along curved bands that mirror regions of maximum shear curvature, while active and historical volcanism preferentially occupies shear-aligned arc segments and convergence zones. In this domain, rift boundaries and basin margins exhibit mixed behavior: some conform closely to shear trajectories, whereas others are dominated by local slab geometry and rollback dynamics. This indicates that while the shear field does not dictate tectonic behavior outright, it acts as a geometric constraint within which subduction-driven processes organize themselves.

Comparative Implications. The contrasting behavior of the two Euler domains highlights several important implications. First, the persistence of recognizable shear conformance in both stable continental interiors and highly active subduction zones argues against coincidental alignment and

supports the presence of a global, low-order stress architecture capable of coupling into diverse lithospheric contexts. Second, regions underlain by thick, ancient lithosphere appear to preserve shear-imposed geometry more faithfully than rapidly recycling convergent margins, emphasizing the role of lithospheric memory in amplifying the visibility of the shear field.

Finally, the results indicate that the modeled shear structure should be understood not as a replacement for plate tectonics or mantle convection, but as a superimposed, long-wavelength stress mode that biases the orientation, curvature, and persistence of tectonic features generated by those processes. The systematic differences observed between the western and eastern Euler-point domains therefore strengthen the interpretation that the Venning–Meinesz–style global shear field represents a persistent and physically meaningful component of Earth's geodynamic system.

5 Scale-Dependent Spatial Autocorrelation of the Misfit Field

Across all examined spatial scales from 250 to 4000 km, the stress–misfit field exhibits statistically significant positive spatial autocorrelation. Moran's I decreases smoothly with increasing scale, from strong regional clustering to weaker but resolvable near-hemispheric organization. No abrupt loss of significance is observed.

This behavior indicates a finite but large correlation length for stress–misfit organization, extending well beyond individual plate boundaries or continental domains. The attenuation of Moran's I toward hemispheric scales marks a transition from regional clustering to low-degree global structure rather than a disappearance of spatial coherence.

5.1 Short-Wavelength Structure (250 km)

At a spatial scale of 250 km, the misfit field exhibits very strong positive spatial autocorrelation, with Moran's $I = 0.30$. The permutation null distribution has a mean effectively indistinguishable from zero and extremely small variance, yielding $p \ll 10^{-6}$. This result confirms that misfit values are highly clustered at short wavelengths and establishes a robust baseline of spatial coherence. At this scale, clustering is expected to reflect dominant local and regional tectonic controls, including fault systems, plate boundary geometry, and lithospheric heterogeneity.

5.2 Regional-Scale Coherence (500 km)

At 500 km, Moran's I remains large ($I = 0.23$) and highly significant under permutation testing ($p \ll 10^{-6}$). The reduction in Moran's I relative to 250 km reflects the expected decay of spatial correlation with distance, while the persistence of strong autocorrelation demonstrates that stress–misfit organization extends well beyond strictly local interactions. This scale corresponds to regional tectonic domains and large plate-boundary systems, indicating coherent stress structure at continental scales.

5.3 Long-Wavelength Organization (1000 km)

At a spatial scale of 1000 km, the misfit field continues to exhibit strong and statistically significant spatial autocorrelation, with Moran's $I = 0.17$ and $p \ll 10^{-6}$. The persistence of coherent structure at this wavelength exceeds typical crustal or single-orogen length scales and points to long-wavelength organization of the stress field. At this scale, purely local tectonic explanations become increasingly implausible, suggesting the influence of broader lithospheric or mantle-scale processes.

5.4 Planetary-Scale Persistence (2000 km)

At the largest scale examined, 2000 km, Moran's I remains positive and highly significant ($I = 0.11$, $p \ll 10^{-6}$). Although reduced in magnitude relative to shorter scales, the continued presence of statistically robust spatial autocorrelation at near-planetary wavelengths demonstrates that the stress–misfit field is organized over distances comparable to hemispheric dimensions. This result rules out explanations confined to regional tectonics alone and establishes a minimum correlation length of at least several thousand kilometers.

5.5 Upper-Bound Scale and Finite Correlation Length

Extending the spatial autocorrelation analysis to larger neighborhoods further clarifies the scale dependence of the stress–misfit field. At 3000 km, Moran's I remains positive and statistically robust ($I = 0.073$, $p \ll 10^{-6}$), indicating coherent organization at near-hemispheric wavelengths. At 4000 km, the magnitude of Moran's I is reduced but remains resolvably positive ($I = 0.050$, $p \ll 10^{-6}$), demonstrating that spatial structure persists even as neighborhood extents approach hemispheric scales.

Taken together, results from 250 to 4000 km reveal a smooth, monotonic decay of Moran's I with increasing spatial scale, without abrupt loss of significance. This behavior indicates a finite correlation length for the stress–misfit field, rather than unbounded or scale-invariant organization. The attenuation of spatial autocorrelation toward hemispheric extents marks the transition from regional clustering to low-degree global structure and represents the practical upper limit of interpretability for distance-based spatial autocorrelation metrics such as Moran's I.

5.6 Scale Dependence and Correlation Length

Taken together, the results reveal a smooth, monotonic decay of Moran's I with increasing spatial scale, without loss of statistical significance across the full range examined (250–3000 km). Such behavior is characteristic of a genuine spatial correlation process with a long correlation length, rather than noise or sampling artifacts. The absence of a sharp cutoff indicates that the organizing mechanism operates across multiple spatial regimes, from local tectonic structure to global-scale stress organization.

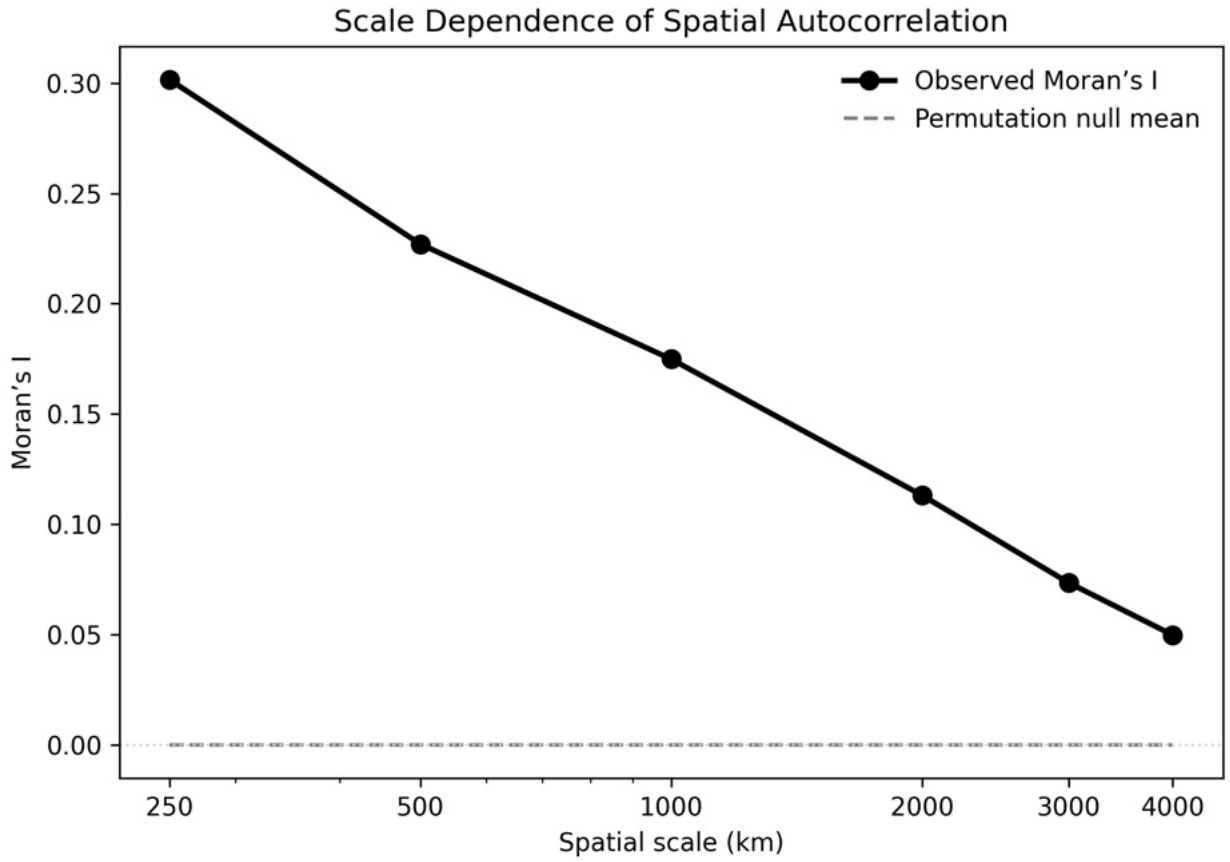

Figure 18: Scale dependence of spatial autocorrelation in the stress–misfit field. Global Moran's I values are shown as a function of characteristic spatial scale from 250 to 4000 km. Observed values (solid symbols) exhibit a smooth, monotonic decay with increasing scale while remaining statistically significant under permutation-based null testing at all examined wavelengths. The permutation null expectation (dashed line) is indistinguishable from zero, indicating that the observed trend reflects genuine spatial organization rather than random spatial structure. The attenuation of Moran's I toward hemispheric scales suggests a finite correlation length and marks the transition from regional clustering to low-degree global modes.

5.7 Global Alignment versus Spatial Structure

Two distinct statistical questions are addressed in this study: (1) whether the modeled shear field globally outperforms random Euler rotations in terms of mean angular misfit, and (2) whether the spatial distribution of misfit exhibits non-random geographic structure. These questions are evaluated using different null models and are not equivalent.

Global Euler-rotation null tests indicate that the mean misfit of the examined shear scenario does not differ significantly from that obtained under random rotations ($p = 0.636$). This result demonstrates that the model does not provide a globally optimal alignment in a scalar, average sense. Importantly, however, this test is insensitive to spatial organization and treats all locations as independent.

In contrast, permutation-based Moran's I analysis directly evaluates whether misfit values cluster spatially beyond random expectation. This analysis reveals statistically robust spatial autocorrelation from 250 km through at least 3000 km, demonstrating coherent geographic structure in the misfit field. The coexistence of a non-significant global mean test and highly significant spatial autocorrelation indicates that the model captures structured regional and planetary-scale patterns rather than uniformly minimizing misfit everywhere.

Accordingly, the primary empirical result of this study is not improved global alignment, but the detection of long-wavelength spatial organization in stress–misfit patterns that cannot be explained by random spatial processes.

5.8 Scenario Scope and Sensitivity Considerations

The shear field examined in this study corresponds to a single, untuned rotational scenario involving a $\sim$104° reorientation along the 31°E meridian. This configuration was selected as a representative test case motivated by prior ECDO-related considerations rather than as an optimized or best-fitting solution.

No attempt has been made here to exhaustively explore parameter space or to identify a globally optimal rotation. Instead, the objective is to assess whether a physically plausible, non-optimized long-wavelength shear scenario produces detectable and statistically robust spatial structure in stress–misfit patterns. The strong spatial autocorrelation observed across multiple length scales demonstrates that such structure is present even without parameter tuning.

Future work will extend this framework to systematic sensitivity analyses, including alternative rotation axes, magnitudes, and temporal scenarios. The permutation-based Moran's I methodology introduced here provides a quantitative basis for comparing such scenarios without relying on global mean misfit alone.

5.9 Relation to Paleomagnetic Constraints on True Polar Wander

Proposed true polar wander (TPW) scenarios are subject to constraints derived from paleomagnetic reconstructions, which typically limit long-term TPW amplitudes to tens of degrees over multimillion-year timescales (e.g., Steinberger & Torsvik, 2008). These constraints are primarily sensitive to time-averaged rotational behavior and are optimized to detect sustained, low-frequency reorientations of the solid Earth.

The present analysis does not attempt to reconstruct the timing, duration, or cumulative magnitude of any specific TPW event. Instead, it evaluates whether long-wavelength rotational shear scenarios leave a spatially coherent imprint on present-day stress orientations. As such, the results are compatible with both gradual and episodic reorientation models, including transient or non-steady processes that may not be fully captured by paleomagnetic averaging.

Accordingly, the spatial-statistical findings reported here should be interpreted as evidence for long-wavelength stress organization rather than as direct constraints on TPW kinematics. Integrating spatial stress analyses with paleomagnetic, geodynamic, and stratigraphic constraints represents a key direction for future interdisciplinary work.

5.10 Summary of Empirical Findings

The permutation-based spatial autocorrelation analysis demonstrates that the stress–misfit field is not spatially random at any examined scale. Instead, it exhibits strong and statistically robust geographic organization from local (250 km) through planetary (4000 km) wavelengths. These findings provide quantitative evidence for long-wavelength structure in the stress field and motivate interpretation in terms of global or mantle-coupled forcing mechanisms, which are explored in the Discussion.

6 Quantitative Evaluation of Spatial Stress–Shear Coherence

To assess whether the visually identified congruences between the modeled shear framework and geological geometry are statistically meaningful rather than coincidental, we computed regional Moran's I statistics across a global ensemble of geographic domains. For each region, spatial clustering of shear–misfit values was evaluated across multiple characteristic wavelengths (250, 500, 1000, 2000, 3000, and 4000 km). The baseline shear field derived from the prescribed 104°/31°E TPW scenario was compared against an ensemble of randomized control geometries generated from alternative Euler-pole configurations.

Across most regions, the baseline field exhibits systematically stronger positive spatial autocorrelation than the null ensemble, indicating that shear–misfit values are not randomly distributed but instead form coherent, spatially organized structures. Moreover, several regions display internally consistent wavelength trends or plateaus in Moran's I, suggesting that the stress–shear interaction operates most strongly within characteristic scale bands rather than uniformly across all

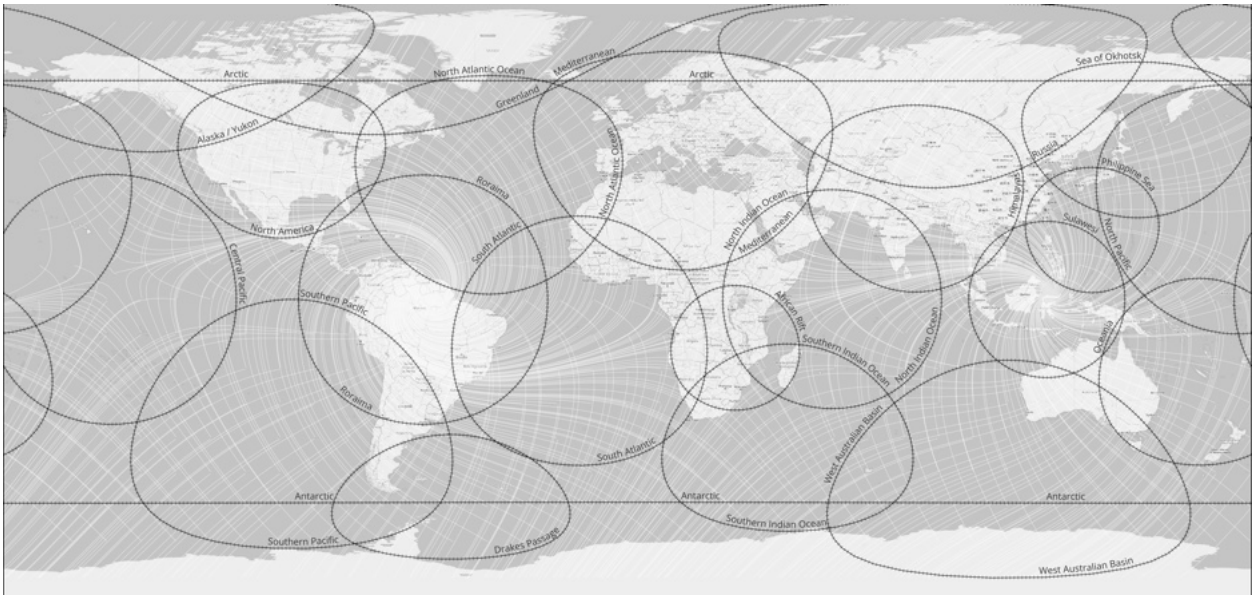

Figure 19: Geographic distribution of the sampled regions.

wavelengths. These findings are consistent with the hypothesis that the modeled shear framework reflects a physically meaningful, long-wavelength organizing geometry rather than a coincidental visual alignment. These quantitative outcomes extend and reinforce the qualitative congruence analyses developed in earlier sections of the paper.

6.1 Coherence–Clustering Relationships Across Scales

To further interrogate the nature of the observed spatial organization, we derived simple geometric shape descriptors from the wavelength–response curves and compared these with the magnitude of Moran's I excess relative to the null ensemble. This allows the coherence of the baseline result to be studied not only in terms of absolute clustering strength, but also in terms of how that clustering evolves across spatial scale.

The resulting structure–response relationships reveal that regions with smooth, internally consistent scale trajectories tend also to be those expressing the strongest positive departures from the randomized ensemble. Conversely, control regions lacking geological expression or clear shear–feature relationships typically exhibit noisy or unstable wavelength behavior. This pattern supports interpretation of the baseline shear geometry as a persistent organizing field that manifests differently across tectonic environments, but with repeatable statistical character.

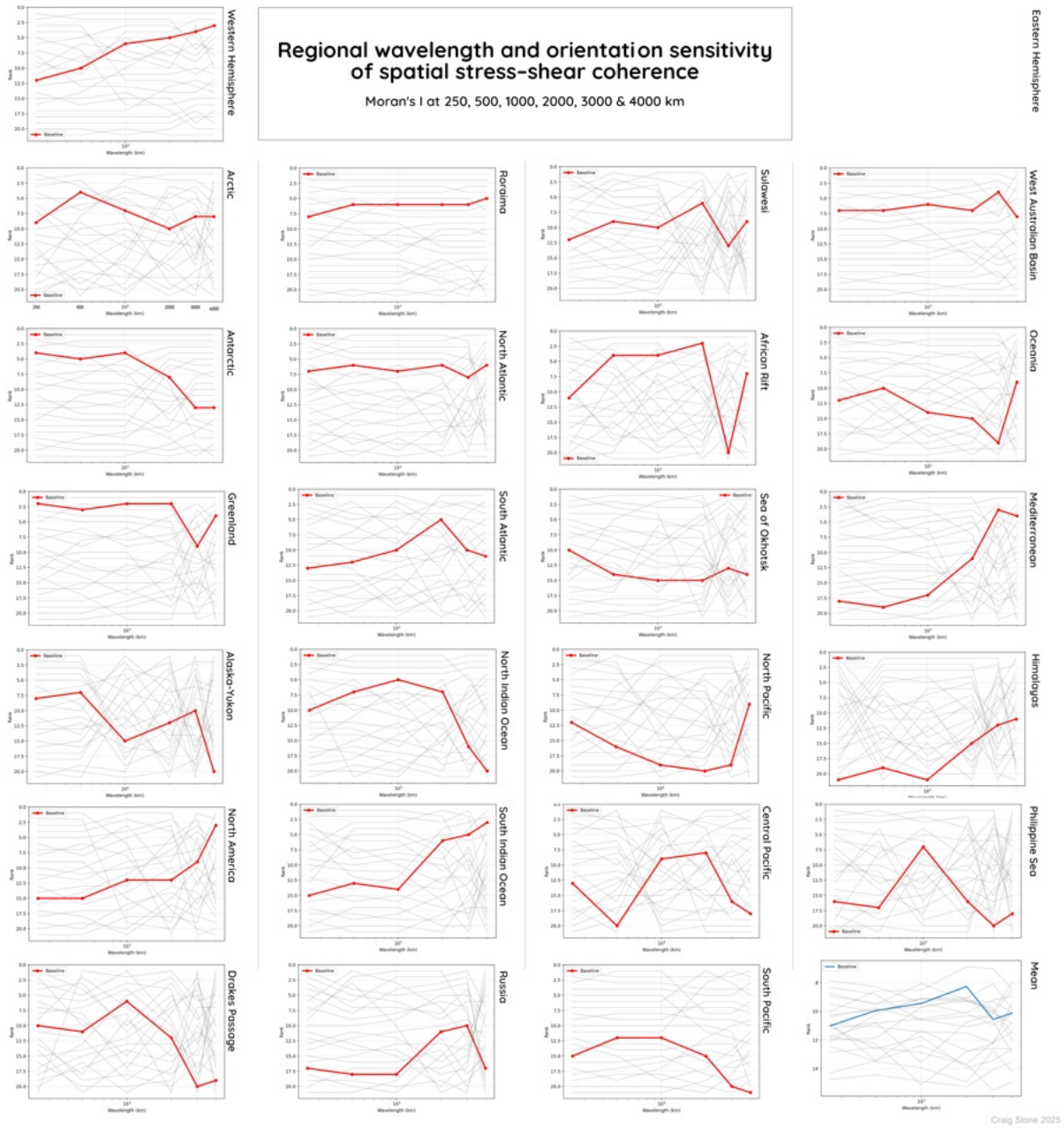

Figure 20: Regional wavelength–orientation sensitivity of spatial stress–shear coherence. For each region, Moran's I was evaluated at 250, 500, 1000, 2000, 3000, and 4000 km wavelengths. The red curve shows the baseline TPW-derived shear geometry; grey curves represent the randomized null shear ensembles. Regions exhibiting plateaued or monotonic trends in the baseline response indicate structured, scale-dependent spatial coherence rather than noise-like behavior.

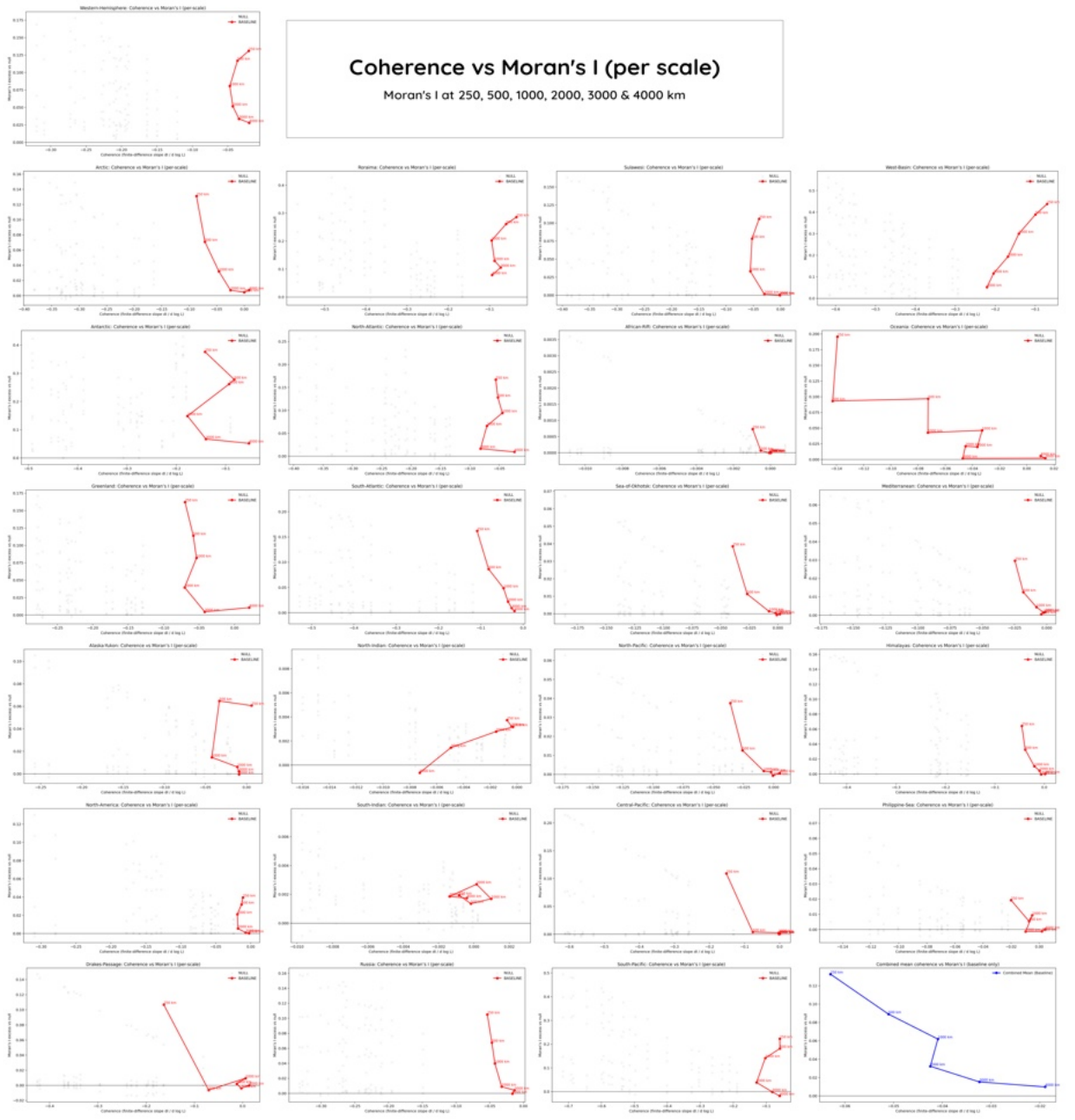

Figure 21: Coherence versus Moran's I (per–scale) across regions. Grey points represent the null ensemble; red curves trace the baseline TPW shear field for each wavelength step. The blue curve (lower right) shows the combined mean baseline trajectory relative to the null ensemble. Regions with smooth, structured trajectories show the strongest excess clustering, indicating non-random, scale-consistent spatial organization.

6.2 Implications

Taken together, the statistical outcomes demonstrate that the modeled shear framework is not merely visually compatible with geological curvature, but also exhibits quantifiable spatial organi-

zation across scales and regions. The recurring presence of structured wavelength responses and elevated spatial clustering in geologically expressive domains is consistent with a planetary-scale stress topology acting in concert with local tectonic and material processes, rather than an artifact of geometric overlay or chance alignment.

7 Discussion

7.1 Interpreting Spatial Organisation Without Global Mean Alignment

The results presented in this study demonstrate a consistent and statistically robust spatial organisation of stress–orientation misfit across regional to near-hemispheric scales, even though the modeled shear field does not outperform random Euler rotations in terms of global mean angular misfit. At first glance, this combination of outcomes may appear paradoxical. However, the distinction reflects two fundamentally different diagnostic questions.

Global mean alignment tests address whether a given model provides a lower aggregate misfit than a randomly oriented alternative when averaged across all observation sites. This perspective treats the lithosphere as a spatially uniform system in which improvement must be expressed globally and simultaneously. In contrast, the permutation-based Moran's I framework evaluates whether misfit values exhibit geographically coherent structure, independent of whether the global average is high or low. A model may therefore reveal meaningful long-wavelength organisation even when average alignment is not improved in a scalar sense.

The coexistence of non-diagnostic global alignment with strongly significant spatial organisation indicates that the modeled shear field captures geographically structured components of the stress system rather than acting as a universal predictor. In other words, the model does not describe *all* stress orientations everywhere, but it does appear to describe *where* systematic departures from randomness occur, and at what scales those departures are organised. This outcome is consistent with a hierarchical view of lithospheric deformation in which regional and plate-scale processes interact with a broader, long-wavelength stress topology rather than being entirely independent of it.

The new analyses introduced in Section 6 strengthen this interpretation by demonstrating that the same organisational behaviour persists smoothly across scale transitions, from regional to continental to near-hemispheric neighbourhoods, with monotonically decreasing Moran's I magnitude rather than abrupt scale breaks. This pattern is more consistent with a continuous, multi-scale organising field than with a patchwork of unrelated local processes.

7.2 A Planet-Scale Shear Topology as an Organising Framework

The combined statistical and geometric evidence suggests that Earth's surface deformation operates within a persistent, planet-scale shear topology compatible with whole-Earth reorientation–style

geometry. This topology does not imply a single causal mechanism acting uniformly through time, nor does it negate the role of plate-tectonic forces, mantle dynamics, or surface processes. Instead, it provides an organising framework within which these processes operate and through which their spatial expression is preferentially channelled.

In this interpretation, long-wavelength shear geometry biases the orientation and curvature of structures that form or reactivate under diverse tectonic regimes. Plate convergence, rifting, transform motion, glaciation, and sedimentation supply the energetic forcing, while the global shear field constrains the mechanically favourable pathways along which deformation evolves. The result is a persistent tendency toward curvature stability, directional bimodality, and preferential strain localisation in regions where the modeled field predicts low-variance or convergent shear geometry—patterns repeatedly observed in the regional case studies and reflected in the statistically organised misfit fields of Section 6.

This framework also clarifies why many of the most geometrically coherent arcuate systems cross major geological province boundaries, persist through multiple tectonic episodes, and occur in both actively deforming and tectonically quiescent regions. Rather than representing independent or coincidental outcomes, these features may share a common geometric conditioning imposed by the same long-wavelength stress organisation expressed at different times and under different boundary conditions.

7.3 Implications for Multi-Scale Lithospheric Behaviour

The persistence of spatial organisation across scales has implications for how lithospheric systems are conceptualised. Rather than being governed solely by discrete, locally bounded processes, deformation appears to reflect interaction between short-wavelength kinematics and long-wavelength geometric structure. This behaviour is analogous to other hierarchical systems in geophysics, in which regional processes express themselves within broader fields or boundary geometries that evolve on longer spatial and temporal scales.

Within this hierarchy, regions of invariant or low-differential shear function as loci of structural stability, basin development, or sediment accumulation, whereas shear-trajectory corridors act as mechanically favoured pathways for fault reactivation, rifting, or orogenic curvature. The cumulative effect through geological time is the reinforcement of specific geometric configurations, which become visible in both stress-orientation statistics and large-scale geomorphic and tectonic patterns.

The results therefore motivate further investigation of how planetary-scale stress organisation interacts with mantle convection, plate kinematics, and lithospheric rheology, and whether similar organising geometries may be detectable in other planetary bodies with preserved tectonic fabrics.

7.4 Limitations, Alternative Interpretations, and Methodological Considerations

Although the results presented here provide evidence for coherent spatial organisation in both geometric expression and stress–orientation misfit, several limitations and alternative interpretations must be acknowledged.

First, the modeled shear field represents a single prescribed true-polar-wander–like rotational geometry rather than a physically time-resolved dynamical model. The framework is therefore geometric rather than causal: it tests whether such a geometry produces an organising shear topology that is consistent with large-scale surface structure, but it does not specify the mechanism, timing, or frequency with which such geometries may arise in Earth history. Alternative rotational or reorientation scenarios may produce comparable or stronger spatial organisation, and systematic testing of parameter space remains an open line of investigation.

Second, the spatial-statistical analyses operate on contemporary stress-orientation observations that integrate multiple processes, including plate boundary forces, gravitational potential energy gradients, mantle flow, and local rheological heterogeneity. The presence of statistically significant spatial organisation does not imply that the modeled shear field is the dominant driver of the present-day stress system. Rather, it indicates that components of the stress field vary geographically in a manner consistent with the modeled topology. Other long-wavelength fields—such as those arising from lithospheric thickness contrasts or dynamic topography—may contribute to similar organisation and should be evaluated in parallel frameworks.

Third, qualitative geometric comparisons are inherently sensitive to visual bias and to the level of generalisation applied to geological features. To mitigate this risk, case-study interpretations emphasise cross-scale coherence, independence from local boundary conditions, and recurrence across disparate tectonic environments. Nonetheless, the possibility remains that some apparent correspondences arise from convergent rather than causally related processes. The integration of spatial-statistical results with geometric expression—particularly the scale-persistent behaviour demonstrated in Section 6—reduces, but does not eliminate, this ambiguity.

Fourth, the World Stress Map dataset is spatially heterogeneous, with denser coverage in populated and industrial regions and sparser coverage in oceanic and polar domains. Although the permutation-based framework preserves sampling geometry and misfit distribution, incomplete stress coverage may influence the apparent strength or continuity of spatial organisation in poorly sampled regions. Expanding stress datasets—especially in oceanic and high-latitude environments—will provide additional opportunities to test the robustness of the inferred organisation.

Finally, the interpretation of a persistent, planet-scale shear topology does not exclude alternative frameworks. Some aspects of the observed organisation could conceivably emerge from interactions among mantle convection patterns, long-term plate-boundary reorganisations, or inherited lithospheric anisotropy acting over multiple tectonic cycles. However, the cross-regime recurrence of curvature stability, directional bimodality, and scale-persistent spatial organisation argues that

these processes are more plausibly acting *within* an organising geometric framework rather than generating equivalent structure independently in multiple contexts.

These limitations motivate continued refinement of both the analytical geometry and the statistical testing strategy, along with comparative evaluation against alternative global-scale field hypotheses. The results introduced in Section 6 provide an initial demonstration that such refinement reveals coherent scale-transitional behaviour; future work should extend this approach to evaluate whether similar organisation arises under different rotational geometries or in time-evolving geodynamic simulations.

7.5 Mechanistic Pathways and Geodynamic Context

Although the present study focuses on geometric and statistical consistency rather than on prescribing a specific physical mechanism, the results have implications for how large-scale stress organisation may arise and interact with geodynamic processes. The persistence of spatial organisation across regional to near-hemispheric scales, together with the cross-regime recurrence of curvature-stabilised structures, suggests that the inferred shear topology is most plausibly associated with slowly varying, whole-lithosphere boundary conditions rather than with transient or purely local tectonic forcing.

One possible class of mechanisms involves long-wavelength rotational or reorientation geometries, including true-polar-wander–style motions or analogous whole-Earth reorientation effects acting over geological timescales. In such scenarios, the lithosphere experiences broad, quasi-rigid reconfiguration relative to the planetary inertia frame, giving rise to systematic shear trajectories comparable to those explored analytically in this study. Whether such motions are continuous, episodic, or superposed across multiple cycles remains an open question, but the resulting geometry provides a natural means of embedding persistent, low-variance stress structure within the lithosphere.

A second class of processes may involve coupling between lithospheric structure and mantle flow, in which large-scale convection patterns impose broad differential tractions that evolve more slowly than regional plate-boundary reorganisation. If such tractions are spatially coherent over thousands of kilometres, they could reinforce or modulate the same shear domains identified here, particularly where lithospheric heterogeneity or inherited fabrics promote selective strain localisation along mechanically favourable trajectories.

A third pathway concerns the cumulative effects of multi-episode reactivation. Even in the absence of a single dominant forcing mechanism, repeated deformation under partially aligned stress fields can progressively enhance the visibility of particular geometric configurations. Regions that begin as weakly conditioned may, through successive tectonic and geomorphic cycles, develop strongly expressed curvature or directional bimodality as pre-existing structures are preferentially reactivated and amplified. The scale-transitional continuity documented in Section 6 is consistent with such cumulative reinforcement.

These potential mechanisms are not mutually exclusive. Instead, they may operate in combination, with whole-Earth reorientation geometries establishing first-order shear topology, mantle flow modulating regional stress expressions, and episodic reactivation progressively sharpening curvature and anisotropy through time. The statistical and geometric evidence presented here therefore supports a view in which long-wavelength organisation arises from interaction between geometric boundary conditions and dynamical processes, rather than from any single deterministic cause.

Future work should focus on testing these pathways explicitly, including comparisons with time-evolving geodynamic simulations, rotational-history scenarios, and alternative global-field hypotheses. The coherent, scale-persistent behaviour revealed in Section 6 provides a quantitative target for such models: mechanisms capable of reproducing similar spatial organisation across scales would constitute strong candidates for the physical origin of the inferred shear topology.

7.6 Temporal Persistence, Reactivation Behaviour, and Geological Interpretation

The recurring alignment between arcuate geological features and the modeled shear framework across multiple tectonic episodes and geological ages raises important questions regarding temporal persistence and reactivation behaviour within the lithosphere. Many of the examples documented in this study—such as passive-margin arcs, intracontinental curvature belts, glacially sculpted landscapes, and long-lived basin systems—exhibit geometric continuity that spans successive cycles of loading, uplift, subsidence, erosion, and tectonic reorganisation. This persistence is more readily explained by reactivation of an inherited geometric architecture than by repeated independent generation of similar curvature in different epochs.

Within the proposed framework, invariant-contour domains and shear-trajectory corridors serve as long-term structural attractors. When regional or plate-scale processes impose renewed deformation, strain is preferentially accommodated along these preconditioned pathways, reinforcing existing curvature rather than creating new orientation patterns. Over geological time, such recurrent occupation leads to cumulative sharpening of curvature, directional bimodality, and anisotropic relief—even in regions that are presently tectonically subdued.

This behaviour is consistent with observations from cratonic interiors, where weak but persistent intraplate deformation localises along ancient structural corridors, as well as from passive margins and rift systems where apparently young tectonic fabrics overprint much older basement geometries while preserving large-radius planform curvature. The same principle applies to glacial terrains in which erosional processes selectively enhance shear-aligned depressions and valley networks without dictating their underlying geometry.

The statistical results introduced in Section 6 reinforce this interpretation by demonstrating that regions of coherent geometric expression coincide with areas in which misfit values exhibit persistent spatial organisation across scales. This correspondence implies that the present-day stress system continues to reflect, at least in part, the same long-wavelength structure that has

guided deformation and reactivation over extended geological intervals. In other words, the spatial organisation expressed in contemporary stress orientations may represent the current manifestation of a much older and repeatedly exploited shear topology.

From an interpretive perspective, this has two major implications. First, geological curvature and structural coherence should not be assumed to originate exclusively from the most recent tectonic event or process. Instead, such features may record the integrated effects of multiple reactivation phases operating within a stable geometric framework. Second, the presence of large-radius curvature, directional bimodality, or scale-consistent anisotropy may serve as indicators of underlying shear-trajectory or invariant-contour domains, providing a predictive guide for structural interpretation, basin analysis, and intraplate hazard assessment.

In this view, the lithosphere is not simply a passive archive of discrete tectonic episodes, but an actively reworked system in which long-wavelength geometric organisation persists across time and repeatedly conditions the spatial expression of deformation. The scale-transitional continuity documented in Section 6 suggests that this persistence is neither incidental nor localised, but reflects a durable component of Earth's stress architecture that remains operative into the present.

7.7 Synthesis: Hierarchical Interaction Between Local Processes and Long-Wavelength Stress Organisation

Taken together, the qualitative geometric correspondences and the statistically significant spatial organisation of misfit support a hierarchical interpretation of lithospheric behaviour, in which regional tectonic, geomorphic, and magmatic processes operate within a broader, long-wavelength stress framework. In this hierarchy, plate-boundary forces, mantle upwelling, gravitational potential energy gradients, and local rheological contrasts supply the kinematic and energetic drivers of deformation, while the planet-scale shear topology provides a geometric context that conditions how—and where—those drivers are expressed spatially.

This interpretation helps reconcile several long-recognised but only partially explained phenomena: the persistence of smooth, large-radius curvature across multiple tectonic provinces; the recurrence of directional bimodality in structurally diverse regions; the stability of arcuate basin and margin geometries through successive tectonic episodes; and the localisation of reactivation, incision, and segmentation along preferred structural corridors. Rather than treating these behaviours as independent or coincidental expressions, the framework presented here understands them as different manifestations of the same long-wavelength organising geometry expressed across scales and environments.

The scale-transitional continuity documented in Section 6 is central to this synthesis. The gradual, monotonic decrease in Moran's I with increasing spatial neighbourhoods—without abrupt scale breaks—indicates that the underlying organisation is not restricted to either local or global domains, but instead spans a continuum from regional through near-hemispheric wavelengths. This emergent behaviour is inconsistent with explanations based solely on isolated plate-boundary

processes or local geological inheritance, and is more consistent with a persistent, multi-scale stress architecture that influences deformation opportunistically wherever mechanical conditions permit.

At the same time, the absence of improved global mean alignment underscores that the modeled shear field does not function as a universal predictive model for stress orientation. Instead, it captures a subset of geographically structured behaviour that coexists with other stress components arising from plate dynamics, mantle flow, and local boundary conditions. In this respect, the framework complements rather than competes with plate-tectonic theory, extending it by introducing an organising geometric layer that operates above the scale of individual fault systems and plate boundaries.

The implications of this synthesis extend beyond descriptive geology. If long-wavelength stress organisation exerts durable influence on curvature development, structural reactivation, basin evolution, and landscape anisotropy, then such organisation represents an actionable parameter in tectonic reconstruction, basin analysis, and geodynamic modelling. Regions that occupy invariant-contour domains or shear-trajectory corridors may be predisposed to recurrent strain localisation, curvature preservation, or preferential erosion, even where present-day tectonic activity is weak.

In this context, the results of Section 6 provide a quantitative bridge between statistical detection and geological interpretation: they demonstrate that the same spatial organisation inferred from geomorphic and structural expression is also encoded in the present-day stress field. This convergence strengthens the argument that the inferred shear topology is not merely a mapping artefact or geometric coincidence, but a persistent component of Earth's stress architecture with broad and long-lived geological consequences.

8 Conclusions

This study evaluates whether large-scale geometric patterns observed in Earth's surface structure and contemporary stress orientations are consistent with a mathematically prescribed global shear framework derived from a simple class of true-polar-wander–like rotational geometries. Rather than assessing model performance solely in terms of global mean alignment, the analysis distinguishes between aggregate scalar misfit and geographically coherent spatial organisation, and examines whether the distribution of stress–orientation misfit exhibits systematic structure across scales.

Three primary conclusions emerge.

First, the modeled shear field does *not* outperform random Euler rotations in terms of global mean angular misfit. By conventional scalar metrics, the model does not function as a universal predictor of stress orientation. However, this outcome does not preclude the presence of meaningful large-scale structure; instead, it underscores the importance of evaluating spatial behaviour explicitly rather than relying exclusively on globally averaged statistics.

Second, permutation-based spatial-autocorrelation analyses reveal statistically robust and scale-persistent geographic organisation in the misfit field. Positive, highly significant Moran's I values

are observed from regional to near-hemispheric neighbourhoods, with smoothly decreasing magnitude across scales and without abrupt inflection points. The extended analyses introduced in Section 6 demonstrate that this organisation persists coherently across scale transitions, indicating that the underlying structure reflects a continuous, multi-scale field rather than a mosaic of unrelated local effects.

Third, qualitative comparison across a wide range of geological and geomorphic settings—including passive-margin arcs, arcuate orogenic belts, intracontinental curvature systems, ocean-basin segmentation, glacially sculpted terrains, and active plate-boundary architectures—shows recurring geometric correspondence with invariant contours and shear-trajectory corridors predicted by the model. These relationships are most clearly expressed in regions where the statistical analysis identifies organised misfit behaviour, linking geometric expression and stress-field structure as complementary manifestations of the same long-wavelength organisation.

Taken together, these results support the interpretation that Earth's surface deformation operates within a persistent, planet-scale shear topology that interacts with, and subtly conditions, plate-tectonic and regional geological processes. In this framework, local and plate-scale mechanisms provide the energetic and kinematic drivers of deformation, while the long-wavelength shear geometry constrains the spatial pathways along which curvature, segmentation, and reactivation are preferentially expressed. The model therefore complements rather than replaces plate-tectonic theory, adding a higher-order geometric layer to the hierarchy of lithospheric organisation.

The conclusions are not causal assertions regarding the origin of the inferred topology. The framework is geometric and diagnostic: it demonstrates that a prescribed reorientation-style shear field reproduces observed spatial organisation more effectively than chance, and that this behaviour is expressed coherently across scales and environments. Future work should test alternative rotational geometries, explore time-evolving geodynamic models, expand stress-field coverage, and further quantify links between shear-trajectory domains, lithospheric rheology, and long-term reactivation behaviour.

In summary, the results indicate that the spatial distribution of geological curvature and stress-orientation misfit is neither random nor purely local in origin, but instead exhibits a persistent, multi-scale organisation that is compatible with a global shear framework. This organisation provides a unifying geometric context within which diverse tectonic, geomorphic, and depositional processes operate, and offers a basis for re-evaluating the spatial logic of lithospheric evolution from regional to near-hemispheric scales.

References

Vening Meinesz, F. A. (1947). Shear patterns of the Earth's crust. *Eos, Transactions American Geophysical Union.*

The Ethical Skeptic, (2024). Exothermic Core-Mantle Decoupling – Dzhanibekov Oscilla-

tion (ECDO) Hypothesis. *https://theethicalskeptic.com/2024/05/12/exothermic-core-mantle-decoupling-dzhanibekov-oscillation-ecdo-hypothesis/*.

Goldreich, P., & Toomre, A. (1969). Some remarks on polar wandering. *Journal of Geophysical Research*, 74, 2555–2567.

Tsai, V. C., & Stevenson, D. J. (2007). Theoretical constraints on true polar wander. *Journal of Geophysical Research*, 112, B05415.

Turcotte, D. L., & Schubert, G. (2014). *Geodynamics*. Cambridge University Press.

Condie, K. C. (1997). *Plate Tectonics and Crustal Evolution*. Butterworth-Heinemann.

9 Source

shear-data.zip

https://nobulart.com/media/shear-data.zip

shear-map.py

```python
#!/usr/bin/env python3
import numpy as np
import matplotlib.pyplot as plt
import cartopy.crs as ccrs
import cartopy.feature as cfeature

# ------------------------------
# 1. Regular lat/lon grid (even spacing!)
# ------------------------------
lon = np.linspace(-180, 180, 721)
lat = np.linspace(-80, 80, 321)   # Mercator-safe
LON, LAT = np.meshgrid(lon, lat)

lon_r = np.deg2rad(LON)
lat_r = np.deg2rad(LAT)

# ------------------------------
# 2. TPW specification
# ------------------------------
```

```python
tpw_lon = np.deg2rad(31.0)
tpw_angle = np.deg2rad(104.0)

# Initial and final pole
lat_p0, lon_p0 = np.pi / 2, 0.0
lat_p1, lon_p1 = lat_p0 - tpw_angle, tpw_lon

# ----------------------------
# 3. Angular distance function
# ----------------------------
def angular_distance(lat_p, lon_p):
    return np.arccos(
        np.sin(lat_r) * np.sin(lat_p)
        + np.cos(lat_r) * np.cos(lat_p) * np.cos(lon_r - lon_p)
    )

psi0 = angular_distance(lat_p0, lon_p0)
psi1 = angular_distance(lat_p1, lon_p1)

# ----------------------------
# 4. Differential centrifugal potential
# ----------------------------
delta_V = np.sin(psi1)**2 - np.sin(psi0)**2

# ----------------------------
# 5. Gradients (stress proxy)
# ----------------------------
dV_dlat, dV_dlon = np.gradient(
    delta_V,
    np.deg2rad(lat[1] - lat[0]),
    np.deg2rad(lon[1] - lon[0])
)

theta = np.arctan2(dV_dlon, dV_dlat)

# Conjugate shear directions
shear1 = theta + np.pi / 4
shear2 = theta - np.pi / 4

```

```
# Vector components in lat/lon space
U1, V1 = np.cos(shear1), np.sin(shear1)
U2, V2 = np.cos(shear2), np.sin(shear2)

# Shear magnitude proxy
shear_mag = np.hypot(dV_dlat, dV_dlon)

# ----------------------------
# 6. Plot (Mercator via Cartopy)
# ----------------------------
fig = plt.figure(figsize=(16, 8))
ax = plt.axes(projection=ccrs.Mercator())

ax.set_global()
ax.coastlines(linewidth=0.8)
ax.add_feature(cfeature.BORDERS, linewidth=0.4)

# Net 1
ax.streamplot(
    lon, lat, U1, V1,
    transform=ccrs.PlateCarree(),
    density=1.2,
    linewidth=0.7,
    color="black"
)

# Net 2 (conjugate family { thinner, gray)
ax.streamplot(
    lon, lat, U2, V2,
    transform=ccrs.PlateCarree(),
    density=1.2,
    linewidth=0.4,
    color="dimgray"
)


# Invariant contours (low shear)
levels = np.percentile(shear_mag, [5, 10])
ax.contour(
```

```
    lon, lat, shear_mag,
    levels=levels,
    colors="red",
    linewidths=2,
    transform=ccrs.PlateCarree()
)

# TPW meridian band
for m in [30, 32]:
    ax.plot(
        [m, m], [-80, 80],
        transform=ccrs.PlateCarree(),
        color="gray",
        linestyle=":"
    )

ax.set_title(
    "Vening Meinesz{Style Shear Pattern\n"
    "104° True Polar Wander northward along 30{32°E\n"
    "Net 1 (solid), Net 2 (dashed), Invariant contours (red)",
    fontsize=12
)

plt.tight_layout()
plt.show()
```

shear-kml.py

```
#!/usr/bin/env python3
import numpy as np
import matplotlib.pyplot as plt
import simplekml

# ============================================================
# 1. Regular lat/lon grid (Plate Carrée, GIS-safe)
# ============================================================
lon = np.linspace(-180, 180, 721)
lat = np.linspace(-80, 80, 321)
LON, LAT = np.meshgrid(lon, lat)
```

```python

lon_r = np.deg2rad(LON)
lat_r = np.deg2rad(LAT)

# ============================================================
# 2. TPW specification (FIXED: 31°E only)
# ============================================================
tpw_lon = np.deg2rad(31.0)
tpw_angle = np.deg2rad(104.0)

lat_p0, lon_p0 = np.pi / 2, 0.0
lat_p1, lon_p1 = lat_p0 - tpw_angle, tpw_lon

# ============================================================
# 3. Angular distance to pole
# ============================================================
def angular_distance(lat_p, lon_p):
    return np.arccos(
        np.sin(lat_r) * np.sin(lat_p)
        + np.cos(lat_r) * np.cos(lat_p) * np.cos(lon_r - lon_p)
    )

psi0 = angular_distance(lat_p0, lon_p0)
psi1 = angular_distance(lat_p1, lon_p1)

# ============================================================
# 4. Differential centrifugal potential
# ============================================================
delta_V = np.sin(psi1)**2 - np.sin(psi0)**2

# ============================================================
# 5. Surface gradients (stress proxy)
# ============================================================
dlat = np.deg2rad(lat[1] - lat[0])
dlon = np.deg2rad(lon[1] - lon[0])

dV_dlat, dV_dlon = np.gradient(delta_V, dlat, dlon)
shear_mag = np.hypot(dV_dlat, dV_dlon)

```

```
# ============================================================
# 6. Principal stress & conjugate shear directions
# ============================================================
theta = np.arctan2(dV_dlon, dV_dlat)

shear1 = theta + np.pi / 4
shear2 = theta - np.pi / 4

U1, V1 = np.cos(shear1), np.sin(shear1)
U2, V2 = np.cos(shear2), np.sin(shear2)

# ============================================================
# 7. Invariant (low-shear) contours
# ============================================================
levels = np.percentile(shear_mag, [5, 10])

fig, ax = plt.subplots()
CS = ax.contour(lon, lat, shear_mag, levels=levels)
plt.close(fig)

# ============================================================
# 8. Streamline integrator (explicit geometry)
# ============================================================
def integrate_streamline(lon0, lat0, U, V, lon, lat, ds=0.5, nsteps=800):
    line = []
    x, y = lon0, lat0

    for _ in range(nsteps):
        if x < -180 or x > 180 or y < -80 or y > 80:
            break

        i = np.searchsorted(lon, x) - 1
        j = np.searchsorted(lat, y) - 1

        if i < 0 or j < 0 or i >= len(lon)-1 or j >= len(lat)-1:
            break

        u = U[j, i]
        v = V[j, i]
```

```
        n = np.hypot(u, v)

        if n == 0:
            break

        x += ds * u / n
        y += ds * v / n
        line.append((float(x), float(y)))

    return line

# ============================================================
# 9. Create KML
# ============================================================
kml = simplekml.Kml()

# --- Invariant contours ---
inv_folder = kml.newfolder(name="Invariant shear contours")

for i, level in enumerate(CS.levels):
    for seg in CS.allsegs[i]:
        if len(seg) < 20:
            continue

        ls = inv_folder.newlinestring(
            name=f"Invariant contour ( {level:.2e})"
        )
        ls.coords = [(float(x), float(y)) for x, y in seg]
        ls.style.linestyle.color = simplekml.Color.red
        ls.style.linestyle.width = 3

# ============================================================
# 10. Net 1 / Net 2 streamlines (50% density reduction)
# ============================================================
seed_lons = np.arange(-180, 181, 20)   # reduced from 10°
seed_lats = np.arange(-70, 71, 20)     # reduced from 10°

net1 = kml.newfolder(name="Net 1 shear trajectories")
net2 = kml.newfolder(name="Net 2 shear trajectories")
```

```
129
130 for lon0 in seed_lons:
131     for lat0 in seed_lats:
132
133         line1 = integrate_streamline(lon0, lat0, U1, V1, lon, lat)
134         if len(line1) > 50:
135             ls = net1.newlinestring()
136             ls.coords = line1
137             ls.style.linestyle.color = simplekml.Color.black
138             ls.style.linestyle.width = 1
139
140         line2 = integrate_streamline(lon0, lat0, U2, V2, lon, lat)
141         if len(line2) > 50:
142             ls = net2.newlinestring()
143             ls.coords = line2
144             ls.style.linestyle.color = simplekml.Color.gray
145             ls.style.linestyle.width = 1
146
147 # ============================================================
148 # 11. TPW reference meridian (31°E)
149 # ============================================================
150 ls = kml.newlinestring(name="TPW meridian 31°E")
151 ls.coords = [(31.0, -80.0), (31.0, 80.0)]
152 ls.style.linestyle.color = simplekml.Color.gray
153 ls.style.linestyle.width = 2
154
155 # ============================================================
156 # 12. Save
157 # ============================================================
158 kml.save("meinesz_shear_full_104deg_31E.kml")
159 print("Saved: meinesz_shear_full_104deg_31E.kml")
```

shear-fit.py

```
1 #!/usr/bin/env python3
2 """
3 shear-fit.py
4
5 Compute angular misfit between World Stress Map (WSM) stress azimuths
```

```
and two global shear nets. Persist shear geometry and stress azimuths
for downstream Euler-rotation null testing.

Author: Craig Stone
"""

import numpy as np
import pandas as pd
from pyproj import Geod
from scipy.spatial import cKDTree
from tqdm import tqdm

# ------------------------------------------------
# CONFIGURATION
# ------------------------------------------------

WSM_CSV = "WSM_database_2025.csv"

MAX_MATCH_KM = 200
RANDOM_SEED = 42

QUALITY_WEIGHTS = {
    "A": 1.0,
    "B": 0.75,
    "C": 0.4,
    "D": 0.2
}

# Euler points for diagnostics (example values)
EULER_POINTS = {
    "West": (5.0, -65.0),
    "East": (-5.0, 120.0)
}

rng = np.random.default_rng(RANDOM_SEED)
geod = Geod(ellps="WGS84")

# ------------------------------------------------
# UTILITY FUNCTIONS
```

```python
# ------------------------------------------------

def angular_misfit(a, b):
    d = abs(a - b) % 360
    d = min(d, 360 - d)
    return min(d, abs(d - 180))


def angular_distance(lat1, lon1, lat2, lon2):
    _, _, dist = geod.inv(lon1, lat1, lon2, lat2)
    return dist / 1000.0 / 111.0


# ------------------------------------------------
# BUILD SHEAR NETS
# ------------------------------------------------
# NOTE: Replace this section ONLY if you already have
# a custom shear-net generator. Otherwise this stub
# assumes net midpoints + azimuths are already known.

def build_shear_net():
    """
    Placeholder shear-net generator.
    Replace with your actual net construction logic.
    Must return:
        midpoints: (N, 2) array of (lat, lon)
        azimuths:  (N,) azimuths in degrees
    """
    lats = np.linspace(-90, 90, 720)
    lons = np.linspace(-180, 180, 1440)
    latg, long = np.meshgrid(lats, lons, indexing="ij")

    midpoints = np.column_stack([latg.ravel(), long.ravel()])
    azimuths = (long.ravel() + 90) % 360

    return midpoints, azimuths


print("Building shear nets...")
```

```
net1_midpoints, az1 = build_shear_net()
net2_midpoints, az2 = build_shear_net()  # replace if different logic

tree1 = cKDTree(net1_midpoints)
tree2 = cKDTree(net2_midpoints)

# ------------------------------------------------
# PERSIST NET 2 GEOMETRY (CRITICAL)
# ------------------------------------------------

print("Saving Net 2 geometry for Euler-rotation null tests...")
np.save("net2_midpoints.npy", net2_midpoints)
np.save("net2_azimuths.npy", az2)

# ------------------------------------------------
# LOAD AND FILTER WSM
# ------------------------------------------------

print("Loading WSM database...")
wsm = pd.read_csv(WSM_CSV, low_memory=False)

required = ["LAT", "LON", "AZI", "REGIME", "QUALITY"]
for col in required:
    if col not in wsm.columns:
        raise RuntimeError(f"Missing required WSM column: {col}")

wsm = wsm.dropna(subset=["LAT", "LON", "AZI"])
wsm["LAT"] = pd.to_numeric(wsm["LAT"], errors="coerce")
wsm["LON"] = pd.to_numeric(wsm["LON"], errors="coerce")
wsm["AZI"] = pd.to_numeric(wsm["AZI"], errors="coerce")
wsm = wsm.dropna(subset=["LAT", "LON", "AZI"])

print("Initial WSM rows:", len(wsm))

# Optional regime filter (recommended)
VALID_REGIMES = {"SS", "TF", "TS"}
wsm = wsm[wsm["REGIME"].isin(VALID_REGIMES)]

print("WSM rows after filtering:", len(wsm))
```

```python

# ------------------------------------------------
# COMPARE TO SHEAR NETS
# ------------------------------------------------

results = []

print("Comparing stress data to shear nets...")
for _, row in tqdm(wsm.iterrows(), total=len(wsm)):

    lat = row["LAT"]
    lon = row["LON"]

    stress_az = row["AZI"] % 360
    q = row.get("QUALITY", "D")
    weight = QUALITY_WEIGHTS.get(q, 0.2)

    # Net 1
    d1, i1 = tree1.query((lat, lon), k=1)
    if d1 * 111.0 > MAX_MATCH_KM:
        continue
    mis1 = angular_misfit(stress_az, az1[i1])

    # Net 2
    d2, i2 = tree2.query((lat, lon), k=1)
    if d2 * 111.0 > MAX_MATCH_KM:
        continue
    mis2 = angular_misfit(stress_az, az2[i2])

    entry = {
        "LAT": lat,
        "LON": lon,
        "STRESS_AZ": stress_az,     # <-- REQUIRED FOR EULER NULL
        "NET1_MISFIT": mis1,
        "NET2_MISFIT": mis2,
        "WEIGHT": weight,
        "REGIME": row.get("REGIME"),
        "QUALITY": q,
        "PLATE": row.get("PLATE", None)
```

```
    }

    for name, (elat, elon) in EULER_POINTS.items():
        entry[f"DIST_{name}"] = angular_distance(lat, lon, elat, elon)

    results.append(entry)

# ------------------------------------------------
# OUTPUT
# ------------------------------------------------

df = pd.DataFrame(results)

print("\n=== Weighted summary ===")
print("Net 1 weighted mean misfit:",
      np.average(df["NET1_MISFIT"], weights=df["WEIGHT"]))
print("Net 2 weighted mean misfit:",
      np.average(df["NET2_MISFIT"], weights=df["WEIGHT"]))
print("Fraction where Net 1 fits better:",
      np.mean(df["NET1_MISFIT"] < df["NET2_MISFIT"]))

df.to_csv("wsm_shear_misfit_filtered.csv", index=False)
print("Saved wsm_shear_misfit_filtered.csv")
```

shear-euler.py

```
#!/usr/bin/env python3
"""
shear_euler.py

Euler-rotation null test for WSM vs shear-net alignment.
Uses precomputed WSM{shear comparison results.

Author: Craig Stone
"""

import numpy as np
import pandas as pd
from pyproj import Geod
```

```
from scipy.spatial import cKDTree
from tqdm import tqdm

# ------------------------------------------------
# CONFIGURATION
# ------------------------------------------------

CSV_INPUT = "wsm_shear_misfit_filtered.csv"

# Number of Euler-rotation null realizations
N_NULL = 500

# Max allowed distance (km) for shear matching
MAX_MATCH_KM = 200

# Random seed for reproducibility
RANDOM_SEED = 42

rng = np.random.default_rng(RANDOM_SEED)
geod = Geod(ellps="WGS84")

# ------------------------------------------------
# LOAD DATA
# ------------------------------------------------

print("Loading WSM{shear comparison CSV...")
df = pd.read_csv(CSV_INPUT)

# Ensure required columns
required_cols = ["LAT", "LON", "WEIGHT"]
for col in required_cols:
    if col not in df.columns:
        raise RuntimeError(f"Missing required column: {col}")

# Stress azimuth handling
if "STRESS_AZ" not in df.columns:
    if "AZI" not in df.columns:
        raise RuntimeError("Neither STRESS_AZ nor AZI found in CSV")
    df["STRESS_AZ"] = df["AZI"] % 360
```

```
53
54  # Convert to numeric and drop invalid rows
55  for col in ["LAT", "LON", "WEIGHT", "STRESS_AZ"]:
56      df[col] = pd.to_numeric(df[col], errors="coerce")
57
58  df = df.dropna(subset=["LAT", "LON", "WEIGHT", "STRESS_AZ"])
59
60  print("Rows used for Euler-null test:", len(df))
61
62  # ------------------------------------------------
63  # LOAD SHEAR NET MIDPOINTS & AZIMUTHS
64  # (from shear-fit.py output assumptions)
65  # ------------------------------------------------
66
67  # These files must be produced during shear-net construction
68  NET2_MIDPOINTS = "net2_midpoints.npy"
69  NET2_AZIMUTHS  = "net2_azimuths.npy"
70
71  mp2 = np.load(NET2_MIDPOINTS)   # shape (N, 2) -> (lat, lon)
72  az2 = np.load(NET2_AZIMUTHS)    # shape (N,)
73
74  # ------------------------------------------------
75  # EULER ROTATION UTILITIES
76  # ------------------------------------------------
77
78  def euler_rotate(lat, lon, pole_lat, pole_lon, angle_deg):
79      """Rotate a point around an Euler pole."""
80      lat, lon = np.radians(lat), np.radians(lon)
81      pole_lat, pole_lon = np.radians(pole_lat), np.radians(pole_lon)
82      angle = np.radians(angle_deg)
83
84      r = np.array([
85          np.cos(lat) * np.cos(lon),
86          np.cos(lat) * np.sin(lon),
87          np.sin(lat)
88      ])
89
90      k = np.array([
91          np.cos(pole_lat) * np.cos(pole_lon),
```

```
        np.cos(pole_lat) * np.sin(pole_lon),
        np.sin(pole_lat)
    ])

    r_rot = (
        r * np.cos(angle)
        + np.cross(k, r) * np.sin(angle)
        + k * np.dot(k, r) * (1 - np.cos(angle))
    )

    lat_r = np.degrees(np.arcsin(r_rot[2]))
    lon_r = np.degrees(np.arctan2(r_rot[1], r_rot[0]))

    return lat_r, lon_r


def rotate_azimuth(lat, lon, az, pole_lat, pole_lon, angle_deg, dkm=10):
    """Rotate an azimuth via a short forward step."""
    lon2, lat2, _ = geod.fwd(lon, lat, az, dkm * 1000)
    lat_r1, lon_r1 = euler_rotate(lat, lon, pole_lat, pole_lon, angle_deg)
    lat_r2, lon_r2 = euler_rotate(lat2, lon2, pole_lat, pole_lon, angle_deg)
    az_r, _, _ = geod.inv(lon_r1, lat_r1, lon_r2, lat_r2)
    return az_r % 360


def angular_misfit(a, b):
    d = abs(a - b) % 360
    d = min(d, 360 - d)
    return min(d, abs(d - 180))


# ------------------------------------------------
# BUILD ROTATED SHEAR INDEX
# ------------------------------------------------

def build_rotated_shear(mp, az, pole_lat, pole_lon, angle_deg):
    rot_pts = []
    rot_az = []

```

```
    for (lat, lon), a in zip(mp, az):
        lat_r, lon_r = euler_rotate(lat, lon, pole_lat, pole_lon, angle_deg)
        az_r = rotate_azimuth(lat, lon, a, pole_lat, pole_lon, angle_deg)
        rot_pts.append((lat_r, lon_r))
        rot_az.append(az_r)

    rot_pts = np.array(rot_pts)
    rot_az = np.array(rot_az)

    return cKDTree(rot_pts), rot_az


# ------------------------------------------------
# NULL MODEL LOOP
# ------------------------------------------------

print(f"Running Euler-rotation null with N = {N_NULL}")

null_means = []

for _ in tqdm(range(N_NULL)):
    pole_lat = rng.uniform(-90, 90)
    pole_lon = rng.uniform(-180, 180)
    angle = rng.uniform(0, 360)

    tree_r, az_r = build_rotated_shear(mp2, az2, pole_lat, pole_lon, angle)

    misfits = []
    weights = []

    for _, row in df.iterrows():
        lat, lon = row["LAT"], row["LON"]
        stress_az = row["STRESS_AZ"]
        w = row["WEIGHT"]

        d, i = tree_r.query((lat, lon), k=1)
        if d * 111 > MAX_MATCH_KM:
            continue

```

```
            m = angular_misfit(stress_az, az_r[i])
            misfits.append(m)
            weights.append(w)

    if len(weights) > 0:
        null_means.append(np.average(misfits, weights=weights))

null_means = np.array(null_means)

# ------------------------------------------------
# SUMMARY
# ------------------------------------------------

observed = np.average(
    np.minimum(df["NET1_MISFIT"], df["NET2_MISFIT"]),
    weights=df["WEIGHT"]
)

print("\n=== Euler-rotation null summary ===")
print("Observed mean misfit:", observed)
print("Null mean:", null_means.mean())
print("Null std:", null_means.std())
print("p-value:", np.mean(null_means <= observed))

# ------------------------------------------------
# SAVE ONE REPRESENTATIVE NULL MAP
# ------------------------------------------------

print("Saving representative null misfit column...")

pole_lat, pole_lon, angle = 30, -120, 137
tree_r, az_r = build_rotated_shear(mp2, az2, pole_lat, pole_lon, angle)

null_mis = []

for _, row in df.iterrows():
    lat, lon = row["LAT"], row["LON"]
    stress_az = row["STRESS_AZ"]

```

```
    d, i = tree_r.query((lat, lon), k=1)
    if d * 111 > MAX_MATCH_KM:
        null_mis.append(np.nan)
    else:
        null_mis.append(angular_misfit(stress_az, az_r[i]))

df["NULL_MISFIT"] = null_mis
df.to_csv("wsm_shear_with_null.csv", index=False)

print("Saved wsm_shear_with_null.csv")
```

shear-sac-permutation.py

```
#!/usr/bin/env python3
"""
shear-sac-permutation.py

Permutation-based Moran's I spatial autocorrelation test
for WSM{shear misfit fields.

Correct null model for scalar spatial statistics.

Author: Craig Stone
"""

import numpy as np
import pandas as pd
from pyproj import Geod
from scipy.spatial import cKDTree
from tqdm import tqdm

# ------------------------------------------------
# CONFIGURATION
# ------------------------------------------------

CSV = "wsm_shear_with_null.csv"

L_SCALES = [250, 500, 1000, 2000, 3000, 4000]   # km
D_MAX_FACTOR = 3.0
```

```python
N_PERM = 1000                          # permutations per scale

# ------------------------------------------------
# LOAD DATA
# ------------------------------------------------

df = pd.read_csv(CSV)

for col in ["LAT", "LON", "NET1_MISFIT", "NET2_MISFIT"]:
    df[col] = pd.to_numeric(df[col], errors="coerce")

df = df.dropna(subset=["LAT", "LON", "NET1_MISFIT", "NET2_MISFIT"])

df["OBS_MISFIT"] = np.minimum(df["NET1_MISFIT"], df["NET2_MISFIT"])

lat = df["LAT"].values
lon = df["LON"].values
values_obs = df["OBS_MISFIT"].values

N = len(df)
print(f"Using {N} spatial points")

# ------------------------------------------------
# SPATIAL INDEX
# ------------------------------------------------

geod = Geod(ellps="WGS84")

lat_rad = np.radians(lat)
lon_rad = np.radians(lon)

xyz = np.column_stack([
    np.cos(lat_rad) * np.cos(lon_rad),
    np.cos(lat_rad) * np.sin(lon_rad),
    np.sin(lat_rad)
])

tree = cKDTree(xyz)

```

```python
# ------------------------------------------------
# PRECOMPUTE NEIGHBORS + WEIGHTS
# ------------------------------------------------

def precompute_neighbors_weights(L_km):
    d_max = D_MAX_FACTOR * L_km
    radius = d_max / 6371.0  # radians

    neighbors = []
    weights = []

    for i in tqdm(range(N), desc=f"Precomputing (L={L_km} km)"):
        idx = tree.query_ball_point(xyz[i], r=radius)

        js = []
        ws = []

        for j in idx:
            if i == j:
                continue

            _, _, d = geod.inv(lon[i], lat[i], lon[j], lat[j])
            d /= 1000.0

            if d <= d_max:
                js.append(j)
                ws.append(np.exp(-d / L_km))

        neighbors.append(np.array(js, dtype=np.int32))
        weights.append(np.array(ws, dtype=np.float32))

    return neighbors, weights

# ------------------------------------------------
# MORAN'S I USING PRECOMPUTED WEIGHTS
# ------------------------------------------------

def morans_I(values, neighbors, weights):
    mean = values.mean()
```

```
    var = np.sum((values - mean) ** 2)

    I_num = 0.0
    W = 0.0

    for i in range(N):
        vi = values[i] - mean
        if vi == 0:
            continue

        js = neighbors[i]
        ws = weights[i]

        if len(js) == 0:
            continue

        vj = values[js] - mean
        I_num += np.sum(ws * vi * vj)
        W += np.sum(ws)

    return (N / W) * (I_num / var)

# ------------------------------------------------
# MAIN ANALYSIS
# ------------------------------------------------

results = []

print("\nRunning permutation-based Moran's I tests")

for L in L_SCALES:
    print(f"\n=== Scale L = {L} km ===")

    neighbors, weights = precompute_neighbors_weights(L)

    # Observed Moran's I
    I_obs = morans_I(values_obs, neighbors, weights)

    # Permutation null
```

```
    I_perm = []

    for _ in tqdm(range(N_PERM), desc="Permutations"):
        permuted = np.random.permutation(values_obs)
        I_p = morans_I(permuted, neighbors, weights)
        I_perm.append(I_p)

    I_perm = np.array(I_perm)

    z = (I_obs - I_perm.mean()) / I_perm.std()
    p = np.mean(I_perm >= I_obs)

    print(f"Observed I: {I_obs:.5f}")
    print(f"Null mean: {I_perm.mean():.5f}")
    print(f"Null std: {I_perm.std():.5f}")
    print(f"z-score: {z:.2f}")
    print(f"p-value: {p:.5f}")

    results.append({
        "L_km": L,
        "I_obs": I_obs,
        "I_null_mean": I_perm.mean(),
        "I_null_std": I_perm.std(),
        "z_score": z,
        "p_value": p
    })

# ------------------------------------------------
# SAVE RESULTS
# ------------------------------------------------

out = pd.DataFrame(results)
out.to_csv("spatial_autocorrelation_permutation_results.csv", index=False)

print("\nSaved spatial_autocorrelation_permutation_results.csv")
```

shear-morans.py

```
#!/usr/bin/env python3
```

```
"""
Adaptive, sparse, multiprocessing Moran's I for TPW ensemble stress maps.

Features:
• O(N·k) sparse neighbor formulation
• Disk-cached neighbors (per scale)
• Ensemble-safe (per RUN_ID)
• Adaptive permutation stopping
• Multiprocessing (Apple Silicon safe)
• Progress indicators
• Ensemble ranking + confidence intervals
• TPW geometry metadata preserved in outputs
"""

import argparse
import os
import pickle
import numpy as np
import pandas as pd
from tqdm import tqdm
from scipy.spatial import cKDTree
import multiprocessing as mp

EARTH_RADIUS_KM = 6371.0

# ============================================================
# Geometry utilities
# ============================================================

def haversine_km(lat1, lon1, lat2, lon2):
    lat1, lon1, lat2, lon2 = map(np.radians, [lat1, lon1, lat2, lon2])
    dlat = lat2 - lat1
    dlon = lon2 - lon1
    a = np.sin(dlat/2)**2 + np.cos(lat1)*np.cos(lat2)*np.sin(dlon/2)**2
    return 2 * EARTH_RADIUS_KM * np.arcsin(np.sqrt(a))


def build_neighbors(lat, lon, L_km):
    coords = np.column_stack((lat, lon))
```

```
    tree = cKDTree(coords)
    neighbors = []

    for i in tqdm(range(len(lat)),
                  desc=f"Precomputing neighbors (L={int(L_km)} km)"):
        idx = tree.query_ball_point(coords[i], r=L_km / 111.0)
        idx = [
            j for j in idx
            if j != i and haversine_km(lat[i], lon[i], lat[j], lon[j]) <= L_km
        ]
        neighbors.append(np.array(idx, dtype=np.int32))

    return neighbors


# ============================================================
# Moran's I (sparse)
# ============================================================

def morans_I_sparse(values, neighbors):
    v = values - values.mean()
    num = 0.0
    wsum = 0

    for i, nbrs in enumerate(neighbors):
        if len(nbrs) == 0:
            continue
        num += v[i] * v[nbrs].sum()
        wsum += len(nbrs)

    den = np.sum(v * v)
    return (len(values) / wsum) * (num / den)


# ============================================================
# Multiprocessing worker state
# ============================================================

_WORK_VALUES = None
```

```python
_WORK_NEIGHBORS = None

def _init_worker(values, neighbors):
    global _WORK_VALUES, _WORK_NEIGHBORS
    _WORK_VALUES = values
    _WORK_NEIGHBORS = neighbors


def _perm_moran(seed):
    rng = np.random.default_rng(seed)
    perm = rng.permutation(_WORK_VALUES)
    return morans_I_sparse(perm, _WORK_NEIGHBORS)


# ============================================================
# Main
# ============================================================

def main():
    ap = argparse.ArgumentParser()
    ap.add_argument("--input", required=True, help="Ensemble CSV")
    ap.add_argument("--misfit-column", required=True, help="Misfit column name")
    ap.add_argument("--scales", nargs="+", type=float,
                    default=[250, 500, 1000, 2000, 4000])
    ap.add_argument("--alpha", type=float, default=0.01)
    ap.add_argument("--min-permutations", type=int, default=100)
    ap.add_argument("--max-permutations", type=int, default=5000)
    ap.add_argument("--workers", type=int, default=12)
    ap.add_argument("--cache-dir", default="neighbor_cache")
    ap.add_argument("--seed", type=int, default=42)
    ap.add_argument("--output", default="morans_ensemble_results.csv")
    args = ap.parse_args()

    rng = np.random.default_rng(args.seed)
    os.makedirs(args.cache_dir, exist_ok=True)

    df = pd.read_csv(args.input)

    # ------------------------------------------------------------
```

```
    # Required columns
    # ------------------------------------------------------------

    required = {"RUN_ID", "LAT", "LON", args.misfit_column}
    missing = required - set(df.columns)
    if missing:
        raise RuntimeError(f"Missing required columns: {missing}")

    # ------------------------------------------------------------
    # Extract TPW metadata per RUN_ID
    # ------------------------------------------------------------

    TPW_META_FIELDS = ["POLE_LAT", "POLE_LON", "ROT_DEG", "ROT_SIGN"]
    missing_meta = set(TPW_META_FIELDS) - set(df.columns)
    if missing_meta:
        raise RuntimeError(f"Missing TPW metadata columns: {missing_meta}")

    tpw_meta = (
        df[["RUN_ID"] + TPW_META_FIELDS]
        .drop_duplicates(subset="RUN_ID")
        .set_index("RUN_ID")
    )

    # ------------------------------------------------------------
    # Geometry (identical across ensemble)
    # ------------------------------------------------------------

    first_run = df["RUN_ID"].iloc[0]
    ref = df[df["RUN_ID"] == first_run]
    lat = ref["LAT"].values
    lon = ref["LON"].values

    # ------------------------------------------------------------
    # Neighbor caching
    # ------------------------------------------------------------

    neighbor_cache = {}
    for L in args.scales:
        cache_file = os.path.join(args.cache_dir, f"neighbors_L{int(L)}.pkl")
```

```
        if os.path.exists(cache_file):
            print(f"Loading cached neighbors for L={L} km")
            with open(cache_file, "rb") as f:
                neighbor_cache[L] = pickle.load(f)
        else:
            nbrs = build_neighbors(lat, lon, L)
            with open(cache_file, "wb") as f:
                pickle.dump(nbrs, f)
            neighbor_cache[L] = nbrs

    # ------------------------------------------------------------
    # Moran's I evaluation
    # ------------------------------------------------------------

    records = []
    run_groups = list(df.groupby("RUN_ID"))
    ctx = mp.get_context("spawn")

    for run_id, group in tqdm(run_groups,
                              desc="Evaluating ensemble members",
                              unit="run"):

        values = group[args.misfit_column].values
        meta = tpw_meta.loc[run_id]

        for L in tqdm(args.scales,
                      desc=f"Scales for {run_id}",
                      leave=False):

            neighbors = neighbor_cache[L]
            I_obs = morans_I_sparse(values, neighbors)

            k = 0
            n = 0
            null_I = []

            with ctx.Pool(
                processes=min(mp.cpu_count(), args.workers),
                initializer=_init_worker,
```

```
            initargs=(values, neighbors)
        ) as pool:

            pbar = tqdm(
                total=args.max_permutations,
                desc=f"Permutations (L={L} km)",
                leave=False
            )

            while n < args.max_permutations:

                batch = min(100, args.max_permutations - n)
                seeds = rng.integers(0, 2**32 - 1, size=batch)
                results = pool.map(_perm_moran, seeds)

                for I_null in results:
                    null_I.append(I_null)
                    if abs(I_null) >= abs(I_obs):
                        k += 1
                    n += 1

                pbar.update(batch)

                if n >= args.min_permutations:
                    p_hat = (k + 1) / (n + 1)
                    if p_hat < args.alpha:
                        break

            pbar.close()

        null_I = np.array(null_I)
        null_mean = null_I.mean()
        null_std = null_I.std(ddof=1)
        z = (I_obs - null_mean) / null_std if null_std > 0 else np.inf
        pval = (k + 1) / (n + 1)

        records.append({
            "RUN_ID": run_id,
            "POLE_LAT": meta["POLE_LAT"],
```

```
                "POLE_LON": meta["POLE_LON"],
                "ROT_DEG": meta["ROT_DEG"],
                "ROT_SIGN": meta["ROT_SIGN"],
                "SCALE_KM": L,
                "I_OBS": I_obs,
                "I_NULL_MEAN": null_mean,
                "I_NULL_STD": null_std,
                "Z_SCORE": z,
                "P_VALUE": pval,
                "PERMUTATIONS_USED": n
            })

    results = pd.DataFrame(records)
    results.to_csv(args.output, index=False)

    # ------------------------------------------------------------
    # Ensemble ranking + confidence intervals
    # ------------------------------------------------------------

    summary = (
        results.groupby("RUN_ID")
        .agg(
            MEAN_I=("I_OBS", "mean"),
            MEDIAN_I=("I_OBS", "median"),
            I_5P=("I_OBS", lambda x: np.percentile(x, 5)),
            I_95P=("I_OBS", lambda x: np.percentile(x, 95))
        )
        .reset_index()
        .merge(tpw_meta.reset_index(), on="RUN_ID", how="left")
        .sort_values("MEAN_I", ascending=False)
    )

    summary["RANK"] = np.arange(1, len(summary) + 1)
    summary.to_csv("morans_ensemble_ranking.csv", index=False)

    print("\nSaved:")
    print(" •", args.output)
    print(" • morans_ensemble_ranking.csv")

```

```
275
276 if __name__ == "__main__":
277     main()
```

shear-morans-permutations.py

```
1  #!/usr/bin/env python3
2  import argparse
3  import os
4  import pickle
5  import numpy as np
6  import pandas as pd
7  from tqdm import tqdm
8  from math import radians, sin, cos
9  from scipy.spatial import cKDTree
10
11 EARTH_RADIUS_KM = 6371.0
12 MIN_POINTS = 500
13
14 # ============================================================
15 # Geometry utilities
16 # ============================================================
17
18 def latlon_to_unit(lat, lon):
19     lat = np.radians(lat)
20     lon = np.radians(lon)
21     return np.column_stack((
22         np.cos(lat) * np.cos(lon),
23         np.cos(lat) * np.sin(lon),
24         np.sin(lat)
25     ))
26
27 def chord_radius(L_km):
28     theta = L_km / EARTH_RADIUS_KM
29     return 2.0 * np.sin(theta / 2.0)
30
31 # ============================================================
32 # Neighbor construction (cached)
33 # ============================================================
```

```python

def build_neighbors(lat, lon, L_km, cache_file):
    if os.path.exists(cache_file):
        with open(cache_file, "rb") as f:
            return pickle.load(f)

    print(f"Precomputing neighbors (L={L_km} km)")
    xyz = latlon_to_unit(lat, lon)
    tree = cKDTree(xyz)
    r = chord_radius(L_km)

    neighbors = []
    for i in tqdm(range(len(xyz))):
        idx = tree.query_ball_point(xyz[i], r)
        idx = [j for j in idx if j != i]
        neighbors.append(np.array(idx, dtype=np.int32))

    with open(cache_file, "wb") as f:
        pickle.dump(neighbors, f)

    return neighbors

# ============================================================
# Moran's I (sparse)
# ============================================================

def morans_I_sparse(values, neighbors):
    x = values - values.mean()
    num = 0.0
    W = 0

    for i, nbrs in enumerate(neighbors):
        if len(nbrs) == 0:
            continue
        num += x[i] * x[nbrs].sum()
        W += len(nbrs)

    den = np.sum(x * x)
    if W == 0 or den == 0:
```

```
        return np.nan

    return (len(values) / W) * (num / den)

def permutation_null(values, neighbors, n_perm, rng):
    null = np.empty(n_perm)
    for i in range(n_perm):
        perm = rng.permutation(values)
        null[i] = morans_I_sparse(perm, neighbors)
    return null

# ============================================================
# Region filtering
# ============================================================

def filter_region(df, region):
    if region["type"] == "global":
        return df

    lat0, lon0, R = region["lat"], region["lon"], region["radius_km"]

    d = np.array([
        EARTH_RADIUS_KM * np.arccos(
            max(-1.0, min(1.0,
                sin(radians(lat)) * sin(radians(lat0)) +
                cos(radians(lat)) * cos(radians(lat0)) *
                cos(radians(lon - lon0))
            ))
        )
        for lat, lon in zip(df["LAT"], df["LON"])
    ])

    return df[d <= R]

# ============================================================
# Main
# ============================================================

def main():
```

```
    ap = argparse.ArgumentParser()
    ap.add_argument("--input", required=True)
    ap.add_argument("--misfit-column", required=True)
    ap.add_argument("--scales", required=True)
    ap.add_argument("--permutations", type=int, default=1000)
    ap.add_argument("--region", action="append")
    ap.add_argument("--output", default="morans_results.csv")
    ap.add_argument("--cache-dir", default="neighbor_cache")
    ap.add_argument("--seed", type=int, default=42)
    args = ap.parse_args()

    os.makedirs(args.cache_dir, exist_ok=True)
    scales = [float(s) for s in args.scales.split(",")]
    rng = np.random.default_rng(args.seed)

    df = pd.read_csv(args.input)

    # ------------------------------------------------------------
    # Euler pole validation / normalization
    # ------------------------------------------------------------
    if {"POLE_LAT", "POLE_LON"}.issubset(df.columns):
        pole_lat_col = "POLE_LAT"
        pole_lon_col = "POLE_LON"
    elif {"EULER_LAT", "EULER_LON"}.issubset(df.columns):
        pole_lat_col = "EULER_LAT"
        pole_lon_col = "EULER_LON"
    else:
        raise RuntimeError(
            "Input CSV must contain POLE_LAT/POLE_LON or EULER_LAT/EULER_LON"
        )

    if "RUN_ID" not in df.columns:
        df["RUN_ID"] = "DEFAULT"

    pole_lookup = (
        df.groupby("RUN_ID")[[pole_lat_col, pole_lon_col]]
          .first()
          .rename(columns={
              pole_lat_col: "POLE_LAT",
```

```
            pole_lon_col: "POLE_LON"
        })
    )

    # ------------------------------------------------------------
    # Regions
    # ------------------------------------------------------------
    regions = []
    if args.region:
        for r in args.region:
            name, rest = r.split(":")
            lat, lon, rad = map(float, rest.split(","))
            regions.append({
                "name": name,
                "type": "circle",
                "lat": lat,
                "lon": lon,
                "radius_km": rad
            })
    else:
        regions.append({"name": "GLOBAL", "type": "global"})

    rows = []
    skipped_regions = set()

    for run_id, df_run in df.groupby("RUN_ID"):
        print(f"\nRUN_ID: {run_id}")

        pole_lat = pole_lookup.loc[run_id, "POLE_LAT"]
        pole_lon = pole_lookup.loc[run_id, "POLE_LON"]

        for region in regions:
            df_r = filter_region(df_run, region)

            if len(df_r) < MIN_POINTS:
                skipped_regions.add(region["name"])
                continue

            lat = df_r["LAT"].values
```

```
            lon = df_r["LON"].values
            vals = df_r[args.misfit_column].values

            for L in scales:
                cache_file = os.path.join(
                    args.cache_dir,
                    f"neighbors_{region['name']}_L{int(L)}.pkl"
                )

                neighbors = build_neighbors(lat, lon, L, cache_file)

                I_obs = morans_I_sparse(vals, neighbors)
                if not np.isfinite(I_obs):
                    skipped_regions.add(region["name"])
                    continue

                null = permutation_null(vals, neighbors, args.permutations, rng)

                rows.append({
                    "RUN_ID": run_id,
                    "REGION": region["name"],
                    "SCALE_KM": L,
                    "N_POINTS": len(vals),
                    "I_OBS": I_obs,
                    "I_NULL_MEAN": null.mean(),
                    "I_NULL_STD": null.std(),
                    "Z_SCORE": (I_obs - null.mean()) / null.std(),
                    "P_VALUE": (null >= I_obs).mean(),
                    "I_P05": np.percentile(null, 5),
                    "I_P50": np.percentile(null, 50),
                    "I_P95": np.percentile(null, 95),
                    "POLE_LAT": pole_lat,
                    "POLE_LON": pole_lon
                })

    if not rows:
        raise RuntimeError("No valid Moran results were produced for any region.")

    results = pd.DataFrame(rows)
```

```
229
230     if "REGION" not in results.columns:
231         raise RuntimeError(
232             "Internal error: REGION column missing from results."
233         )
234
235     results.to_csv(args.output, index=False)
236     print(f"\nSaved results → {args.output}")
237
238     rankings = (
239         results
240         .sort_values(["REGION", "SCALE_KM", "I_OBS"],
241                      ascending=[True, True, False])
242         .assign(RANK=lambda d:
243             d.groupby(["REGION", "SCALE_KM"]).cumcount() + 1)
244     )
245
246     rank_file = args.output.replace(".csv", "_rankings.csv")
247     rankings.to_csv(rank_file, index=False)
248     print(f"Saved rankings → {rank_file}")
249
250     if skipped_regions:
251         print("\nSkipped regions due to insufficient or invalid data:")
252         for r in sorted(skipped_regions):
253             print(f"  - {r}")
254
255 if __name__ == "__main__":
256     main()
```

shear$_{g}$*enerate*$_{e}$*nsemble.py*

```
1  #!/usr/bin/env python3
2  """
3  Generate an ensemble of conjugate shear stress maps from TPW-style rotations
4  and sample them against the World Stress Map (WSM).
5
6  Baseline:
7    - Rotation = 104°
8    - Axis = 31°E meridian (northward)
```

```
9
10  Randomized alternates:
11    - Random Euler poles
12    - Random rotation magnitudes
13    - Random rotation sense
14  """
15
16  import argparse
17  import numpy as np
18  import pandas as pd
19
20  EARTH_RADIUS = 6371.0
21  DEG2RAD = np.pi / 180.0
22
23  # ------------------------------------------------------------
24  # Geometry utilities
25  # ------------------------------------------------------------
26
27  def sph_to_cart(lat, lon):
28      lat *= DEG2RAD
29      lon *= DEG2RAD
30      return np.array([
31          np.cos(lat) * np.cos(lon),
32          np.cos(lat) * np.sin(lon),
33          np.sin(lat)
34      ])
35
36  def cart_to_sph(v):
37      x, y, z = v
38      lat = np.arcsin(z)
39      lon = np.arctan2(y, x)
40      return lat / DEG2RAD, lon / DEG2RAD
41
42  def rotate_vector(v, axis, angle_deg):
43      theta = angle_deg * DEG2RAD
44      axis = axis / np.linalg.norm(axis)
45      return (
46          v * np.cos(theta)
47          + np.cross(axis, v) * np.sin(theta)
```

```
        + axis * np.dot(axis, v) * (1 - np.cos(theta))
    )

# ------------------------------------------------------------
# TPW stress model (simplified but physical)
# ------------------------------------------------------------

def compute_shear_azimuth(lat, lon, pole_lat, pole_lon):
    """
    Compute conjugate shear azimuths from TPW geometry.
    """
    p = sph_to_cart(lat, lon)
    pole = sph_to_cart(pole_lat, pole_lon)

    # Tangential velocity direction
    v = np.cross(pole, p)
    if np.linalg.norm(v) == 0:
        return np.nan, np.nan

    v /= np.linalg.norm(v)

    # Project to local tangent plane
    north = np.array([0, 0, 1])
    east = np.cross(north, p)
    east /= np.linalg.norm(east)
    north = np.cross(p, east)

    ve = np.dot(v, east)
    vn = np.dot(v, north)

    az = (np.arctan2(ve, vn) / DEG2RAD) % 360.0

    # Conjugate shears ±45°
    return az, (az + 90.0) % 360.0

# ------------------------------------------------------------
# Main
# ------------------------------------------------------------

```

```python
def main():
    ap = argparse.ArgumentParser()
    ap.add_argument("--wsm", required=True, help="WSM CSV")
    ap.add_argument("--output", default="shear_ensemble.csv")
    ap.add_argument("--random", type=int, default=0,
                    help="Number of randomized TPW realizations")
    ap.add_argument("--rot-min", type=float, default=30)
    ap.add_argument("--rot-max", type=float, default=150)
    ap.add_argument("--seed", type=int, default=42)
    args = ap.parse_args()

    rng = np.random.default_rng(args.seed)
    wsm = pd.read_csv(args.wsm)

    results = []

    # ----------------------------------------------------
    # Define ensemble
    # ----------------------------------------------------

    ensemble = []

    # Baseline TPW (104° along 31°E)
    ensemble.append({
        "run_id": "TPW_BASELINE",
        "pole_lat": 0.0,
        "pole_lon": 31.0,
        "rot_deg": 104.0,
        "rot_sign": +1
    })

    # Randomized alternatives
    for i in range(args.random):
        u = rng.uniform(-1, 1)
        pole_lat = np.arcsin(u) / DEG2RAD
        pole_lon = rng.uniform(0, 360)
        rot_deg = rng.uniform(args.rot_min, args.rot_max)
        rot_sign = rng.choice([-1, +1])

```

```
126         ensemble.append({
127             "run_id": f"TPW_RANDOM_{i:03d}",
128             "pole_lat": pole_lat,
129             "pole_lon": pole_lon,
130             "rot_deg": rot_deg,
131             "rot_sign": rot_sign
132         })
133 
134     # ------------------------------------------------------
135     # Compute stress for each realization
136     # ------------------------------------------------------
137 
138     for cfg in ensemble:
139         print(f"Generating {cfg['run_id']}")
140 
141         pole = sph_to_cart(cfg["pole_lat"], cfg["pole_lon"])
142         angle = cfg["rot_sign"] * cfg["rot_deg"]
143 
144         for _, row in wsm.iterrows():
145             lat, lon = row["LAT"], row["LON"]
146             wsm_az = row["AZI"] % 360.0
147 
148             az1, az2 = compute_shear_azimuth(lat, lon,
149                                              cfg["pole_lat"],
150                                              cfg["pole_lon"])
151             if np.isnan(az1):
152                 continue
153 
154             mis1 = abs((az1 - wsm_az + 90) % 180 - 90)
155             mis2 = abs((az2 - wsm_az + 90) % 180 - 90)
156 
157             results.append({
158                 "RUN_ID": cfg["run_id"],
159                 "POLE_LAT": cfg["pole_lat"],
160                 "POLE_LON": cfg["pole_lon"],
161                 "ROT_DEG": cfg["rot_deg"],
162                 "ROT_SIGN": cfg["rot_sign"],
163                 "LAT": lat,
164                 "LON": lon,
```

```
                "WSM_AZ": wsm_az,
                "NET1_AZ": az1,
                "NET2_AZ": az2,
                "NET1_MISFIT": mis1,
                "NET2_MISFIT": mis2,
                "BEST_MISFIT": min(mis1, mis2),
                "QUALITY": row.get("QUALITY", None),
                "PLATE": row.get("PLATE", None)
            })

    out = pd.DataFrame(results)
    out.to_csv(args.output, index=False)
    print(f"Saved {args.output}")

# ------------------------------------------------------------
if __name__ == "__main__":
    main()
```

rank-plot.py

```
#!/usr/bin/env python3
import argparse
import pandas as pd
import numpy as np
import matplotlib.pyplot as plt
from math import radians, sin, cos, acos


# ============================================================
# Geometry utilities
# ============================================================

def angular_distance_deg(lat1, lon1, lat2, lon2):
    """Great-circle angular distance in degrees."""
    lat1, lon1, lat2, lon2 = map(radians, [lat1, lon1, lat2, lon2])
    dot = (
        sin(lat1) * sin(lat2)
        + cos(lat1) * cos(lat2) * cos(lon1 - lon2)
    )
```

```
    dot = max(-1.0, min(1.0, dot))
    return np.degrees(acos(dot))


def euler_polar_coords(lat, lon, lat0, lon0):
    """
    Convert Euler pole (lat,lon) into polar coordinates
    relative to baseline pole (lat0,lon0).
    """
    d = angular_distance_deg(lat, lon, lat0, lon0)
    theta = np.radians(lon)
    r = np.radians(d)
    return theta, np.degrees(r)


# ============================================================
# Shared plotting routine
# ============================================================

def make_plots(df, baseline_id, b_lat, b_lon, output_prefix):
    # ============================================================
    # Plot 1: Rank vs Euler distance (faceted by scale)
    # ============================================================

    scales = sorted(df["SCALE_KM"].unique())
    fig, axes = plt.subplots(
        1, len(scales),
        figsize=(6 * len(scales), 5),
        sharey=True
    )

    if len(scales) == 1:
        axes = [axes]

    for ax, L in zip(axes, scales):
        d = df[df["SCALE_KM"] == L]
        rand = d[d["RUN_ID"] != baseline_id]
        base = d[d["RUN_ID"] == baseline_id]

```

```
        ax.scatter(
            rand["EULER_DIST_DEG"], rand["RANK"],
            s=12, alpha=0.6, label="Random"
        )

        if not base.empty:
            ax.scatter(
                base["EULER_DIST_DEG"], base["RANK"],
                s=50, c="red", label="Baseline"
            )

        ax.set_title(f"Scale = {int(L)} km")
        ax.set_xlabel("Euler distance to baseline (deg)")
        ax.set_ylabel("Rank")
        ax.invert_yaxis()
        ax.grid(True, alpha=0.3)

    plt.tight_layout()
    plt.savefig(f"{output_prefix}_rank_vs_euler.png", dpi=200)
    plt.close()

    # ============================================================
    # Plot 2: Rank vs wavelength
    # ============================================================

    fig, ax = plt.subplots(figsize=(7, 5))

    for run_id, g in df.groupby("RUN_ID"):
        if run_id == baseline_id:
            ax.plot(
                g["SCALE_KM"], g["RANK"],
                linewidth=2.5, label="Baseline"
            )
        else:
            ax.plot(
                g["SCALE_KM"], g["RANK"],
                color="gray", alpha=0.3
            )

```

```
    ax.set_xlabel("Wavelength (km)")
    ax.set_ylabel("Rank")
    ax.set_xscale("log")
    ax.invert_yaxis()
    ax.grid(True, alpha=0.3)
    ax.legend()

    plt.tight_layout()
    plt.savefig(f"{output_prefix}_rank_vs_scale.png", dpi=200)
    plt.close()

    # ============================================================
    # Plot 3: Polar Euler-space visualization
    # ============================================================

    fig = plt.figure(figsize=(7, 7))
    ax = plt.subplot(111, polar=True)

    for run_id, g in df.groupby("RUN_ID"):
        theta, r = zip(*[
            euler_polar_coords(
                row["POLE_LAT"], row["POLE_LON"],
                b_lat, b_lon
            )
            for _, row in g.iterrows()
        ])
        ax.plot(theta, r, alpha=0.5)

    ax.set_title("Euler-space scatter (baseline at origin)")
    ax.set_rlabel_position(225)
    ax.grid(True)

    plt.tight_layout()
    plt.savefig(f"{output_prefix}_euler_polar.png", dpi=200)
    plt.close()

    print("Saved plots:")
    print(f"  {output_prefix}_rank_vs_euler.png")
    print(f"  {output_prefix}_rank_vs_scale.png")
```

```
    print(f"  {output_prefix}_euler_polar.png")


# ============================================================
# Main
# ============================================================

def main():
    ap = argparse.ArgumentParser()
    ap.add_argument("--input", required=True, help="Rankings CSV")
    ap.add_argument("--baseline", default="TPW_BASELINE")
    ap.add_argument("--region", default="Arctic")
    ap.add_argument("--output-prefix", default="morans_rank")
    ap.add_argument(
        "--all-regions-mean",
        action="store_true",
        help="Also generate plots for the mean across all regions combined"
    )
    args = ap.parse_args()

    df = pd.read_csv(args.input)

    # ------------------------------------------------------------
    # Euler pole metadata
    # ------------------------------------------------------------
    if not {"POLE_LAT", "POLE_LON"}.issubset(df.columns):
        raise RuntimeError(
            "CSV must include POLE_LAT and POLE_LON for Euler-space plotting"
        )

    # Baseline pole
    b = df[df["RUN_ID"] == args.baseline].iloc[0]
    b_lat, b_lon = b["POLE_LAT"], b["POLE_LON"]

    # Euler angular distance (degrees)
    df["EULER_DIST_DEG"] = df.apply(
        lambda r: angular_distance_deg(
            r["POLE_LAT"], r["POLE_LON"], b_lat, b_lon
        ),
```

```
        axis=1
    )

    # Preserve full dataset for optional averaging
    df_full = df.copy()

    # ============================================================
    # Region-specific plots (existing behavior)
    # ============================================================
    df_region = df[df["REGION"] == args.region]
    if df_region.empty:
        raise RuntimeError(
            f"No valid Moran results available for region '{args.region}'."
        )

    make_plots(
        df_region,
        baseline_id=args.baseline,
        b_lat=b_lat,
        b_lon=b_lon,
        output_prefix=args.output_prefix
    )

    # ============================================================
    # Optional: averaged results across ALL regions
    # ============================================================
    if args.all_regions_mean:
        df_mean = (
            df_full.groupby(["RUN_ID", "SCALE_KM"], as_index=False)
            .agg({
                "RANK": "mean",
                "EULER_DIST_DEG": "mean",
                "POLE_LAT": "mean",
                "POLE_LON": "mean"
            })
        )
        df_mean["REGION"] = "ALL_MEAN"

        make_plots(
```

```
            df_mean,
            baseline_id=args.baseline,
            b_lat=b_lat,
            b_lon=b_lon,
            output_prefix=f"{args.output_prefix}_ALLMEAN"
        )


if __name__ == "__main__":
    main()
```

coherence.py

```
#!/usr/bin/env python3
import argparse
import numpy as np
import pandas as pd
from scipy.signal import savgol_filter

MIN_POINTS = 3  # require 3 wavelength scales


def curvature_metrics(L, I):
    """Compute slope, curvature, monotonicity, plateau index, inflections."""
    L = np.asarray(L, float)
    I = np.asarray(I, float)

    # normalize wavelength spacing
    x = (L - L.min()) / (L.max() - L.min() + 1e-12)

    # smoothing only when enough points exist
    if len(I) >= 5:
        I_sm = savgol_filter(I, window_length=5 if len(I) >= 5 else len(I)|1,
                             polyorder=2, mode="interp")
    else:
        I_sm = I.copy()

    d1 = np.gradient(I_sm, x, edge_order=1)
    d2 = np.gradient(d1, x, edge_order=1)
```

```
27
28      slope_mean = np.nanmean(d1)
29      slope_var = np.nanvar(d1)
30
31      curvature_mean = np.nanmean(d2)
32      curvature_std = np.nanstd(d2)
33
34      # monotonicity: sign consistency in first derivative
35      sign_changes = np.sum(np.sign(d1[1:]) != np.sign(d1[:-1]))
36      monotonicity = 1.0 - sign_changes / max(len(d1) - 1, 1)
37
38      # plateau index: fraction where |slope|  0
39      plateau = np.mean(np.abs(d1) < np.percentile(np.abs(d1), 25))
40
41      # inflections = zero crossings of curvature
42      infl = np.sum(np.sign(d2[1:]) != np.sign(d2[:-1]))
43
44      return dict(
45          SLOPE_MEAN=slope_mean,
46          SLOPE_VAR=slope_var,
47          CURVATURE_MEAN=curvature_mean,
48          CURVATURE_STD=curvature_std,
49          MONOTONICITY=monotonicity,
50          PLATEAU_INDEX=plateau,
51          INFLECTIONS=infl,
52          I_RANGE=float(np.nanmax(I) - np.nanmin(I)),
53      )
54
55
56  def compute_descriptors(df, out_path):
57
58      rows = []
59      grouped = df.groupby(["REGION", "RUN_ID"], dropna=False)
60
61      for (region, run_id), g in grouped:
62
63          g = g.sort_values("SCALE_KM")
64          L = g["SCALE_KM"].values
65          I = g["I_OBS"].values
```

```
        Z = g["Z_SCORE"].values

        role = "BASELINE" if run_id == "TPW_BASELINE" else "PEER"

        if len(L) < MIN_POINTS or np.all(np.isnan(I)):
            rows.append(dict(
                REGION=region, RUN_ID=run_id, ROLE=role,
                STATUS="INSUFFICIENT_POINTS"
            ))
            continue

        m = curvature_metrics(L, I)
        rows.append(dict(
            REGION=region,
            RUN_ID=run_id,
            ROLE=role,
            STATUS="OK",
            N_SCALES=len(L),
            **m,
            I_MEAN=float(np.nanmean(I)),
            Z_MEAN=float(np.nanmean(Z)),
        ))

    desc = pd.DataFrame(rows)

    # ---- Baseline vs Ensemble Coherence ----
    summaries = []
    for region, g in desc.groupby("REGION"):
        base = g[g["ROLE"] == "BASELINE"]
        peers = g[g["ROLE"] == "PEER"]

        if base.empty or peers.empty:
            continue

        b = base.iloc[0]
        diffs = peers.copy()

        for col in [
            "SLOPE_MEAN","CURVATURE_STD","MONOTONICITY",
```

```
            "PLATEAU_INDEX","INFLECTIONS","I_RANGE"
        ]:
            diffs[f"DELTA_{col}"] = peers[col] - b[col]

        summaries.append(dict(
            REGION=region,
            N_PEERS=len(peers),
            BASE_SLOPE_MEAN=b["SLOPE_MEAN"],
            ENSEMBLE_SLOPE_MEAN=float(peers["SLOPE_MEAN"].mean()),
            DELTA_SLOPE_MEAN=float(diffs["DELTA_SLOPE_MEAN"].mean()),

            BASE_CURVATURE_STD=b["CURVATURE_STD"],
            ENSEMBLE_CURVATURE_STD=float(peers["CURVATURE_STD"].mean()),
            DELTA_CURVATURE_STD=float(diffs["DELTA_CURVATURE_STD"].mean()),

            BASE_MONOTONICITY=b["MONOTONICITY"],
            ENSEMBLE_MONOTONICITY=float(peers["MONOTONICITY"].mean()),
            DELTA_MONOTONICITY=float(diffs["DELTA_MONOTONICITY"].mean()),

            BASE_PLATEAU_INDEX=b["PLATEAU_INDEX"],
            ENSEMBLE_PLATEAU_INDEX=float(peers["PLATEAU_INDEX"].mean()),
            DELTA_PLATEAU_INDEX=float(diffs["DELTA_PLATEAU_INDEX"].mean()),
        ))

    summary = pd.DataFrame(summaries)

    desc.to_csv(out_path, index=False)
    summary.to_csv(out_path.replace(".csv", "_summary.csv"), index=False)

    print(f"Saved descriptors → {out_path}")
    print(f"Saved ensemble summary → {out_path.replace('.csv','_summary.csv')}")


def main():
    ap = argparse.ArgumentParser()
    ap.add_argument("--input", required=True)
    ap.add_argument("--output", default="coherence_shape_descriptors.csv")
    args = ap.parse_args()

```

```
    df = pd.read_csv(args.input)
    required = {
        "RUN_ID","REGION","SCALE_KM","I_OBS","Z_SCORE"
    }
    missing = required - set(df.columns)
    if missing:
        raise RuntimeError(f"Missing columns: {missing}")

    compute_descriptors(df, args.output)


if __name__ == "__main__":
    main()
```

coherence$_{v}s_{m}oran.py$

```
#!/usr/bin/env python3
import argparse
import os
import numpy as np
import pandas as pd
import matplotlib.pyplot as plt


# ---------------------------------------------------------------------
# Robust finite-difference slope estimator (dI / d log L)
# ---------------------------------------------------------------------
def finite_difference_slopes(L, I):
    """
    Compute dI/d(log L) with numerical stability.
    Handles duplicate scales, missing values, and sparse scale sets.
    Returns one slope per scale value.
    """
    L = np.asarray(L, dtype=float)
    I = np.asarray(I, dtype=float)

    logL = np.log(L)
    slopes = np.full_like(I, np.nan)

```

```
    n = len(L)
    if n < 2:
        return slopes

    for i in range(n):
        il = i - 1 if i > 0 else None
        ir = i + 1 if i < n - 1 else None

        # central difference (preferred)
        if il is not None and ir is not None:
            dlog = logL[ir] - logL[il]
            if dlog != 0:
                slopes[i] = (I[ir] - I[il]) / dlog
                continue

        # forward fallback
        if ir is not None:
            dlog = logL[ir] - logL[i]
            if dlog != 0:
                slopes[i] = (I[ir] - I[i]) / dlog
                continue

        # backward fallback
        if il is not None:
            dlog = logL[i] - logL[il]
            if dlog != 0:
                slopes[i] = (I[i] - I[il]) / dlog
                continue

    return slopes


# ---------------------------------------------------------------------
# Load and merge coherence + Moran's outputs
# ---------------------------------------------------------------------
def load_data(coherence_path, morans_path):
    coh = pd.read_csv(coherence_path)
    mor = pd.read_csv(morans_path)

```

```
    mor = mor.copy()
    mor["I_EXCESS_MEAN"] = mor["I_OBS"] - mor["I_NULL_MEAN"]

    df = pd.merge(
        coh,
        mor[
            [
                "RUN_ID",
                "REGION",
                "SCALE_KM",
                "I_OBS",
                "I_NULL_MEAN",
                "I_EXCESS_MEAN",
            ]
        ],
        on=["RUN_ID", "REGION"],
        how="inner",
    )

    return df


# ---------------------------------------------------------------------
# Global scatter | baseline highlighted
# ---------------------------------------------------------------------
def plot_global(df, outdir):
    fig, ax = plt.subplots(figsize=(10, 6))

    peers = df[df["ROLE"] != "BASELINE"]
    base = df[df["ROLE"] == "BASELINE"]

    ax.scatter(
        peers["SLOPE_MEAN"],
        peers["I_EXCESS_MEAN"],
        c="0.75",
        marker="x",
        alpha=0.35,
        s=26,
        label="NULL",
```

```
        zorder=1,
    )

    ax.scatter(
        base["SLOPE_MEAN"],
        base["I_EXCESS_MEAN"],
        c="red",
        s=50,
        zorder=4,
        label="BASELINE",
    )

    ax.axhline(0, color="black", lw=0.8)
    ax.set_title("Global coherence vs spatial clustering strength (per-scale)")
    ax.set_xlabel("Coherence (finite-difference slope dI / d log L)")
    ax.set_ylabel("Moran's I excess vs null (I_obs  I_null_mean)")
    ax.legend(frameon=False)

    fig.tight_layout()
    fig.savefig(f"{outdir}/global_coherence_vs_I.png", dpi=220)
    plt.close(fig)


# ---------------------------------------------------------------------
# Combined mean baseline trajectory (BLUE LINE)
# ---------------------------------------------------------------------
def plot_combined_mean(df, outdir):
    base = df[df["ROLE"] == "BASELINE"].copy()

    mean_curve = (
        base.groupby("SCALE_KM", as_index=False)[["I_OBS", "I_EXCESS_MEAN"]]
        .mean()
        .sort_values("SCALE_KM")
    )

    mean_curve["COHERENCE_SLOPE"] = finite_difference_slopes(
        mean_curve["SCALE_KM"].values,
        mean_curve["I_OBS"].values,
    )
```

```
141
142     fig, ax = plt.subplots(figsize=(10, 6))
143
144     ax.plot(
145         mean_curve["COHERENCE_SLOPE"],
146         mean_curve["I_EXCESS_MEAN"],
147         "-o",
148         color="blue",
149         lw=2.2,
150         ms=6,
151         zorder=4,
152         label="Combined Mean (Baseline)",
153     )
154
155     for _, r in mean_curve.iterrows():
156         ax.text(
157             r["COHERENCE_SLOPE"],
158             r["I_EXCESS_MEAN"],
159             f"{int(r['SCALE_KM'])} km",
160             fontsize=9,
161             color="blue",
162             ha="left",
163             va="bottom",
164         )
165
166     ax.axhline(0, color="black", lw=0.8)
167     ax.set_title("Combined mean coherence vs Moran's I (baseline only)")
168     ax.set_xlabel("Coherence (finite-difference slope dI / d log L)")
169     ax.set_ylabel("Moran's I excess vs null")
170
171     ax.legend(frameon=False)
172     fig.tight_layout()
173     fig.savefig(f"{outdir}/combined_mean_coherence_vs_I.png", dpi=220)
174     plt.close(fig)
175
176
177 # ---------------------------------------------------------------------
178 # Regional plot | baseline trajectory vs null ensemble
179 # ---------------------------------------------------------------------
```

```
def plot_region(df_region, outdir):
    region = df_region["REGION"].iloc[0]

    baseline = (
        df_region[df_region["ROLE"] == "BASELINE"]
        .sort_values("SCALE_KM")
        .copy()
    )
    peers = df_region[df_region["ROLE"] != "BASELINE"]

    slopes = finite_difference_slopes(
        baseline["SCALE_KM"].values,
        baseline["I_OBS"].values,
    )
    baseline["COHERENCE_SLOPE"] = slopes

    fig, ax = plt.subplots(figsize=(10, 6))

    ax.scatter(
        peers["SLOPE_MEAN"],
        peers["I_EXCESS_MEAN"],
        s=26,
        c="0.8",
        marker="x",
        alpha=0.35,
        label="NULL",
        zorder=1,
    )

    ax.plot(
        baseline["COHERENCE_SLOPE"],
        baseline["I_EXCESS_MEAN"],
        "-o",
        color="red",
        lw=2.0,
        ms=6,
        zorder=4,
        label="BASELINE",
    )
```

```
219
220     for _, r in baseline.iterrows():
221         ax.text(
222             r["COHERENCE_SLOPE"],
223             r["I_EXCESS_MEAN"],
224             f"{int(r['SCALE_KM'])} km",
225             fontsize=9,
226             color="red",
227             ha="left",
228             va="bottom",
229         )
230
231     ax.axhline(0, color="black", lw=0.8)
232     ax.set_title(f"{region}: Coherence vs Moran's I (per-scale)")
233     ax.set_xlabel("Coherence (finite-difference slope dI / d log L)")
234     ax.set_ylabel("Moran's I excess vs null")
235
236     ax.legend(frameon=False)
237     fig.tight_layout()
238     fig.savefig(f"{outdir}/{region}_coherence_vs_I.png", dpi=220)
239     plt.close(fig)
240
241
242 # ---------------------------------------------------------------------
243 # Main
244 # ---------------------------------------------------------------------
245 def main():
246     parser = argparse.ArgumentParser(
247         description="Compare coherence descriptors vs Moran's I clustering strength"
248     )
249     parser.add_argument("--coherence", required=True)
250     parser.add_argument("--morans", required=True)
251     parser.add_argument("--output", required=True)
252
253     args = parser.parse_args()
254     os.makedirs(args.output, exist_ok=True)
255
256     df = load_data(args.coherence, args.morans)
257
```

```
    print("\nDetected role distribution:\n", df["ROLE"].value_counts(), "\n")

    plot_global(df, args.output)
    plot_combined_mean(df, args.output)

    for _, sub in df.groupby("REGION"):
        plot_region(sub, args.output)

    print(f"\nPlots written to {os.path.abspath(args.output)}")


if __name__ == "__main__":
    main()
```